

CLIMATE INTERPOLATION FOR LAND RESOURCE  
AND LAND USE STUDIES IN MOUNTAINOUS REGIONS

---

Guillermo A. Baigorria Paz

Proefschrift  
ter verkrijging van de graad van doctor  
op gezag van de rector magnificus  
van Wageningen Universiteit,  
Prof.dr.ir. L. Speelman,  
in het openbaar te verdedigen  
op dinsdag 19 april  
des namiddags te 16:00 in de Aula

Promotor

Prof dr. A. Veldkamp

Hoogleraar Bodeminventarisatie en Landevaluatie

Co-Promotor

dr. ir. J.J. Stoorvogel

Universitair Hoofddocent Bodeminventarisatie en Landevaluatie

Promotiecommissie

Prof.dr.ir. E.M.A. Smaling

Prof.dr. A.A.M. Holtslag

Prof.dr.ir. L. Stroosnijder

Dr J.W. Hansen

ITC, Enschede

Wageningen Universiteit, Nederland

Wageningen Universiteit, Nederland

International Research Institute for

Climate Prediction, Palisades, USA

**CLIMATE INTERPOLATION FOR LAND RESOURCE  
AND LAND USE STUDIES IN MOUNTAINOUS REGIONS**

Guillermo A. Baigorria Paz

2005

PhD. Thesis  
Laboratory of Soil Science and Geology,  
Wageningen University and Research Centre,  
The Netherlands

ISBN: 90-8504-238-0

*“Unfortunately, all these really valuable treasures of a science remain inaccessible to the people and do not bring to him benefit, which can from them be expected... it is necessary to reduce all available scientific riches in one connected whole and to state the given results by popular language.”*

*V.V. Dokuchaev, 1879*

*Dedicated to the memory*

*of my father Guillermo and my nephew Jean*

## Acknowledgements

---

First, I want to express my gratitude to Wageningen University and Research Centre (WU) and to the International Potato Center (CIP), both providing me a home to develop myself as a future researcher.

I want to especially thank the United States Agency for International Development (USAID), through its Soil Management Collaborative Research Program (SM-CRSP) financing a project entitled 'Tradeoffs in Sustainable Agriculture and the Environment in the Andes: A Decision Support System for Policy Makers' (Grant # 291488). This project was the umbrella of the development of my PhD research.

To Dr. Walter T. Bowen, who gave me the opportunity to work at CIP under his supervision, and to begin my PhD program. Thanks for transmitting your knowledge and for your pieces of advice as a friend.

To Dr. Antonie Veldkamp, full professor of Soil Science and Land Evaluation Chair of the Laboratory of Soil Science and Geology – WU, who accepted me as his student and guided me during my last stage at WU.

To the TOA team: Dr. John Antle from Montana State University, Dr. Jetse Stoorvogel from WU, and Dr. Charles Crissman from CIP for believing in me on developing the Tradeoffs issues in Peru and Ecuador. For supporting not only economically to my PhD, but also guiding me on my instruction as a future researcher. My gratitude to Jetse, my advisor during all my research at WU.

To Dr. Roberto Quiroz, head of the Natural Resources Management Division. Thank you for your availability, stimulating discussions and human qualities.

I wish to express my sincere gratitude to my close friend Fina Bokhorst, who extended her hands to my wife and me in Holland, teaching us that our studies were not all in live. Thanks for your time, for a space on your life and your mind, and for your unconditional friendship.

I want to express my gratitude to the Secretariat of the 'Global change SysTem for Analysis, Research and Training (START)' for co-funding chapter 5 of this thesis. To the International Research Institute for Climate Prediction (IRI),

especially to Dr. James Hansen and Dr. Neil Ward, for the training received at the Advance Training Institute (ATI) funded by START and the 'David and Lucille Packard Foundation'.

To the Meteorological and Hydrological National Service of Peru (SENAMHI), to support the research of atmospheric transmissivity in Peru. Specially thanks to my friends, MSc. Irene Trebejo and MSc. Esequiel Villegas.

To Dr. Corinne Valdivia from Missouri University for supporting the field-workshop of chapter 5, but also for her valuable pieces of advice. Also thanks to Dr. Carlos León-Velarde from CIP, who gave me pieces of advice to properly make important decisions.

To Mrs. Ivonne Valdizán, Mrs. Rosario Marcovich, Mrs. Karina Petrovich, and Miss Yasmín Raygada supporting me with the administrative issues at CIP. To Mrs. Henny van den Berg-Koolhout and Thea van Hummel supporting me with the administrative issues at WU. To Mr. Alex García supporting me in the computational area, Jorge de la Cruz and PhD<sub>(c)</sub> Mariana Cruz for supporting GIS and Delphi's programming issues, and to Alicia Levine in the edition of some parts of the present thesis work.

The field work conducted in Cajamarca would not be possible without the special support of the people in charge of the project there, my friends, Eng. Estuardo Regalado, Mrs. Noemí Cabanillas, Tech. Lucinda Chávez, Eng. William Regalado, and Tech. Alcides Rosas. Also to my students, MSc. Liliana Sánchez and Eng. Janeth Pizarro who supported the field work made on chapter 5.

To the 'Asociación para el Desarrollo Forestal' (ADEFOR), providing the meteorological historical records of the three main weather stations in the Peruvian study area. To the farmers in charge of my weather stations Mrs. Rosa Abanto, Mrs. Graciela Díaz and Mr. Simón Mires. At last but not least, to the farmers of La Encañada and Tambomayo watersheds in Peru and Chitán and San Gabriel watersheds in Ecuador, who provided valuable information to the present work.

To my friends in Holland, specially the ones in Ede and Wageningen. To Petra and Indiana.

To my family and wife for their support, patient and their understanding.



## Table of Contents

1. INTRODUCTION	1
1.1 Objectives	2
1.2 Study area	2
1.3 Outline of the study	4
2. ATMOSPHERIC TRANSMISSIVITY: DISTRIBUTION AND EMPIRICAL ESTIMATION AROUND THE CENTRAL ANDES	7
2.1 Introduction	8
2.2 Data	9
2.3 Methods	12
2.3.1 Spatial distribution of the atmospheric transmissivity coefficient	12
2.3.2 Model based on sunshine hours: Ångström-Prescott model	13
2.3.3 Model based on temperatures	13
2.3.4 Calibration and validation	15
2.4 Results and discussion	16
2.4.1 Factors affecting the spatial distribution of $\tau$	16
2.4.2 Model based on sunshine hours	21
2.4.3 Models based on temperatures	22
2.5 Conclusions	28
3. INTERPOLATING MINIMUM AND MAXIMUM TEMPERATURES AND SOLAR IRRADIATION IN MOUNTAIN AREAS	31
3.1 Introduction	32
3.2 Materials and methods	33
3.2.1 Data	33
3.2.2 Model rationale	34
3.2.3 Mathematical structure of the model	35
3.3 Results and discussion	39
3.4 Conclusions	45
4. MODELING THE SPATIAL DISTRIBUTION OF RAINFALL IN COMPLEX TERRAINS BASED ON THE DIGITAL MOUNTAIN WAVE MODEL	47
4.1 Introduction	48
4.2 Background	49
4.2.1 Formation of precipitation	49
4.2.2 Spatial rainfall distribution	50
4.2.3 Circulation patterns and topography	50
4.2.4 Mountain waves	51
4.3 Methodology	52
4.3.1 Study area and data sources	52
4.3.2 Mountain Wave Model	53
4.3.3 Rainfall interpolation model	56
4.3.4 Validation	62

4.4 Results and Discussion	62
4.4.1 Software	62
4.4.2 The Digital Mountain Wave Model (DMWM)	63
4.4.3. Rainfall interpolation	65
4.5 Conclusions	69
5. WEATHER AND SEASONAL-CLIMATE FORECASTS TO SUPPORT AGRICULTURAL DECISION-MAKING AT DIFFERENT SPATIAL AND TEMPORAL SCALES	71
5.1 Introduction	72
5.2 Data and methods	74
5.2.1 Data collection and standardization	75
5.2.2 Spatial and temporal downscaling of seasonal-climate forecast	76
5.2.3 Evaluation of land management	78
5.3 Results	79
5.3.1 Data collection and standardization	79
5.3.2 Spatial and temporal downscaling of seasonal-climate forecast	83
5.3.3 Yield forecast and risk evaluation	84
5.4 Discussion and conclusions	86
5.4.1 Current decision-making processes	86
5.4.2 Downscaling the GCM's forecast to the field level	88
5.4.3 Yield forecast, risk evaluation, and training	91
5.4.4 Improving decision-making at different levels	94
6. CLIMATE VARIABILITY EXPLAINING SOIL VARIABILITY IN VOLCANIC ASH SOILS IN THE ECUADORIAN ANDES	97
6.1 Introduction	98
6.2 Data and methods	100
6.2.1 Study area	100
6.2.2 Data collection	102
6.2.3 Weather data interpolation and climate maps	104
6.2.4 Development and validation of multiple regression models	105
6.3 Results and discussion	106
6.3.1 Weather data interpolation and climate maps	106
6.3.2 Soil organic matter	109
6.3.3 Other soil characteristics	115
6.4 Conclusions	118
7. THE EFFECT OF THE RESOLUTION OF CLIMATE AND SOIL DATA ON A LAND USE STUDY IN THE ECUADORIAN ANDES	119
7.1 Introduction	120
7.2 Study area	121
7.3 Data and methods	122
7.3.1 The Tradeoff Analysis System	122

7.3.2 Farm survey data	124
7.3.3 Climate and soil data	124
7.3.4 Model simulations	128
7.4 Results and discussion	131
7.5 Conclusions	138
8. SYNTHESIS	139
8.1 Generalization: taking care	140
8.2 Modeling spatial and temporal variation of meteorological variables	140
8.3 Supporting decision makers	141
8.4 Explaining spatial and temporal variation of soil characteristics	143
8.5 Measuring the effect of the resolution of input data	143
REFERENCES	153
Annex I	167



# Chapter 1

---

## Introduction

Researchers in the field of environmental sciences often face a lack of climatic data. This results in the usage of a number of easy, but very rough, solutions. Examples include the use of simple linear relationships with altitude to estimate temperature differences. Another approximation includes the use of Thiessen polygons to identify weather stations that are nearest to each location. Thiessen polygons ignore the spatial variation within the polygons and the weather stations are considered to be representative for them. Although the impact of these generalizations is not very well known, it is likely that they may result in large errors. This is especially true for complex mountainous areas where short distance variation in climate and weather conditions is likely to occur. Recent technological developments in e.g. geostatistics, modeling, remote sensing and GIS have made an enormous impact on the analytical capacity in environmental sciences. These developments allow for new, innovative approaches to tackle data scarcity through the use of secondary data. In addition, these new tools led to more efficient ways to structure the collection of additional data. For climatic data, this includes the use of geostatistics to interpolate weather data and the use of weather generators

In the Peruvian and Ecuadorian Andes, land use and land resource studies find themselves in a data-scarce environment where only few weather stations are available. Although climate is a very important driving factor behind the processes in land resources and land use researchers have to rely on crude generalizations. In this thesis new interpolation methods are developed for weather data. These models have been developed for the complex mountainous terrain of the Andes. To check the

validity and use of these models they were tested in a number of land resource and land use studies dealing with climate forecasting for agricultural land use, digital soil mapping and regional land use analysis.

## 1.1 Objectives

The main objective of the present thesis is:

- To resolve the data crisis in climate and weather data for land resource and land use studies.

Specific objectives of the present thesis are:

- To develop new efficient methods to interpolate weather and climate data using mechanistic and/or empirical techniques.
- To analyze the use of global seasonal-climate forecast models at the local level in combination with crop growth simulation models and local predictors.
- To evaluate the interpolated, high-resolution weather data for land resource and land use studies.

## 1.2 Study area

This study has been carried out in the Andean highlands of Peru and Ecuador (Figure 1.1). The study area in Peru is located near the town of Cajamarca and includes the La Encañada and Tambomayo watersheds. The two watersheds measure 165 km<sup>2</sup> and range in altitudes from 2950 to 4000 meters above sea level. Soils are classified as Entisols, Inceptisols and Mollisols following the Soil Taxonomy (USDA and NRCS, 1998). Production systems are mainly based on natural and improved pastures and crops, basically Andean roots and tubers (e.g. potato, oca and olluco), wheat and barley (Tapia, 1995). Agriculture in the area is marginal and it is

located on steep hillsides of up to 65% slope (Romero and Stroosnijder, 2001). Per hectare annual income value ranges from US\$ 400 to US\$ 3200 (Valdivia, 2002) and per capita income is usually less than US\$ 1 per day (Baigorria et al., 2002). The department of Cajamarca where the watersheds are located is considered one of the most economically depressed areas in Peru.

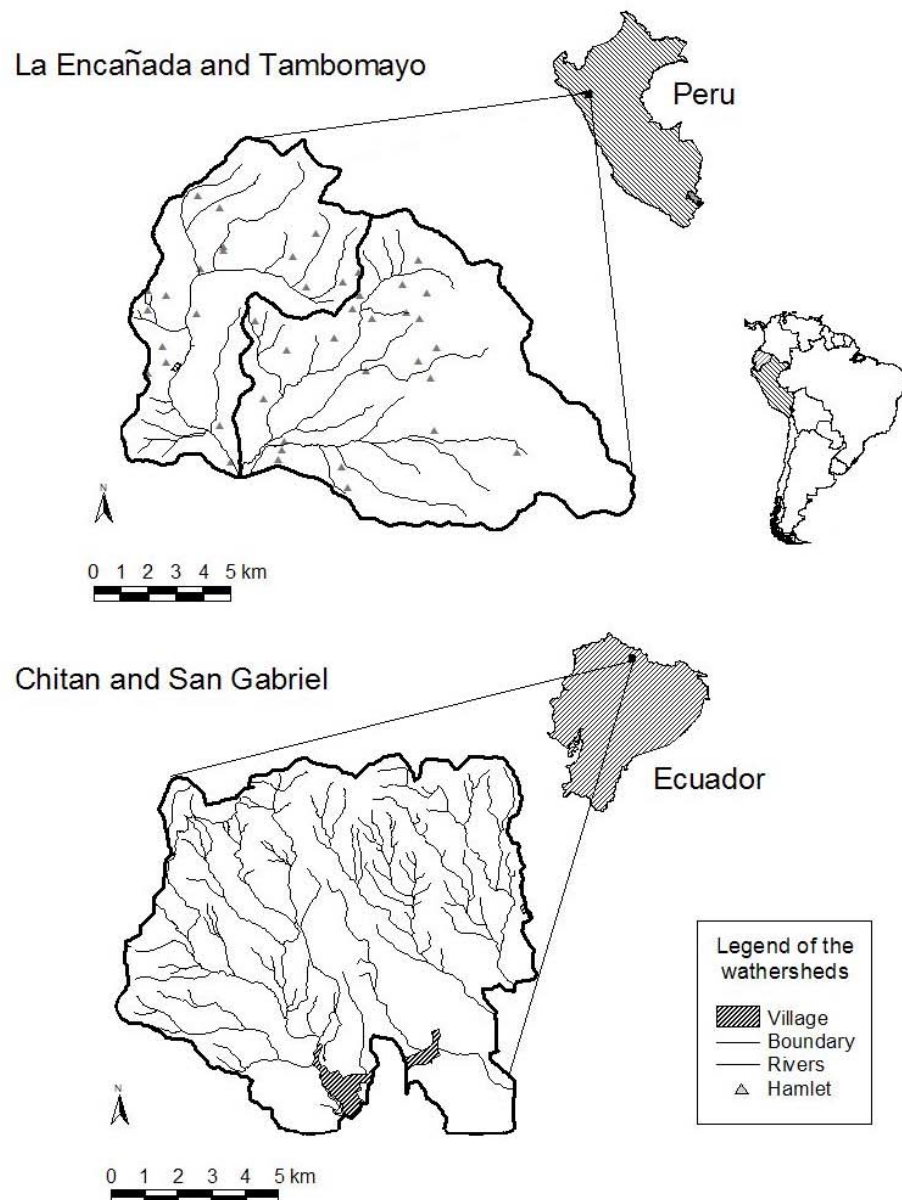


Fig. 1.1. Location of La Encañada and Tambomayo watersheds in Peru and Chitan and San Gabriel watersheds in Ecuador.

The second study area corresponds to the Chitan and San Gabriel watersheds in northern Ecuador. The two watersheds cover 95 km<sup>2</sup> and range in altitude from 2700 to 3840 meters above sea level. Production systems are mainly based on a potato-pasture rotation where potato and milk are the two main commercial products. Crops like wheat, maize, peas, barley, beans, broad beans and some Andean roots and tubers are minor components of the cropping systems (Crissman et al., 1998). Agriculture in the area is developed on steep hillsides. The province of Carchi where the watersheds are located is considered the most important potato production area in Ecuador (Crissman et al., 1998). Soils are classified as Andisols following the Soil Taxonomy (USDA and NRCS, 1998).

### **1.3 Outline of the study**

The different chapters in this thesis deal with the interpolation techniques (Chapter 2-4), the use of seasonal climate-forecasts for local agricultural decisions (Chapter 5) and the application of high-resolution climatic data for land resource (Chapter 6) and land use studies (Chapter 7).

Chapter 2 deals with the spatial and temporal distribution of the atmospheric transmissivity in complex terrain. The variation in the atmospheric transmissivity is an important starting point for further interpolation of weather data. The chapter shows that in complex terrains, it is not possible to generalize atmospheric transmissivity as often done in more homogeneous conditions. It is necessary to differentiate the factors that control climate, topography, and even sea currents affecting the incoming solar radiation in a specific area. In this chapter empirical models to estimate this variable as a function of sunshine hours as well as temperature swing are calibrated and validated for its use in future chapters of this thesis.



In Chapter 3-4 interpolation techniques for weather data are developed for the la Encañada and Tambomayo watersheds in Peru. Chapter 3 deals with the development of a process-based interpolation model for maximum and minimum temperatures, based on the net radiation balance when these temperatures occur twice in a day. The output maps are used in combination with the empiric models for atmospheric transmissivity developed in Chapter 2 resulting in detailed resolution maps of incoming solar radiation. Chapter 4 deals with the development of a process-based interpolation model of rainfall based on the digital mountain wave model (DMWM). This DMWM is defined as a digital representation of the three-dimensional cloud-route determined by the interaction between topography and wind direction. The DMWM establishes a displacement surface for movement of the bottom of an air mass following a predetermined wind direction. Chapter 3 and 4 face the lack of data as well as the representativeness of the weather stations data in complex terrains leading to inconveniences in applying conventional geostatistical methods.

Chapter 5 analyzes the possibility to use seasonal-climate forecasts produced at global scales (pixel sizes of 220 x 220km) to decision makers at the farm level and watershed level (pixel sizes of 100 x 100 m). The chapter analyzes the different levels of information that farmers and agricultural related institutes currently use to make operational, tactical and strategic decisions (Bouma et al., 1999). Weather and seasonal-climate forecast, soils, and land use management are integrated and translated to the farmers as forecasted crop productions.

In chapter 6, the interpolation models developed in the previous chapters are applied in the Ecuadorian Andes to produce high-resolution maps of the different meteorological variables. The high-resolution climatic data are subsequently used for a digital soil mapping exercise. In digital soil mapping we use auxiliary information to explain the variation in soils. Besides parent material, topography, vegetation and time, climate is one of the five main soil-forming factors. The high-resolution climatic data provide

an excellent entry point to obtain better insight in the spatial variability of key soil properties like soil organic matter.

Chapter 7 illustrates the value of the newly generated high-resolution data in a regional land use analysis project. In the project, the tradeoff analysis model (Crissman et al., 1998, Stoorvogel et al., 2004a) is applied for the watersheds in the Ecuadorian Andes to estimate the tradeoffs between economic and environmental indicators. The land use analysis relies heavily on high resolution climatic and soil data to estimate expected crop productions with crop growth simulation models and pesticide leaching with the corresponding leaching models. Key question that is being answered in this chapter is how the use of the high-resolution data changes the outcomes of the model application.

The individual chapters have been submitted as publications in a peer reviewed scientific journals; therefore some descriptive information about the watersheds is some times duplicated.

## Chapter 2

---

### Atmospheric transmissivity: distribution and empirical estimation around the Central Andes

This study of the distribution in space and time of atmospheric transmissivity  $\tau$  takes into account the fact that, in complex terrain, many factors affect this variable; thus, it is not possible to use the generalizations that can be applied under more homogeneous conditions. Climatic controls, topography and even sea currents have important effects on clouds and aerosols affecting  $\tau$ , simultaneously leading to differences in the distribution of incoming solar radiation. Different models exist to estimate incoming solar radiation as a function of relative sunshine hours (observed sunshine hours/theoretical sunshine hours,  $n/N$ ) or differences between maximum and minimum temperatures  $\Delta T$ . We calibrated, validated and evaluated four of these empirical relations based on data from 15 weather stations in Peru. Models were calibrated using 66% of the daily historical record available for each weather station; the rest of the information was used for validation and comparison. The Ångström-Prescott model was used to estimate incoming solar radiation based on  $n/N$ , and gave the best performance of all the models tested. The other models (Bristow-Campbell, Hargreaves, and Garcia) estimated incoming solar radiation based on  $\Delta T$ . Of all the models in this group, the Bristow-Campbell model performed best; it is also valuable because of the physical explanation involved. The empirical coefficients of all the models evaluated are presented here. Two empirical equations are proposed with which to estimate values of the coefficients  $b_B$  and  $c_B$  in the Bristow-Campbell model, as a function of  $\Delta T$  and latitude, allowing the model to be applied to other study areas.

## 2.1 Introduction

Atmospheric transmissivity  $\tau$  in Peru is mainly affected by climatic controls, such as the semi-permanent high-pressure cells over the Pacific and Atlantic Oceans, the Bolivian high (a high-pressure cell in the upper levels of the troposphere), the near-equatorial trough, the cool Humboldt or Peruvian Current, and the Andes mountain range. Over space and time, the interactions of all these climatic controls over complex terrains cause different moisture features in the atmosphere affecting  $\tau$ . In conjunction with the apparent movement of the sun from one hemisphere to the other, a complex pattern of incoming solar radiation develops that does not just correspond to the effects of altitude and latitude.

Incoming solar radiation  $H$  is one of the most important variables in meteorology, since it is the energy source underlying the majority of processes on our planet. Both the total amount of incoming solar radiation and the distribution of that radiation are becoming increasingly important variables in agricultural sciences, due to the introduction of process-based models used to simulate crop growth (Tsuji et al., 1998). The development of photovoltaic panels has provided another reason for understanding the variation that occurs in incoming solar radiation over space and time, since its availability and distribution determine the size of the photovoltaic panels needed for a given application or location. However, despite their importance, measurements of incoming solar radiation are infrequent, since the equipment is costly and highly specialized. In developing countries like Peru, stations where incoming solar radiation can be measured are few and far between. The high spatial variability that occurs both in topography and climate means that irradiation measurements are representative of only very small areas.

Several methods to estimate incoming solar radiation using radiative transfer models and satellites have been developed around the world (Atwater and Ball, 1978; Weymouth and Le Marshall, 1994; Bastos et al.,

1996; Ceballos and Moura, 1997; Dissing and Wendler, 1998; Garatuza-Payan et al., 2001; Gultepe et al., 2001). However, they have all been developed away from mountainous areas because the lack of data for calibration and validation, and because of the complexities in topography, thus needing more complex algorithms to explain the radiative fluxes.

Therefore, it is necessary to generate and calibrate empirical relationships that estimate incoming solar radiation as a function of other known meteorological variables, e.g. as performed by Ångström (1924), Prescott (1940), Frère et al. (1975), Cengiz et al. (1981), Hargreaves and Samani (1982), Bristow and Campbell (1984), García (1994), Goodin et al. (1999), Mahmood and Hubbard (2002). Relative sunshine hours, cloudiness and temperature are frequently measured by weather stations. The use of these variables to estimate incoming solar radiation can help in understanding its variation in time and space.

## **2.2 Data**

Peru is located between latitudes  $0^{\circ}01'48''\text{S}$  and  $18^{\circ}21'03''\text{S}$ , and between longitudes  $68^{\circ}39'27''\text{W}$  and  $81^{\circ}20'11''\text{W}$ . Ranging in altitude from 0 to 6768 meters above sea level, the country has a surface area of 1.29 million  $\text{km}^2$ . Fifteen weather stations from the Peruvian national meteorology and hydrology service (SENAMHI), all containing instruments for measuring incoming solar radiation, sunshine hours and maximum and minimum temperatures, were used in the present work. These weather stations (Table 2.1) are located throughout Peru and cover the variation that occurs between the coastal, highland and jungle areas going from west to east as well as the length of the country from north to south (Figure 2.1). The climatic variation in these locations is presented in Table 2.2.

**Table 2.1.** Geographical location, historical records and instruments used to measure incoming solar radiation in Peru.

ID Location	Latitude (°S)	Longitude (°W)	Altitude (m)	Historical records	Instrument
1 Miraflores	5°10'	80°37'	30	1979-1992	Pyranometer
2 San Ramon SM	5°56'	76°05'	184	1972-1982	Actinograph
3 El Porvenir	6°35'	76°19'	230	1964-1971	Actinograph
4 Bambamarca	6°40'	78°31'	2536	1967-1977	Actinograph
5 Bellavista	7°03'	76°33'	247	1971-1973	Actinograph
6 Weberbauer	7°10'	78°30'	2536	1980-1985	Pyranometer
7 Huayao	12°02'	75°19'	3308	1977-1996	Pyranometer
8 A. von Humboldt	12°05'	76°56'	238	1968-1999	Pyranometer
9 Cosmos	12°09'	75°34'	4575	1986-1988	Pyranometer
10 Granja Kcayra	13°33'	71°52'	3219	1980-1988	Pyranometer
11 San Camilo	14°04'	75°43'	398	1978-1988	Pyranometer
12 Chuquibambilla	14°47'	70°44'	3971	1980-1984	Pyranometer
13 Puno	15°49'	70°00'	3820	1977-1993	Pyranometer
14 Characato	16°27'	71°29'	2451	1978-1987	Pyranometer
15 La Joya	16°35'	71°55'	1295	1967-1993	Actinograph

**Table 2.2.** Main climatic characteristics of the locations.

Location	Incoming solar radiation (MJ m <sup>-2</sup> day <sup>-1</sup> )	Relative sunshine duration (%)	Maximum temperature (°C)	Minimum temperature (°C)	Total annual rainfall (mm)
<b>Coast</b>					
Miraflores	20.7	56	30.7	19.3	216
A. von Humboldt	14.6	40	23.3	15.5	16
San Camilo	21.3	61	28.7	13.4	11
La Joya	25.3	75	27.0	10.1	77
<b>Highlands</b>					
Bambamarca	16.4	44	19.4	9.5	737
Weberbauer	17.7	49	21.3	7.6	644
Cosmos	17.7	46	9.2	-0.7	1047
Huayao	21.6	56	19.6	4.4	765
Granja Kcayra	19.6	53	20.7	3.7	674
Chuquibambilla	21.9	59	16.8	-2.4	715
Puno	22.9	70	14.7	2.6	753
Characato	23.4	73	22.8	6.8	78
<b>Jungle</b>					
San Ramon SM	16.8	41	31.3	20.8	2158
El Porvenir	14.0	41	32.5	20.4	1041
Bellavista	17.2	40	32.2	20.9	928

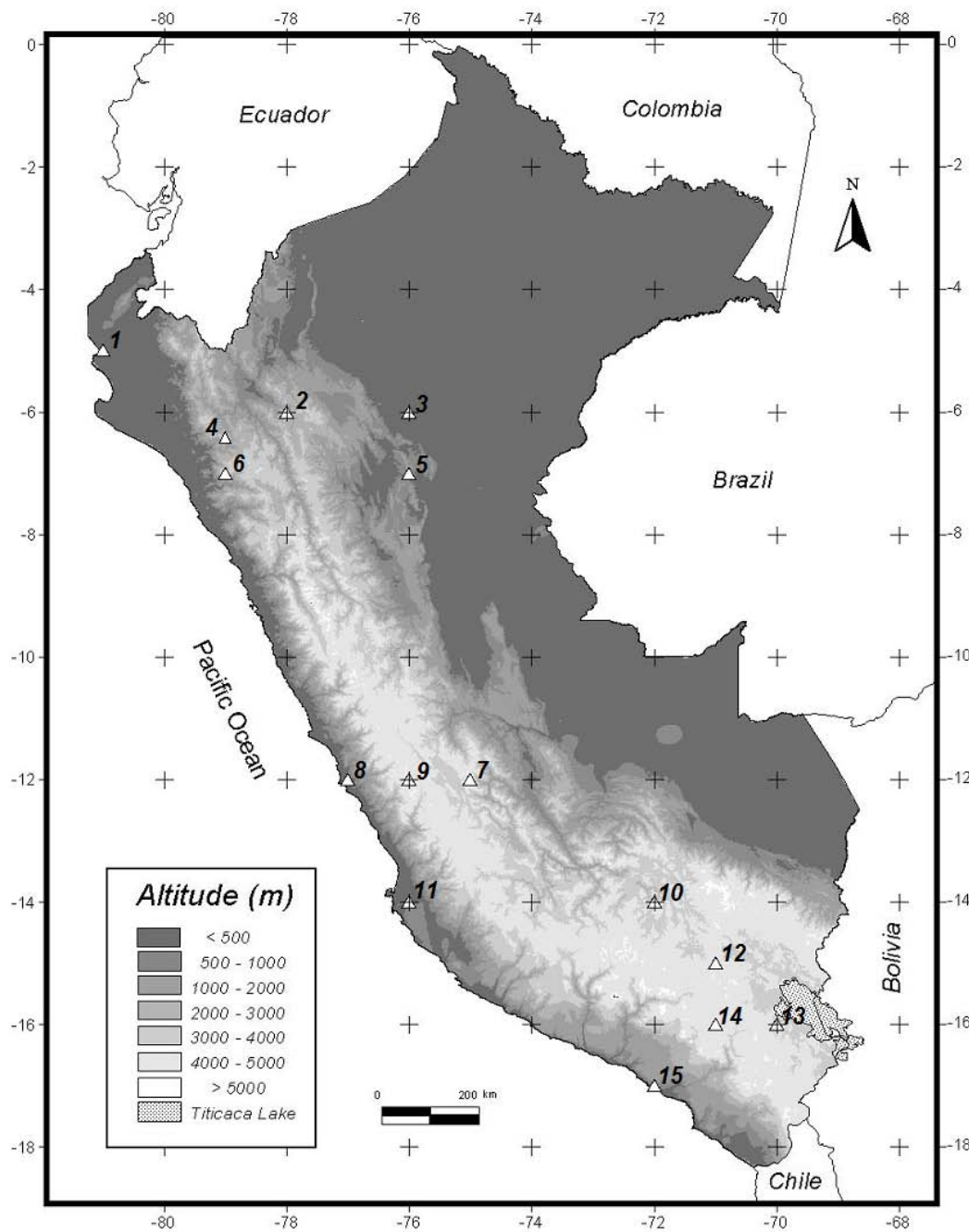


Fig. 2.1. Digital elevation model (DEM) of Peru and location of the weather stations used. Identification numbers are related with table 2.1.

Data on incoming solar radiation were obtained from pyranometers and actinographs; sunshine hours were read from Campbell-Stokes heliographs. All the information used was recorded at hourly intervals, and was taken from the complete historical record of each weather station.

After the aggregation of the hourly data from all the meteorological stations into daily intervals, consistency analyses were performed. These analyses included: the identification of transcription errors caused when transferring data from manual files; the detection of systematic errors caused by instruments and present in bands; the identification of errors related to the reading of bands; and the identification of errors associated with measurement units and the use of conversion factors. In addition, comparisons were made of extraterrestrial incoming solar radiation  $H_o$  (Peixoto and Oort, 1992) and potential or theoretical sunshine hours  $N$  according to latitude. The behavior of the parameters over time was also included, in order to identify jumps within the historical record. Questionable data were analyzed individually, including checks of the synoptic characteristics for a specific day. Outliers in the data for which there was not apparent explanation were disposed of in order to avoid errors in the analysis.

## 2.3 Methods

### 2.3.1 Spatial distribution of the atmospheric transmissivity coefficient $\tau$

The  $\tau$  (%) was calculated for all the weather stations considered in this paper using

$$\tau = \frac{H}{H_o} \times 100 \quad (1)$$

where  $H$  ( $\text{MJ m}^{-2} \text{ day}^{-1}$ ) is the measured incoming solar radiation,  $H_o$  ( $\text{MJ m}^{-2} \text{ day}^{-1}$ ) is the extraterrestrial incoming solar radiation (calculated as a function of the ratio between actual and mean sun–Earth distance, latitude, solar declination and solar angle at sunrise). These values were plotted onto a map of the topography of the area. To allow spatial analysis of this variable, lines joining points with equal values of  $\tau$  were plotted.



### 2.3.2 Model based on sunshine hours: Ångström-Prescott model

The Ångström-Prescott model is the most frequently used model to estimate the relative incoming solar radiation  $H/H_o$ , equivalent to the atmospheric transmissivity coefficient  $\tau$ . It is based on relative sunshine hours  $n/N$ . This equation suggested by Prescott (1940), is a modification of that proposed by Ångström (1924):

$$\frac{H}{H_o} = a + b \frac{n}{N} \quad (2)$$

where  $n$  is the number of effective sunshine hours measured with a heliograph and  $N$  is the potential or theoretical number of sunshine hours. The coefficients  $a$  and  $b$  are empirical; however, they have some physical explanation. The  $a + b$  value represents the maximum atmospheric transmission coefficient  $\tau$ , and  $a$  represents the minimum value of  $\tau$ .

Frère et al. (1975) proposed values of  $a = 0.29$  and  $b = 0.42$  as being applicable not only to Peru, but also to all the Andean highlands. These values were based on both the high rates of incoming solar radiation that occur as a result of the altitude of these zones and an annual mean of relative sunshine hours (taken to be around 50% as a general value). This idea was rejected for Peru by García (1994), who proposed the application of empirical coefficients at regional scales because of the different climatic conditions that prevail.

### 2.3.3 Model based on temperatures

According to Bristow and Campbell (1984), the size of the difference between daily maximum and minimum air temperatures depends on the Bowen ratio (i.e. the relationship between sensible heat and latent heat). Sensible heat depends on daily incoming solar radiation and is responsible for maximum air temperatures. At night, sensible heat is lost into space as long wave radiation; together with radiative fluxes, this results in a

decrease in air temperature until the daily minimum temperature is reached, usually just before sunrise. This physical explanation justifies the use of these kinds of models, with the advantage given by the use of a widespread network of weather stations that allow measurements to be made of daily extremes of temperature.

### 2.3.3.1 Bristow-Campbell model

Bristow and Campbell (1984) proposed a model with which to estimate relative incoming solar radiation as a function of the difference between maximum and minimum temperatures  $\Delta T$  ( $^{\circ}\text{C}$ ):

$$\frac{H}{H_o} = a_B [1 - \exp(-b_B \Delta T^{c_B})] \quad (3)$$

The empirical coefficients ( $a_B$ ,  $b_B$  and  $c_B$ ) have some physical explanation. The coefficient  $a_B$  represents the maximum value of  $\tau$ , is characteristic of a study area, and depends on pollution and elevation. The coefficients  $b_B$  ( $^{\circ}\text{C}^{-1}$ ) and  $c_B$  determine the effect of increments in  $\Delta T$  on the maximum value of the  $\tau$  (Meza and Varas, 2000).

### 2.3.3.2 Hargreaves model

Hargreaves and Samani (1982) proposed an empirical equation that took the form of a linear regression between the relative incoming solar radiation and the square root of  $\Delta T$ :

$$\frac{H}{H_o} = a_H + b_H \Delta T^{0.5} \quad (4)$$

### 2.3.3.3 Garcia model

The model described by Garcia (1994) is the only attempt made to estimate incoming solar radiation in Peru. The model is an adaptation of the Ångström-Prescott model:

$$\frac{H}{H_o} = a_G + b_G \frac{\Delta T}{N} \quad (5)$$

Using monthly estimates, Garcia (1994) proposed the following values:

- $a = 0.060$  and  $b = 0.640$  for the central coast;
- $a = 0.360$  and  $b = 0.211$  for the northern coast;
- $a = 0.457$  and  $b = 0.207$  for the central highlands;
- $a = 0.230$  and  $b = 0.380$  for the southern highlands.

### 2.3.4 Calibration and validation

To calibrate and validate the Ångström-Prescott model, historical records from each weather station were used for those periods in which parallel information on incoming solar radiation and sunshine hours were available. The values of  $H_o$  and  $N$  were calculated according to the day of the year and the latitude of each locality (Peixoto and Oort, 1992). The database was split into two parts. The first subset, 66% of the total data, was used to calibrate the model, using a linear regression analysis to find the empirical coefficients ( $a$  and  $b$ ) of the Ångström-Prescott model. The remaining data were used to validate the model. The adequacy of the model was assessed by calculating the Pearson product moment correlation coefficient  $r$ , relative error and mean-square error (MSE). Analyses of residuals, as well as normal plots, were used to identify possible inadequacies in the models or problems in the data.

To estimate incoming solar radiation using temperatures recorded on a daily basis, the models proposed by Garcia (1994), Hargreaves and Samani (1982), and Bristow-Campbell (1984) were tested in order to evaluate which was the best to apply to the study area. As in the previous case, all the available information for each location was split into two sets. It should be noted that the empirical coefficient  $a_B$  used in the Bristow-Campbell model was calculated as the sum of the empirical coefficients  $a$  and  $b$  found for the Ångström-Prescott model, since they share the same physical explanation. The statistical analyses performed to validate the model were similar to those described for the Ångström-Prescott model.

## 2.4 Results and discussion

### 2.4.1 Factors affecting the spatial distribution of $\tau$

Figure 2.2 shows an overview of climatic variability in Peru, using monthly values of maximum and minimum temperatures and precipitation, for the coast, the mountains and the jungle. However, within these zones, major variations occur that or caused by other climatic factors.

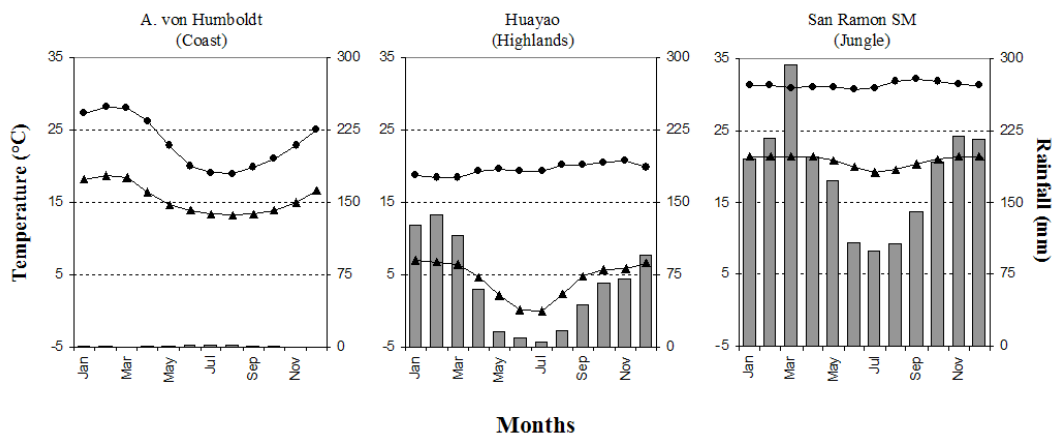


Fig. 2.2. Climatic differences in maximum temperature (●), minimum temperature (▲) and rainfall (■) for three weather stations representative of the coast, the highlands and the jungle of Peru.

Figure 2.3 shows lines connecting points with the same values of atmospheric transmissivity; these lines represent the variation in time and space of this variable. The lines corresponding to the minimum and maximum values of atmospheric transmissivity, i.e. 30% and 80%, occur on the central and southern arid coastal zones, respectively. However, monthly climate values, recorded at weather stations, reached 29% in August at Alexander von Humboldt and 85% in November at La Joya. The highest coefficient of variation was reached on the central arid coastal zone (17%), while the lowest value (4%) occurred on the northern arid coastal zone.

The South Pacific high anticyclone, the Andes mountain range and the Humboldt Current (cool water) affect the arid coastal zone. The effect of the latter decreases to the north of latitude 10°S, where it interacts with the warm water current of El Niño.

The subsidence layer caused by the South Pacific high results in the development of a strong temperature inversion over the coastal waters and the coastline. This layer may extend up to 110 km offshore (normally from 10 to 30 km), reaching heights of 1800 m a.s.l. and trapping stratus cloud, fog, mist, and light drizzle beneath it (Gilford et al., 1992). In July, the South Pacific high reaches its northernmost position, and the lowest sea-surface temperature occurs along the Pacific arid coastal zone. The conjunction of these two phenomena forms the very strong inversion layer, reducing  $\tau$  throughout the area due to the presence of clouds. However, the low-level jet stream named 'Paracas' (usually found below 600 m a.s.l., parallel to the coastline, between the latitudes of 13°S and 19°S), in combination with a sea breeze causes strong local winds that alter the moisture profile. This clears the atmosphere, thus increasing  $\tau$  in the southern coastal arid zone despite its low altitude.

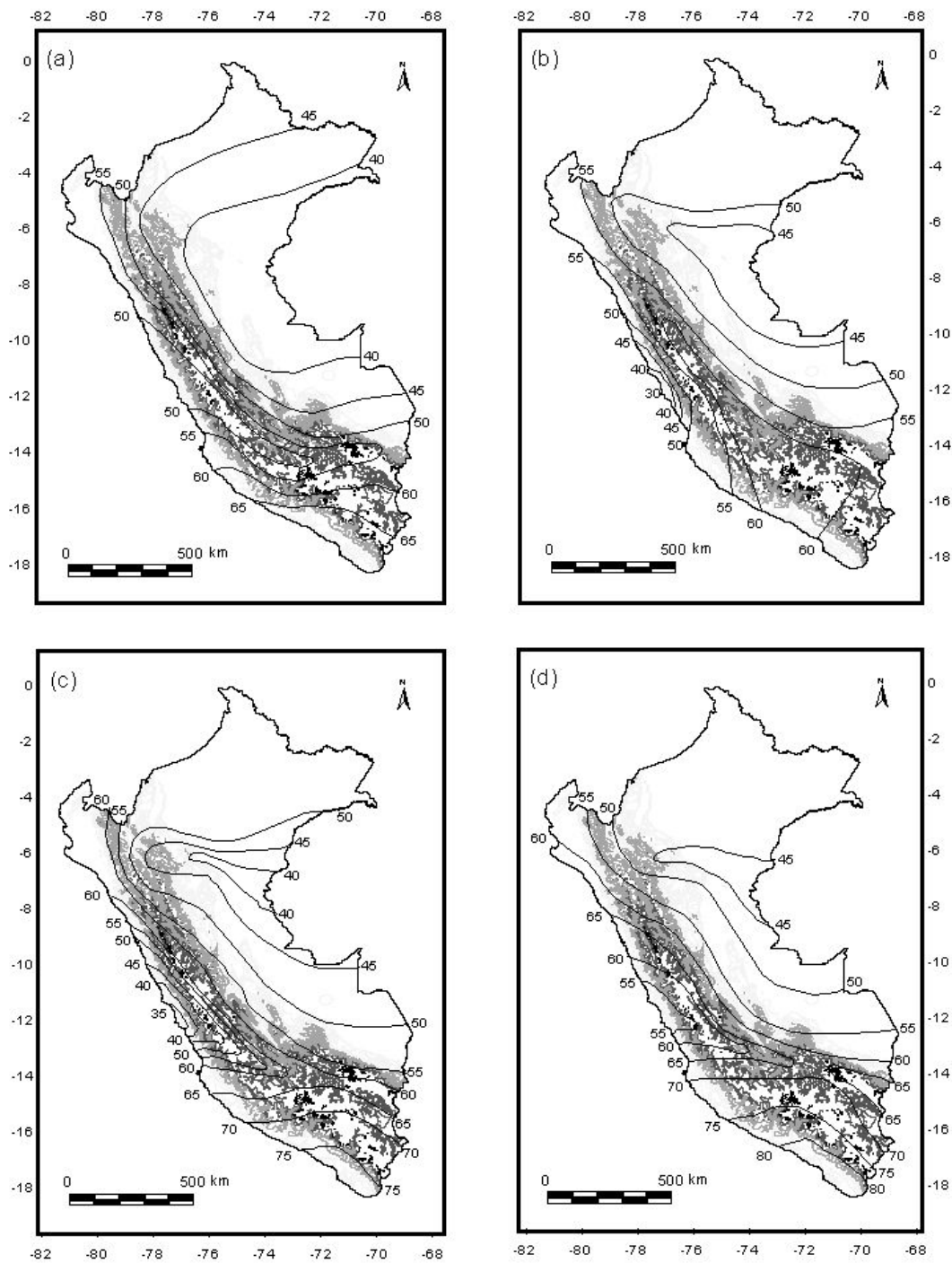


Fig. 2.3. Climate maps of atmospheric transmissivity (%) in different seasons in Peru: (a) March, (b) June, (c) September and (d) December. Latitude and longitude ( $^{\circ}$ ) are shown at the top or bottom and side respectively of each map.

In the northern arid coastal zone, the effect of the subsidence is lost as a result of the warm water current of El Niño and the large distance to the South Pacific high, which moves southwards from December to February. However, during these summer months, the southward movement of the near equatorial trough (NET) in the north of Peru does not lead to an increase in  $\tau$  on the northern arid coastal zone despite the mountainous terrain in northern South America, which breaks up the NET (Gilford et al., 1992).

Figure 2.3(a) to (d) are characterized by a gradient of  $\tau$  parallel to the Andes, as a result of altitude and topographic barrier effects over clouds and aerosols in the atmosphere. At higher altitudes in the mountains the atmospheric thickness is decreased, in turn decreasing the filter effects that govern incoming solar radiation. The mountains are also the major topographic barriers to weather systems and airflow below 2500 m a.s.l., thus preventing the regular exchange of air between the Pacific and Atlantic air masses. This leads to a difference in the atmospheric moisture content on both sides of the Andes, which is eventually expressed in the values of  $\tau$ .

Precipitation over the Andean High Plateau exhibits a pronounced annual cycle, with more than 70% of the rain being concentrated in the 2 to 3 month wet season that occurs during the austral summer (Aceituno and Montecinos, 1993). This wet season precipitation is also associated with the development of convective clouds over the Central Andes and the southwestern part of the Amazon Basin (Horel et al., 1989). Within this rainy season, the Andean High Plateau experiences both rainy and dry periods, which range between 5 and 10 days in duration (Aceituno and Montecinos, 1993). About 50% of the area is covered by cold clouds during the afternoons during these rainy episodes, whereas convective clouds are almost non-existent during the dry episodes (Garreaud, 1999). These observations explain both the occurrence of  $\tau$  values lower than 65% during the winter and the occurrence of rainfall during the summer, despite

the fact that in some areas the altitude is more than 4000 m a.s.l. However,  $\tau$  values that are higher than 75% can be reached during spring, due to the sun being positioned over the Southern Hemisphere and the cloud systems not yet being formed. The intense heating of the Andean High Plateau that occurs in the summer, as a result of the incoming solar radiation, forms the warm-cored, thermal anticyclone known as the Bolivian high. This is responsible for lifting and spreading moist, unstable, low-level Amazonian air over the central Andes, so governing  $\tau$ .

The distribution of  $\tau$ , over space and time, in the jungle zone corresponds to the cloud cover maps presented by Gilford et al. (1992). Characteristics of the dry season are a decrease in afternoon cloud cover and an increased number of clear days. This results in  $\tau$  being higher during the dry season than it is during the wet season.

**Table 2.3.** Values of the coefficients  $a$ ,  $b$  and  $r$  for the Ångström-Prešcott model, the total number of days of data  $n$  used in the estimation process, and the relative error and MSE found during the validation process.

Location	$a$	$b$	$r$	$n$	Error (%)	MSE $\times 10^{-4}$
<b>Coast</b>						
Miraflores	0.355	0.392	0.895	2454	-2.4	25
A. von Humboldt	0.211	0.467	0.892	8124	12.9	47
San Camilo	0.321	0.468	0.766	1494	-0.4	57
La Joya	0.593	0.181	0.781	7534	2.8	127
<b>Highlands</b>						
Bambamarca	0.322	0.336	0.803	1798	6.6	37
Weberbauer	0.231	0.521	0.883	1239	-2.7	40
Cosmos	0.320	0.384	0.826	619	7.4	39
Huayao	0.397	0.379	0.810	4190	2.2	51
Granja Kcayra	0.376	0.364	0.768	1466	3.4	65
Chuquibambilla	0.395	0.384	0.750	1261	-2.1	102
Puno	0.378	0.438	0.775	1870	9.2	72
Characato	0.367	0.396	0.656	813	10.7	94
<b>Jungle</b>						
San Ramon SM	0.301	0.377	0.803	1828	6.6	48
El Porvenir	0.278	0.320	0.792	1075	7.0	36
Bellavista	0.355	0.341	0.784	476	5.9	44



#### 2.4.2 Model based on sunshine hours

The results obtained from the process of validating the model based on sunshine hours, and the empirical coefficients for each weather station, are presented in Table 2.3. Figure 2.4 (a), (c), and (e) show observed versus estimated values from three representative weather stations. The empirical coefficients show high variation in terms of spatial distribution; this was also true for the values that occurred in the regions corresponding to the regions defined in the Garcia (1994) study. The relationships that exist between the relative sunshine hours and the empirical coefficients are not straightforward; this agrees with the findings of Frère et al. (1975). Therefore, it is very difficult to justify the use of a single set of empirical coefficients with regard to a vast region (country). This is especially true where there is a high diversity of ecological environments, as there is in Peru. A literature review undertaken by Martínez-Lozano et al. (1984), addresses the use of relationships between the two empirical coefficients and a number of individual variables (latitude, altitude, albedo, mean solar altitude, natural or artificial pollution and water vapor concentration). Glover and McCulloch (1958) related the coefficient  $a$  to latitude ( $\phi$ ), proposing the expression  $a = 0.01 + 0.27\cos\phi$ . Neuwirth (1980) proposed an equation relating both empirical coefficients to altitude using 19 weather stations in Austria. However, after many analyses, we concluded that the empirical coefficients found in Peru are related to neither latitude nor altitude. Climatic factors, mountain chains and sea currents, are the factors that determine the spatial distribution of incoming solar radiation.

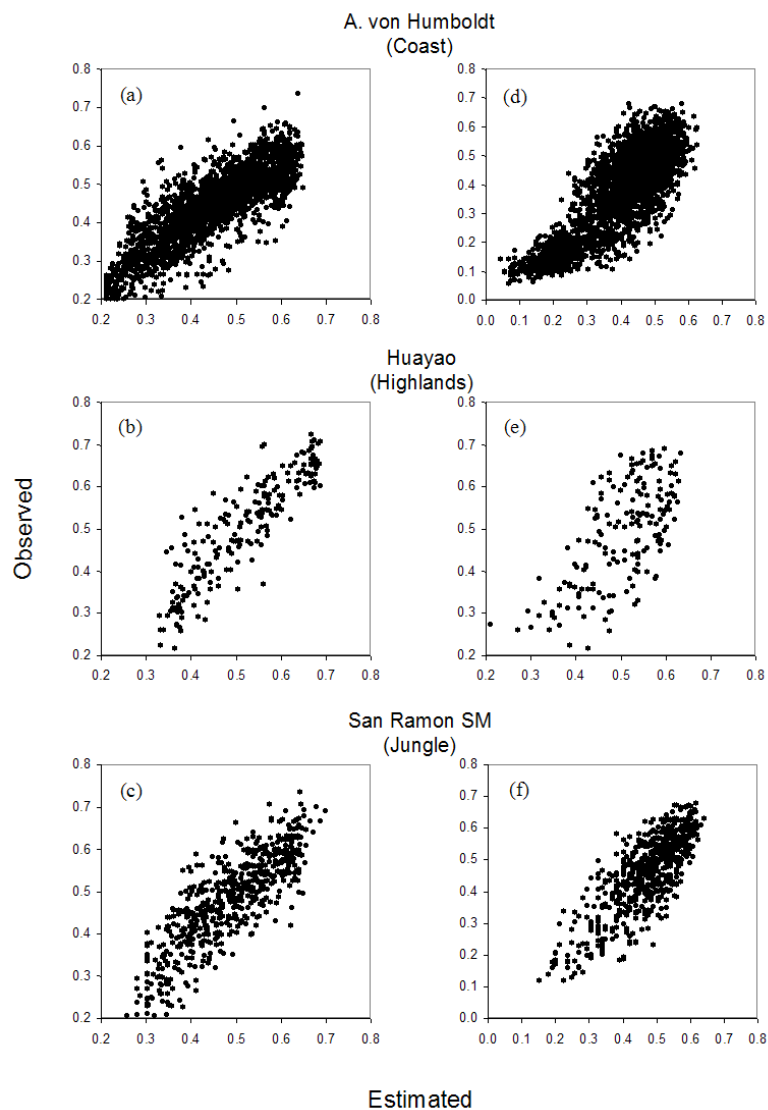


Fig. 2.4. Observed versus estimated data at the time of validation from three weather stations representative of the coast, the highlands, and the jungle of Peru. (a), (c), and (e) correspond to the validation of the Ångström-PreScott model, and (b), (d), and (f) correspond to the validation of the Bristow-Campbell model.

### 2.4.3 Models based on temperatures

Figure 2.5 shows an example of the relationship that exists between the daily relative incoming solar radiation and the difference between maximum and minimum temperatures for three weather stations: one on the coast, one in the highlands and one in the jungle of Peru. The trends shown in these graphs suggest that a meaningful relationship may exist between these two variables for different areas of the country.

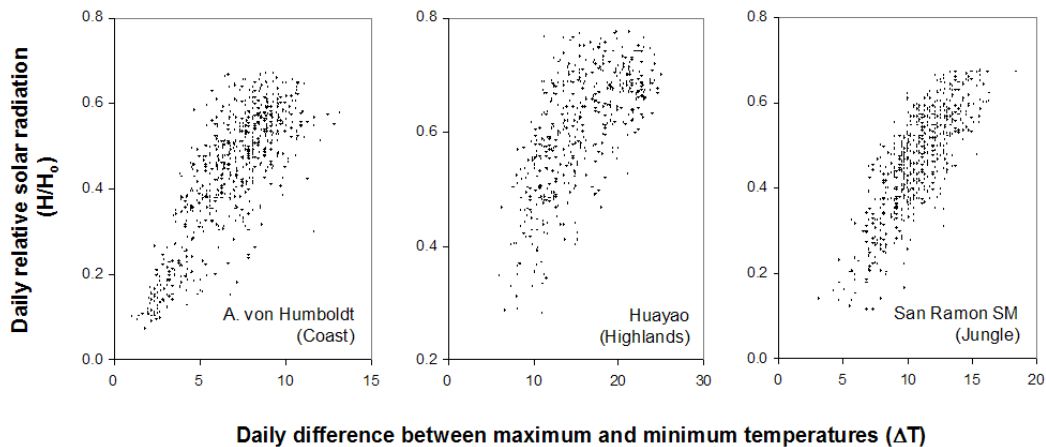


Fig. 2.5. Relationship between daily relative solar radiation  $H/H_0$  and daily difference between maximum and minimum temperatures  $\Delta T$  for three weather stations representative of the coast, the highlands and the jungle of Peru.

The values of the empirical coefficients found when calibrating the three evaluated models are presented in Table 2.4. Table 2.5 shows the correlation coefficient  $r$  for the relationship between the observed and estimated incoming solar radiation values obtained in the validation, and Figure 2.4 (b), (d), and (e) show this relationship for three representatives weather stations.

The Bristow-Campbell model showed the best fit for most of the localities in Peru (Table 2.5). The Hargreaves model gave similar correlation values. However, despite these high correlations, in areas where minimum temperatures are negative and values of  $\Delta T$  are low, the results obtained by using this model are strongly biased. This can be seen in the relative error and MSE of the locality of Cosmos in Table 2.5. In addition, the parameters determined by the Bristow-Campbell model have a better physical explanation.

With regard to data from weather stations in the highlands, coast and jungle, the worst cases found during the analysis of residuals are shown in Figure 2.6. In most of the cases, the residuals were randomly distributed around zero, with more than 95% of the data points falling within

the interval defined by  $e = \pm 2s$ , thus indicating the acceptability of the model used.

**Table 2.4.** Values of the empirical coefficients found in the calibration process and the total number of days of data used for each location.

Location	Models						n (days)	
	Garcia		Hargreaves		Bristow-Campbell			
	$a_G$	$b_G$ (h °C <sup>-1</sup> )	$a_H$	$b_H$ (°C <sup>-0.5</sup> )	$a_B$	$b_B$ (°C <sup>-1</sup> )		$c_B$
<b>Coast</b>								
Miraflores	0.200	0.395	-0.167	0.221	0.75	0.04	1.49	2398
A von Humboldt	0.074	0.571	-0.235	0.246	0.68	0.06	1.42	9141
San Camilo	0.463	0.120	0.075	0.138	0.79	0.09	1.05	1496
<b>Highlands</b>								
Bambamarca	0.294	0.233	0.117	0.118	0.66	0.23	0.80	1355
Weberbauer	0.187	0.259	-0.160	0.173	0.75	0.04	1.28	1071
Cosmos	0.088	0.486	-0.299	0.250	0.70	0.03	1.62	515
Huayao	0.390	0.170	0.121	0.123	0.78	0.11	0.97	3591
Granja Kcayra	0.363	0.137	0.102	0.110	0.74	0.11	0.92	1307
Chuquibambilla	0.471	0.106	0.239	0.089	0.78	0.19	0.76	984
Puno	0.467	0.178	0.192	0.133	0.82	0.20	0.87	1437
Characato	0.252	0.044	0.166	0.121	0.76	0.16	0.91	2089
<b>Jungle</b>								
San Ramon SM	0.045	0.466	-0.364	0.253	0.68	0.02	1.86	1909
El Porvenir	0.174	0.223	-0.110	0.148	0.60	0.06	1.21	1564
Bellavista	0.195	0.302	-0.105	0.175	0.70	0.06	1.22	692

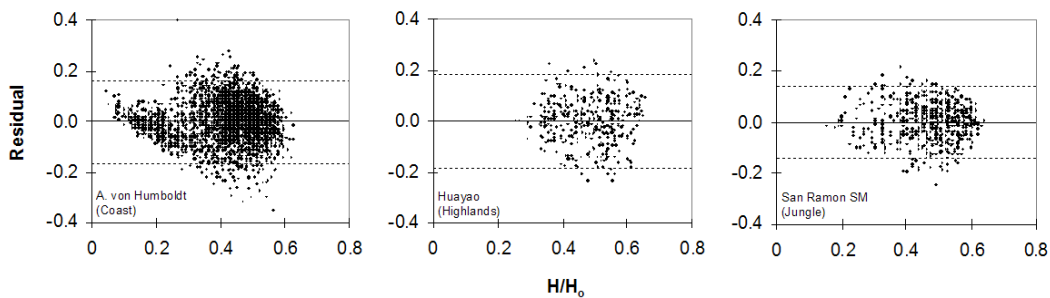


**Fig. 2.6.** Residual plots from three weather stations representative of the coast, the highlands and the jungle of Peru, at the time of validation of the Bristow-Campbell model.

**Table 2.5.** Comparison of three models, in terms of correlation coefficient, relative error and MSE, between observed and estimated incoming solar radiation at the time of validation; n is the number of days of data used.

Location	Garcia			Hargreaves			Bristow-Campbell			n
	r	Error (%)	MSE x10 <sup>-4</sup>	r	Error (%)	MSE x10 <sup>-4</sup>	r	Error (%)	MSE x10 <sup>-4</sup>	
<b>Coast</b>										
Miraflores	0.716	3	48	0.733	3	45	0.741	4	43	816
A von Humboldt	0.752	18	89	0.800	16	74	0.816	1	70	3108
San Camilo	0.280	3	90	0.471	2	76	0.445	4	74	509
<b>Highlands</b>										
Bambamarca	0.629	11	70	0.646	11	69	0.647	1	73	461
Weberbauer	0.621	5	84	0.676	2	81	0.666	3	82	365
Cosmos	0.716	10	81	0.732	452	40905	0.714	9	85	176
Huayao	0.592	5	76	0.664	3	65	0.649	5	64	1221
Granja Kcayra	0.525	12	98	0.585	10	83	0.587	1	84	445
Chuquibambilla	0.480	7	100	0.567	3	86	0.606	4	81	339
Puno	0.441	8	104	0.516	6	90	0.500	7	92	795
Characato	0.062	-47	972	0.245	5	80	0.379	8	81	711
<b>Jungle</b>										
San Ramon SM	0.792	8	55	0.799	7	54	0.802	8	54	650
El Porvenir	0.685	5	43	0.695	5	42	0.709	4	41	532
Bellavista	0.772	2	47	0.794	2	41	0.789	2	41	461

The normal plot (Figure 2.7) shows an s-shaped curve indicating the possibility of skewness in the distribution. The data from the jungle seems to be the most affected by a possible departure from normality.

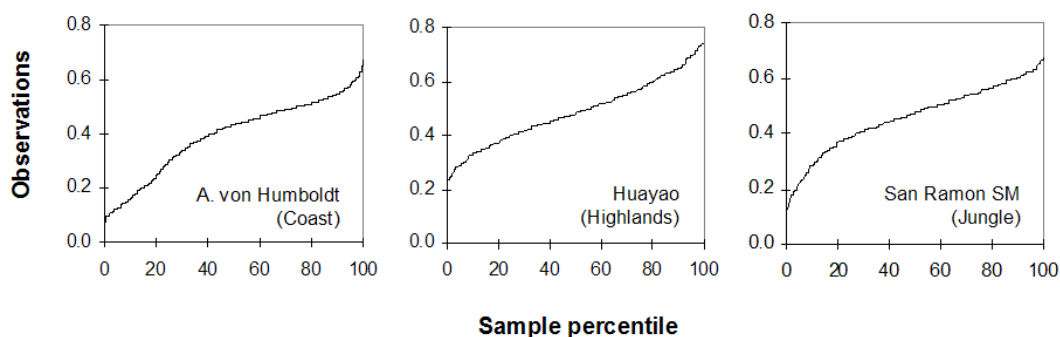


Fig. 2.7. Normal probability plots from three weather stations representative of the coast, the highlands and the jungle of Peru, at the time of validation of the Bristow-Campbell model.

Since the absolute values of the maximum and minimum temperatures, and the differences between them, are greatly influenced by topography, latitude and altitude, among other factors, the coefficients  $b_B$  and  $c_B$  proposed should be applied only in areas where similar thermal regimes prevail. Therefore, in order to increase the applicability of this work, empirical relationships were found which could be used to determine values of  $b_B$  and  $c_B$  as a function of  $\Delta T$  and latitude.

Figure 2.8 (a) shows the relationship between the coefficients  $b_B$  and  $c_B$  derived from the Bristow-Campbell model, while Figure 2.8 (b) and (c) show the relationship between the values presented in Table 2.4 and those estimated by Equations 6 and 7.

$$c_B = 2.116 - 0.072 \Delta T + 57.574 \exp(\phi) \quad (6)$$

$$b_B = 0.107 c_B^{-2.6485} \quad (7)$$

The validation analyses showed high residual values at Puno. This weather station is on the boundaries of the Titicaca Lake, which covers an area of 8300 km<sup>2</sup> and has a regulatory effect on the temperature of the surrounding area, preventing the occurrence of the extremely low minimum temperatures characteristic of high altitudes. This leads to a decrease in  $\Delta T$ , giving non-representative values when used to produce a generic equation. Therefore, this set of coefficients was eliminated when determining the parameters for Equation 6.

It should be noted that pyranometers are more accurate than actinographs when measuring incoming solar radiation. This could have affected the values of the empirical coefficients obtained for San Ramon SM, El Porvenir, Bambamarca, Bellavista and La Joya. However, there are no pyranometers at these places. Therefore, use of the information provided by actinographs constitutes the best approach available.

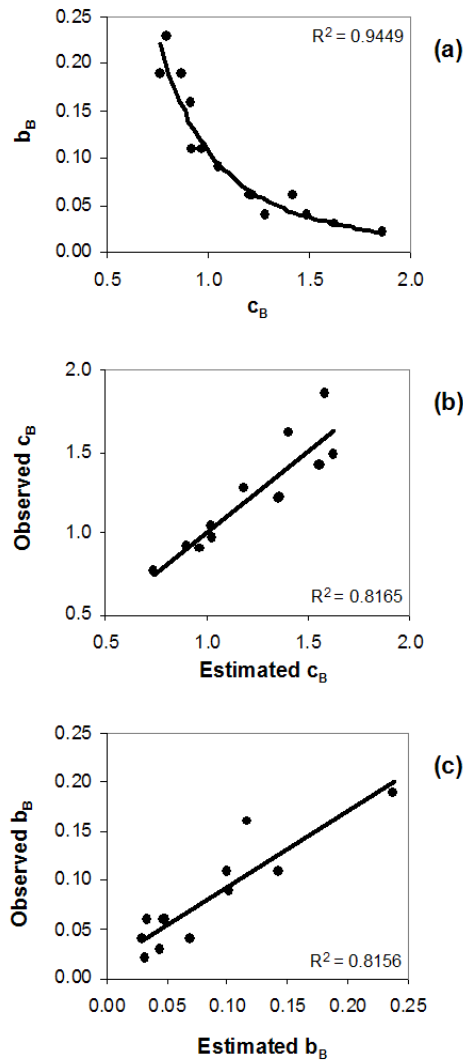


Fig. 2.8. Relationship between  $c_B$  and  $b_B$ , the empirical coefficients of the Bristow-Campbell model (a), and plots of observed versus estimated values for each of the coefficients:  $c_B$  (b) and  $b_B$  (c).

Applications of the present work are strongly related to areas around central Andes; however, because most of the new techniques based on radiative fluxes and/or satellite have still not been calibrated and validated for use in complex terrains like mountains, the empirical alternatives can be applied to other mountain chains around the world, using previously calibrated coefficients.

## 2.5 Conclusions

Many factors other than altitude affect, directly and/or indirectly, atmospheric transmissivity in complex terrains. The South Pacific high, the NET, the Bolivian high, low-level Jets, the Andes mountain range and the Humboldt and El Niño currents, both separately and when interacting, can modify the distribution of the incoming solar radiation in space and time. The interactions of all the above produce the widely differing scenarios of incoming solar radiation observed.

Using the Ångström-Prescott model, the spatial variation obtained for the values of empirical coefficients throughout the different regions of the country casts doubt upon the validity of applying only a single set. Owing to the higher correlation coefficients and the lower relative errors and MSEs obtained for the relationship between relative incoming solar radiation and relative sunshine hours, the empirical coefficients of the Ångström-Prescott model are recommended for use in the regions they represent.

Among the tested models used to estimate incoming solar radiation as a function of temperature, the Bristow-Campbell model is recommended as that most applicable to Peru.

The empirical relationships used to estimate incoming solar radiation based on relative sunshine hours demonstrated more accuracy than those based on temperature. Values of the empirical coefficients given here are on an annual basis. Their utilization for estimating incoming solar radiation must be done only on an annual basis.

## Acknowledgements

We would like to thank the Global Environment Facility (GEF) for funding this project (PER/98/G31 'Photovoltaic-based rural electrification in Peru') and the Ministry of Energy and Mines of Peru (DEP-MEM) for the



support it gave to the project. Special thanks are given to Eng. Emilio Mayorga.

Thanks are also due to the directors of SENAMHI for the facilities they extended to us in the development of the present work, and to the project's workgroup, the members of which contributed to the quality control process applied to the data. We would also like to thank Dr Jetse Stoorvogel, for the contributions made to the present paper, and the United States Agency for International Development (USAID), through its Soil Management Collaborative Research Program (SM-CRSP) financing the project 'Tradeoffs in Sustainable Agriculture and the Environment in the Andes: A Decision Support System for Policy Makers'. Last, but not least, the Consultative Group on International Agricultural Research–Libraries and Information Services Consortium (CGIAR-LIS) are thanked.



## Chapter 3

---

### **Interpolating minimum and maximum temperatures and incoming solar radiation in mountain areas**

In mountain areas, topography and the low water vapour content of the atmosphere due to the high altitude result in a high variability of microclimates over relatively short distances. In addition, scarcity of weather stations often restricts the accurate depiction of spatial variation in the weather. Geostatistical interpolation techniques have been applied to estimate meteorological variables but are unsuitable in complex terrain with a low number of observations. Here, we describe a process-based model for interpolating minimum and maximum temperatures. These temperatures are determined by atmospheric conditions as well as by terrain characteristics. Twice a day, net radiation is zero when maximum and minimum temperatures occur. These temperatures are measured at weather stations. Therefore, the atmospheric conditions estimated at these moments are known. These in combination with topographic characteristics derived from a Digital Elevation Model (DEM) were fed into a model that simulates minimum and maximum temperatures. The resolution of the resulting maps is controlled by the resolution of the DEM. Outputs from the interpolation are used as inputs into an empirical relationship used to estimate the daily total incoming solar radiation, based on the Bristow-Campbell model. A case study in La Encañada and Tambomayo watersheds (northern Andes, Peru) is presented. Validation entailed comparing the observed data from weather stations with the model-estimated data for the available points. Despite slight overestimation of the daily minimum and maximum temperatures and incoming solar radiation, the model performed very well in describing the spatial variation in weather conditions.

### 3.1 Introduction

Detailed meteorological data are becoming increasingly important as inputs for spatially explicit landscape in both regional and global models. Given the fact that weather stations are scarce in many areas, methods are required for the interpolation of weather data. The need for interpolation techniques is especially high in mountainous regions where weather stations are extremely sparse and weather conditions may vary greatly over short distances.

Geostatistical interpolation techniques have been applied to estimate meteorological variables at unsampled locations (Collins and Bolstad, 1996; Hartkamp et al., 1999). These include studies that compare the geostatistical techniques individually (Hartkamp et al., 1999; Wörten et al., 1999; Collins and Bolstad, 1996; Bonan, 1989), thus giving recommendations regarding the most suitable geostatistical technique for each climatic variable. Sometimes, different techniques are recommended for the same variable at different locations and under different conditions (for example dry and wet seasons). Therefore, it is difficult to determine *a priori* which geostatistical technique is most suitable for use when considering specific local conditions and variables. In addition, geostatistical techniques typically require a large number of observation points, often unavailable for weather data. Therefore, there is an urgent need for more generally applicable interpolation models.

In mountain areas, topography is a major factor determining the amount of solar energy incident at a location on the Earth's surface. Variability in elevation, slope, aspect, and shade can create strong local gradients in the incoming solar radiation that directly and indirectly affect such biophysical processes such as air and soil heating, energy and water balances, and primary production (Dubayah and Rich, 1995). When the variation in topography is known from Digital Elevation Models (DEM), the information provides a solid basis for the description of variation in weather conditions.

This paper describes a process-based model to interpolate maximum and minimum temperatures and incoming solar radiation. The model is based on processes capable of describing variation due to topographic parameters such as altitude, aspect, and slope, which are provided by a DEM.

### **3.2 Materials and methods**

#### **3.2.1 Data**

The study was undertaken in the La Encañada and Tambomayo watersheds (160 km<sup>2</sup>) located at south latitude 7°4', west longitude 78°16'. Altitude in the watersheds varies between 2950 meters and 4000 meters above sea level. The grid size of the DEM was 30 meters, in a grid of 628 columns by 482 rows (De la Cruz et al., 1999).

The area contained three weather stations. For the purpose of model validation, five additional (automatic) weather stations were installed in the study area in December 1999. Further information on location, and periods over which records were kept, is presented in Table 3.1. Basic statistics obtained from the three base weather stations and concerning climate characteristics are presented in Table 3.2.

**Table 3.1:** Weather stations in the La Encañada watershed.

Location	Latitude (°S)	Longitude (°W)	Elevation (m asl)	Historical record
Calvario	7°5.08'	78°20.59'	3250	1999-2001
Chacmapampa	7°5.38'	78°19.37'	3300	1999-2001
La Toma-Progreso	7°3.72'	78°16.92'	3590	1995-2001
Las Manzanas	7°7.08'	78°18.60'	3020	1995-2001
Paulino Rios	7°4.64'	78°19.90'	3250	1999-2001
Quinuamayo	7°3.31'	78°18.40'	3500	1999-2001
Sogoron Alto	7°4.21'	78°20.97'	3400	1999-2001
Usnio	7°5.34'	78°18.96'	3260	1983-2001

**Table 3.2:** Summary of climate data for the three weather stations used as reference.

Weather station	Incoming solar radiation (MJ m <sup>-2</sup> d <sup>-1</sup> )	Maximum temperature (°C)	Minimum temperature (°C)	Total rainfall (mm)
Las Manzanas	18.3	16.2	5.9	782.1
Usnio	19.2	14.2	6.1	717.3
La Toma	19.9	10.8	2.8	801.0

### 3.2.2 Model rationale

The interpolation procedure is based on the calculation of the atmospheric transmissivity coefficient ( $\tau$ ) and atmospheric irradiation ( $F_{LW}^{\downarrow}$ ) for those locations where actual weather conditions are measured. If the relationships between  $\tau$  and topographic conditions and also between  $F_{LW}^{\downarrow}$  and topographic conditions are known, we can calculate minimum and maximum temperatures as well as incoming solar radiation. Ideally, surface albedo is also known, though this was not the case for the study area.

Many atmospheric processes depend on the net flux of radiation at the earth's surface ( $F_{rad}^{sfc}$ ) resulting from a balance between the solar (short wave) and terrestrial (long wave) fluxes (Peixoto and Oort, 1992). Daily processes of warming and cooling depend on this balance, which is negative at night and positive during the day. Therefore,  $F_{rad}^{sfc}$  is at zero twice a day, when temperature extremes occur.

Estimations of short and long wave radiation balances are possible at weather stations. Total incoming direct ( $H_i$ ) and diffuse ( $h_i$ ) solar radiation (both in short wave) are measured by pyranometers. Net short wave radiation ( $F_{sw}$ ) can be estimated according to the surface albedo. The Stefan-Boltzmann Law is used to estimate long wave terrestrial radiation ( $F_{LW}^{\uparrow}$ ) using the surface temperature in the estimation. Given the fact that

$F_{rad}^{sc}$  is zero twice a day, when minimum and maximum temperatures occur,  $F_{LW}^{\downarrow}$  can be estimated precisely at these moments by a simple subtraction.

Subsequently, the minimum and maximum temperatures can be calculated for locations between weather stations using  $\tau$  and  $F_{LW}^{\downarrow}$  in combination with topography. The final outputs of minimum and maximum temperatures are used as inputs into the model to estimate incoming solar radiation. This is an empirical model proposed by Bristow and Campbell (1984). Previously, the model had been calibrated, validated, and evaluated in relation to Peruvian conditions (Chapter 2).

### 3.2.3 Mathematical structure of the model

#### 3.2.3.1 Calibration of atmospheric conditions

The Extraterrestrial Irradiation ( $H_o$ ) is the radiation intensity incident just outside the atmosphere and is calculated for each weather station using the following equation (Peixoto and Oort, 1992):

$$H_o = \frac{24}{\pi} S (dm/d)^2 \sin\phi \sin\delta (\rho - \tan\rho) \quad (1)$$

where  $S$  is the solar constant,  $(dm/d)^2$  is the square of the ratio between the medium ( $dm$ ) and actual ( $d$ ) earth-sun distance,  $\phi$  is the latitude,  $\delta$  is the solar declination, and  $\rho$  the hour angle at sunset and sunrise.

$H_i'$  is the incoming direct solar radiation incident on a sloping surface where  $\tau = 1$  and is estimated by Dubayah and Rich (1995) as:

$$H_i' = S(dm/d)^2 [\cos\theta_z \cos\beta + \sin\theta_z \sin\beta \cos(\gamma - a')] \quad (2)$$

where  $\theta_z$  is the zenith angle,  $\beta$  is the slope angle,  $\gamma$  is the azimuth angle, and  $a'$  the wall azimuth angle, which is merely the aspect of the slope from the south (Keith and Kreider, 1978).

It is important to consider that the effective horizon determines the amount of hours during which the sun can be seen from the slope. This means that the potential amount of direct irradiation received by the slope is determined not only by the slope, aspect, and angle of the receiving site but also by the landform opposing the slope.

The effective horizon was taken into account by calculating an obstruction constant ( $K_{obst}$ ) which relates  $H_o$  and the irradiation measured by pyranometers:

$$K_{obst} = \frac{\tau H_o}{(H_i + h_i)} \quad (3)$$

Finally, the effect of  $K_{obst}$  is included in equation (4) which calculates atmospheric transmissivity:

$$\tau = (\sec\theta_z - 1) \sqrt{\frac{H_o \cos\theta_z \cos\beta}{H_i}} \quad (4)$$

The value of  $\tau$  depends on clouds (both the amount and type) and other scattering components (dust, CO<sup>2</sup>, etc.). According to Lee (1978), a transmissivity coefficient of 0.9 is common for clear skies in mountainous areas. Values of  $\tau$  were estimated for each weather station.

The final objective was to apply the model for the purposes of interpolation. Because in mountain regions altitude differences are an important source of variation in transmissivity, a logarithmic function between altitude and  $\tau$  was estimated.

In order to fulfil the need for inputs to estimate the net radiation, the incoming direct ( $H_i$ ) and diffuse ( $h_i$ ) solar radiations at the surface level were calculated using equations (5) and (6). In this way, the effects of topographic parameters (such as slope and aspect) were included:

$$H_i = H_i' \tau^{\sec\theta_z} \quad (5)$$

Incoming diffuse solar radiation is given by (Hungerford et al., 1989):



$$h_i = h'_i \text{Cos}\left(\frac{\beta}{2}\right)^2 \quad (6)$$

where  $h'_i$  is the incoming diffuse solar radiation on a flat surface given using:

$$h'_i = \left[ (S \text{Cos}\theta_z)^2 \tau^{\text{Sec}\theta_z} \right]^{0.5} \left[ 1 - S \text{Cos}\theta_z \tau^{\text{Sec}\theta_z} \right]^{0.5} \quad (7)$$

To find the value of  $F_{LW}^\downarrow$  it was necessary to consider those moments, which occur twice a day, when  $F_{rad}^{sfc}$  is zero (when the extremes of temperatures occur). Minimum temperature occurs around an hour before sunrise; maximum temperature occurs two hours after noon (approximately). Having identified those moments,  $F_{LW}^\downarrow$  is estimated using the following equation:

$$F_{rad}^{sfc} = (H_i + h_i)(1 - \alpha) - F_{LW}^\uparrow + F_{LW}^\downarrow = 0 \quad (8)$$

where  $\alpha$  is the surface albedo.

Finally, values of  $F_{LW}^\downarrow$  were obtained for each weather station at the time of maximum and minimum temperatures. These values were used separately, to construct linear functions with the values of altitude according to a daily or monthly time step.

### 3.2.3.2 Model execution (interpolation)

To produce the final extreme temperature maps, topographical information ( $\phi$ ,  $\beta$ , aspect, and elevation) was derived from the DEM for each individual cell of the raster. Using the elevation values,  $\tau$  and  $F_{LW}^\downarrow$  were estimated cell by cell using the functions generated in the preceding step. Values of  $\phi$ ,  $\beta$  and aspect along with  $\tau$ , were used to estimate  $(H_i + h_i)$  at each cell level. Data on surface albedo were unavailable; therefore, it was assumed constant and estimated to be 0.11 for the entire

grid (Lenters and Cook, 1997). Cell values of  $F_{LW}^{\uparrow}$  were obtained by applying equation (8). Finally, maximum and minimum temperatures were derived from the Stefan-Boltzmann equation for the whole study area.

To estimate incoming solar radiation, the empirical relation proposed by Bristow and Campbell (1984) was applied. This model is expressed as:

$$(H_i + h_i) = H_o a_B \left[ 1 - \exp(-b_B \Delta T^{c_B}) \right] \quad (9)$$

where  $\Delta T$  is the difference between daily maximum and minimum temperatures ( $^{\circ}\text{C}$ ). The constants previously calculated by Baigorria et al. (2004) and specific to the study area were  $a_B = 0.75$ ,  $b_B = 0.04$ , ( $^{\circ}\text{C}^{-1}$ ) and  $c_B = 1$ .

### 3.2.3.3 Validation

#### a. Extreme temperatures

Daily maps of the minimum and maximum temperatures were produced for the year 2000 using the model. The minimum and maximum temperatures for the five weather stations that were available for validation were derived from these maps.

The average residual between the predicted and observed temperatures, standard deviation of the residual, relative error and correlation index (R) were analysed.

#### b. Incoming solar radiation

Because only the reference weather stations have pyranometer sensors in the study area, validation of the incoming solar radiation model was performed using only these points. Interpolated values of maximum and minimum temperatures were obtained from the output maps acquired in the previous step. These values were used to construct a daily database

that was then used to estimate the incoming solar radiation according to the Bristow-Campbell model, applying the coefficients proposed in Chapter 2. The estimated values were compared with the observed values for the three weather stations. The correlation index, relative error, and Mean Absolute Error (MAE) were analysed.

### **3.3 Results and discussion**

As an example of the results, daily maps of maximum and minimum temperatures, and incoming solar radiation, are presented for May 15<sup>th</sup> and November 15<sup>th</sup> in Figure 3.1. Statistical analyses are presented in Table 3.3. Comparisons between the observed and estimated minimum and maximum temperatures, and incoming solar radiation for each weather station are shown as scatter plots in Figures 3.2 and 3.3.

The model is a tool that can be used to interpolate maximum and minimum temperatures, as well as incoming solar radiation, integrating the capabilities of GIS. The model can also be applied to other places without prior calibration, due to self-calibration using the geographical information and databases provided by an existing DEM and weather station network.

To properly apply the model under conditions with a limited number of weather stations, all of them must represent climatically the study area. Weather stations need to be exposed to the same synoptic weather conditions in order to achieve the highest levels of accuracy. Because models are process-based, phenomena such as temperature inversions or frost events can be captured, avoiding the “bird’s eye” effect around the weather stations (Collins and Bolstad, 1996).

Visual analyses of the resulting maps allowed us to identify an error related to the DEM and the position of the weather stations. The pixel size used in the DEM of mountainous surfaces can cause homogenisation of areas by amalgamating different conditions (*i.e.* areas with steep slopes close to flat areas can be misrepresented by the use of an average slope

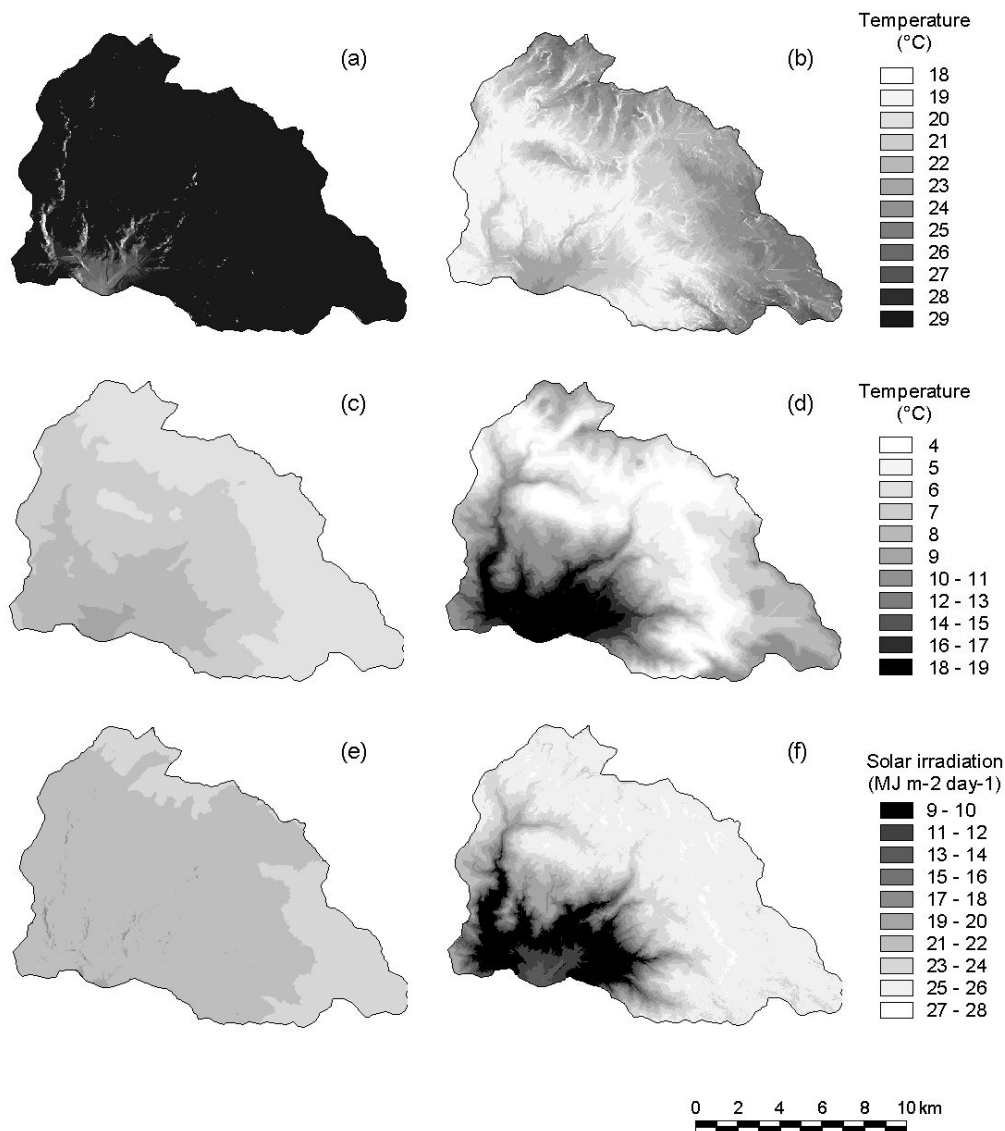


Fig. 3.1. Daily maps of the interpolated variables in La Encañada and Tambomayo watersheds. Maps (a), (c) and (e) correspond to maximum temperature, minimum temperature and incoming solar radiation on May 15<sup>th</sup> respectively. Maps (b), (d) and (f) correspond to the same variables on November 15<sup>th</sup>.

value in one pixel). This assumption leads to incorrect topographic information inputs in locations where the model makes its auto-calibrations. This error explains the fact that the highest values of MAE and median error were obtained at the control weather station of Quinuamayo at the time of the interpolation of maximum temperatures (Table 3.3). This was

due to its location in a narrow gorge. Wind is one factor that can strongly influence temperature, especially at the time of maximum temperatures. This phenomenon is due to the convective movements of air which occur close to the surface of the ground as a result of its warming. Consequently, turbulence breaks the boundary layers, mixing the air and introducing other processes. Knowledge of these processes allows the accurate explanation of maximum temperature behaviour (Rosenberg, 1974). However, to more easily apply the model and to allow a relatively small data set to be used, the accuracy obtained by the model is considered to be satisfactory.

The direct relationship extant between temperature and altitude is only shown when the vertical structure of the atmosphere is analysed but not when topography and land characteristics are taken into account. This is due to the effects that oceans and continents have on the atmosphere that diminishes with height (Peixoto and Oort, 1992). For this reason,

**Table 3.3:** Statistical analyses of minimum and maximum temperatures and incoming solar radiation (number of observations = 258).

<b>Weather station</b>	<b>Mean relative error (%)</b>	<b>Mean absolute error</b>	<b>Median error</b>	<b>Standard deviation of residuals</b>	<b>Correlation index</b>
<b>Minimum temperature</b>					
Calvario	-12.0	1.4	-0.6	1.6	0.74
Chacmapampa	-12.9	0.9	-0.5	1.1	0.86
Paulino Rios	-31.0	1.9	-1.9	0.8	0.89
Quinuamayo	-4.2	0.9	0.7	0.9	0.95
Sogoron Alto	-24.2	1.3	-1.2	0.8	0.86
<b>Maximum temperature</b>					
Calvario	12.2	1.7	1.7	0.9	0.91
Chacmapampa	-0.6	1.1	-0.2	1.3	0.74
Paulino Rios	0.2	0.9	-0.1	1.1	0.85
Quinuamayo	22.8	3.0	2.8	1.1	0.76
Sogoron Alto	2.6	0.6	0.3	0.7	0.92
<b>Incoming solar radiation</b>					
La Toma	-12.0	4.0	-3.2	3.8	0.82
Usnio	3.7	3.7	-0.1	4.4	0.72
Manzanas	10.4	4.1	1.1	4.7	0.63

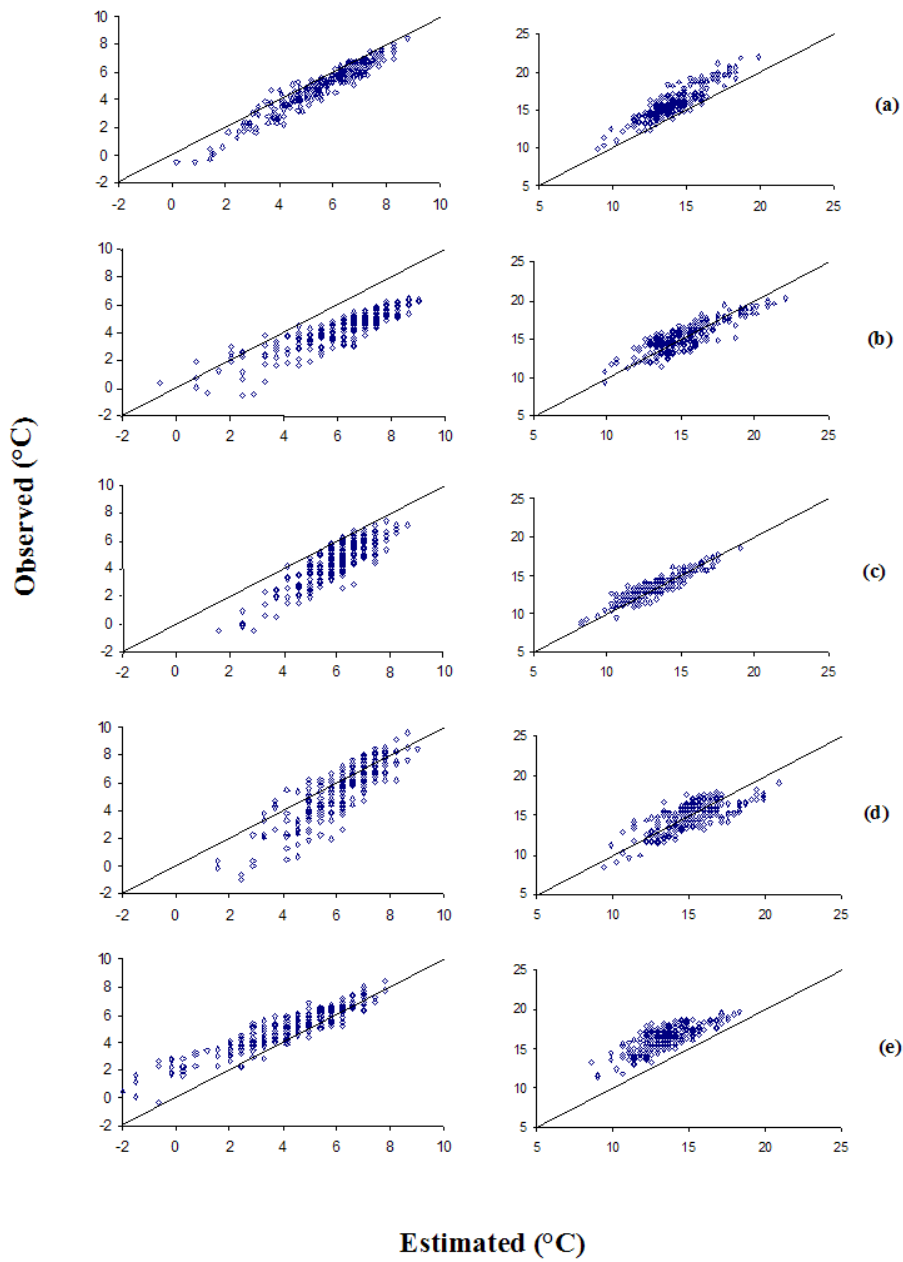


Fig. 3.2. Scatter plots of observed versus estimated data of minimum (left-hand column) and maximum (right-hand column) temperatures (°C) on a daily timestep. (a) Calvario, (b) Paulino Rios, (c) Sogoron Alto, (d) Chacmapampa and (e) Quinamayo.

Avissar and Mahrer (1988) demonstrated that topography is not clearly correlated with minimum temperature ( $r^2=0.13$ ), thus questioning the reliability of the isothermal lines procedures in a topo-climatologic survey (e.g. Avissar, 1993).

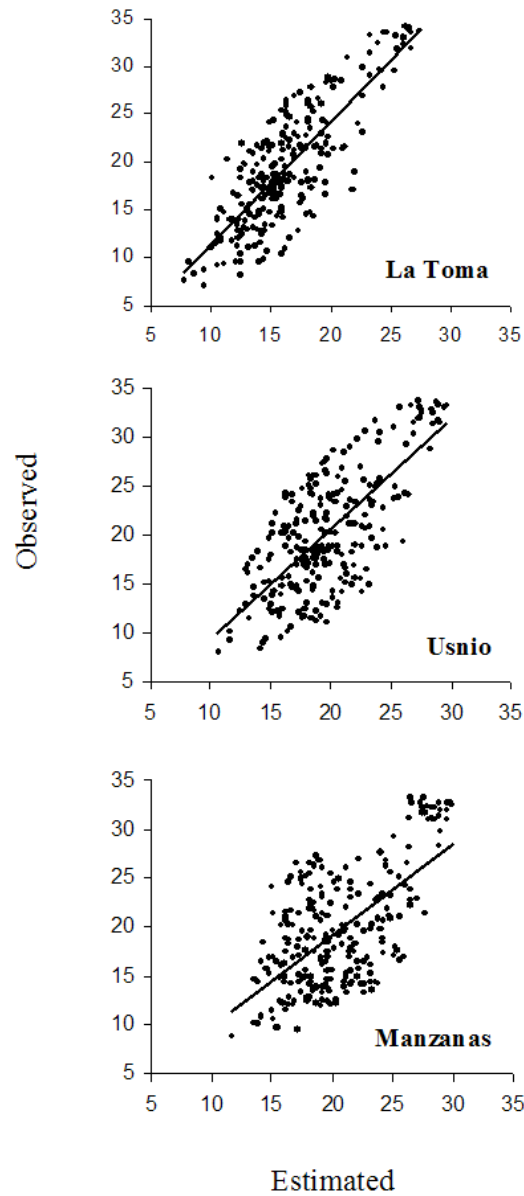


Fig. 3.3. Scatter plots of observed versus estimated data of incoming solar radiation ( $\text{MJ}\cdot\text{m}^{-2}\cdot\text{d}^{-1}$ ) on a daily timestep from the reference weather stations of La Toma, Usnio and Manzanillas.

In Table 3.3, MAE, median error, and standard deviation of the residuals are shown in order to analyse the residual values and also the residual distribution (Isaaks and Srivastava, 1989). The predicted and observed data were quite similar, as shown by the relationship between these datasets, which has a similar slope to the 1:1 line (Figure 3.2). The

offset of the predicted versus observed line was reflected in the values of the MAE and the median error.

Errors associated with the model result from both a lack of spatial variation in the albedo values, which are considered a constant in this study, and the logarithmic definition of the relationship between the transmissivity coefficient and altitude. Alternative definitions of this function should be tried for each day or month, giving more flexibility to the relationship, strongly influenced by the type and quantity of clouds. However, accuracy in terms of the results obtained can be improved using albedo grids provided by remote sensing or field surveys, as well as by improving the resolution of the DEM.

Another way of improving the model is through the addition of subroutines concerned with soil temperature estimations—in order to deal with the buffer effect that soil water content has on soil temperature. This means that it will be necessary to develop a rainfall model, in order to link both the rainfall and the water balance subroutines and generate a feedback process which produces data that have a distribution close to that of the real (observed) data.

The spatial validation of the incoming solar radiation outputs was not completely comprehensive because of the lack of pyranometers in the control weather stations. However, validation was conducted using independent databases of daily observations made at the three weather stations used for the interpolation. The correlation indexes obtained were statistically acceptable (Table 3.3). The relationship between observed and estimated incoming solar radiation is shown in Figure 3.3. The predictions made using the Bristow-Campbell model closely approximated the observed data. Incoming solar radiation results depend upon the accuracy with which the spatial distribution of minimum and maximum temperatures were calculated in the previous steps, as well as upon the empirical model used. If data on incoming solar radiation and daily minimum and maximum temperatures is available, it is recommended that a new set of empirical



coefficients be found for the Bristow-Campbell Model. Figure 3.1 (e and f) shows the effect topography has on the distribution of incoming solar radiation in the area under evaluation. A site-independent model, as suggested here, could replace incoming solar radiation subroutines. However, the aspect and slope of the area, as well as sun obstruction (the effective horizon), should always be taken into account.

### **3.4 Conclusions**

The model proposed here for the spatial interpolation of minimum and maximum temperatures performs very well describing spatial variation in complex terrain at daily and monthly intervals. Because it is based on a minimum data set and GIS, it can be applied to other places without a large number of weather stations or expertise in geostatistical techniques. The empirical incoming solar radiation model gives temporal accuracy when applied at spatial scales. However, it is important that the model be calibrated in regards to the empirical parameters relevant to different locations.

### **Acknowledgements**

The authors would like to thank Jorge de la Cruz for the technical assistance and advice he provided. Thanks are also due to ADEFOR for the support in making weather data available.

The present work is supported by the Grant # 291488 from USAID & Soil Management Collaborative Research Support Program (SM-CRSP)



## Chapter 4

---

### **Modeling the spatial distribution of rainfall in complex terrains based on the Digital Mountain Wave Model**

Rainfall has one of the highest spatio-temporal variabilities of all climatic variables. This is especially true in mountain areas, for which there is also a lack of data to cover large heterogeneous areas producing a large impact on the process of rainfall interpolation using geo-statistic. However, interpolation errors are not caused by the geo-statistical interpolation techniques themselves, but the inability of the point data to capture the high variability of this variable. Therefore, it is necessary to include additional information, such as topography, atmospheric circulation patterns and physical processes involved at the time of interpolation, since they directly affect the spatial distribution of rainfall. This paper describes the approach used to incorporate these variables into a rainfall interpolation model for complex terrain, in data-scarce environments requiring medium to high-resolution rainfall maps. For each wind direction, a Digital Mountain Wave Model (DMWM) was generated using topographic data provided by a Digital Elevation Model and the wind direction at the cloud level (provided by sequences of Infrared images from the GOES-8 satellite). The 8 DMWMs created (one for each of the eight main wind directions) describe the three-dimensional cloud-route over a mountainous area. These DMWMs, together with information from weather stations on daily rainfall and extreme temperatures, were used as inputs into the rainfall interpolation model. The model is based on the mountain waves and the atmospheric processes involved in the formation of rainfall. Results are presented as daily maps, in which resolution is controlled by the resolution of the DEM. The case study was done in La Encañada and Tambomayo watersheds in the Andean Highlands of Peru, using multi-year daily data provided by six automatic weather stations. Although simulations were performed at daily time steps; the cross-validation analysis to measure the accuracy of the model was performed at monthly steps. The model explained more than 85% of the variation observed in space and time. The whole model was implemented using user-friendly software.

Based on: Baigorria, G.A., R. Quiroz, C.C. Romero and J.J. Stoorvogel. Modeling the spatial distribution of rainfall in complex terrains based on the Digital Mountain Wave Model.

© Submitted. Journal of Hydrology. October 2003.

## 4.1 Introduction

Rain-fed agriculture constitutes around 85% of global agriculture (UNESCO, 2000). This percentage of agriculture dependent on rainfall rises to almost 100% when only those systems managed by resource-poor farmers are considered. Irrigated systems also depend on rainfall to replenish surface water resources or aquifers. Therefore, an understanding of the spatial distribution of rainfall is of paramount importance when judging the potential agricultural production of a region and—ultimately—the sustainability of agricultural production systems in a given area (Göbel et al., 1996).

In order to gather rainfall data across the area of interest, the ideal methodology entails on-site collection of near-surface meteorological data. However, as the size of the target area increases, this approach becomes prohibitively expensive (Thornton et al., 1997). There are two main alternatives usually used to estimate the spatial distribution of precipitation—geostatistical techniques and atmospheric modeling.

During the past decades, geostatistics have developed different interpolation techniques based on the spatial correlations between observations and later using correlations with different terrain attributes (Hevesi, 1992; Kyriakidis et al., 2001; Marquínez et al., 2003). However, in mountainous areas with a lack of both: weather stations and spatial representativeness, errors in the application of these techniques are frequent due to the inability of the point data to capture the high variability of the rainfall.

The use of atmospheric models based on physical and dynamic processes are an alternative. General circulation models (GCM) operating at large grids scales are limited to resolve small-scale distribution of orographic precipitation. Mesoscale models as well as models including orographically induced dynamics (Barros and Lettenmaier, 1993; Sinclair, 1994; Smith, 2003) need to be initialized from a large-scale numerical

model, radiosonde data, radar data and/or surface observations. These models require substantial amounts of input data, and even in developed countries where meteorological networks exist, the applications are not detailed enough to support decision making from watershed to farming levels.

Simulation of climatic variables across large areas demands an acceptable level of accuracy on one hand, and also the implementation of the minimum data set concept to assure cost effectiveness. The model described in this paper is intended to respond to both of these criteria. In addition to being designed to simulate rainfall and its spatial distribution, the model was also designed to generate data in the standard format used by crop growth models (IBSNAT, 1988 and Hunt et al., 2000) in order to simulate the spatial variability in crop production.

## **4.2 Background**

### **4.2.1 Formation of precipitation**

When unsaturated air is lifted, it cools at the thermodynamically determined rate of  $9.8^{\circ}\text{C km}^{-1}$ . This is known as the dry adiabatic lapse rate. Once the air becomes so cold that it can no longer maintain water as a vapor, the vapor condenses forming cloud droplets. The condensation process releases heat, which adds to the buoyancy of the air, causing it to rise more rapidly. However, because the air is now saturated, it cools at a slower rate, and this is referred to as the saturated adiabatic lapse rate ( $\gamma_s$ ) (Whiteman, 2000).

The mechanisms by which air is lifted, and which thus result in the condensation process are: (a) gradual air elevation over large areas associated with low pressure systems; (b) thermal convection (at the scale of local cumulus); (c) elevation by mechanical turbulence ('forced convection'); and (d), orographic lifting (Barry and Chorley, 1980).

#### 4.2.2 Spatial rainfall distribution

Rainfall typically presents a high spatio-temporal variability. In the case of flat areas (if weather stations are uniformly distributed and if rainfall measurements do not vary considerably around the mean) use of an arithmetic average can be an acceptable method for estimating the average rainfall received by an area (Chow et al., 1988). However, in mountain areas, the spatial distribution of rainfall exhibits high levels of variation due to the influence topography has on terrain-forced and convective airlifting mechanisms.

Rainfall distribution is affected not only by terrain height (Hevesi et al., 1992), but also by proximity to moisture sources, terrain relief, and aspect (i.e., the direction a slope is facing) relative to the direction of the approaching wind (Benichou and Le Breton, 1987a, 1987b; Daly et al., 1994; Göbel et al., 1996; Mellor, 1996; Whiteman, 2000; Marquínez et al., 2003). Kyriakidis et al. (2001) demonstrated that the empirical correlation of terrain characteristics and atmospheric variables as specific humidity integrated from 850 hPa to 1000 hPa levels and horizontal wind components at the 700 hPa levels, produces good descriptions of the spatial distribution of precipitation. However, extrapolation of this empiric model is restricted to data availability and previous calibration.

Maps showing the distribution of precipitation in mountainous areas are of limited value when detailed information about a particular site is needed, such as in the example of modeling processes such as crop growth or soil erosion. Therefore, it is necessary to include additional information such as topography and atmospheric circulation patterns at the time of interpolation in a more physical and dynamic manner.

#### 4.2.3 Circulation patterns and topography

It is obvious that there exists a close relationship between atmospheric circulation and climatic variables. Bürger (1958, cited by

Bardossy and Plate 1992) studied the relationships that exist between atmospheric circulation patterns and each of the three variables: temperature, rainfall, and cloudiness, using a time series from 1890 to 1950. A good correspondence between them was reported. Lamb (1977, cited in Bardossy and Plate, 1992), stated that even highly variable rainfall is strongly linked to atmospheric circulation. Hay et al. (1991) developed a daily rainfall model based on atmospheric circulation recorded at stations, which were widely spaced. It was found that the only link connecting different stations was the circulation pattern.

Topographic details are important because the steeper the underlying terrain, the higher the precipitation rate when air is forced directly up the slope (Whiteman, 2000). Surface roughness produces variation in the wind fluxes, and according to the amount of roughness, generates special air mass movements, such as mountain waves. These result in airlifting and condensation processes. Models based on the estimation of topographically forced vertical motions and advection to simulate orographic precipitation (Barros and Lettenmaier, 1993; Sinclair, 1994; Smith, 2003) better describe this kind of processes on a small scale.

Furthermore, airflow acceleration over the crest of barriers with steep and narrow upwind faces may displace the precipitation maximum to the lee side of the crest (Daly et al., 1994); this phenomenon may be related to the horizontal displacement of the mountain wave.

#### 4.2.4 Mountain waves

Mountain chains have an important effect on the airflows crossing them. Air is forced to rise in order to pass such obstacles, becoming cooler and denser than the surrounding air, and under the influence of gravity, sink on the lee side of the barrier. The air then overshoots, and oscillates about its equilibrium level, forming mountain waves (Barry and Chorley, 1980; Whiteman, 2000). During the lifting process, water vapor condenses

in the crests of the waves, so forming clouds across and downwind from the mountain barrier.

The amplitude of the waves depends on the initial displacement of the flow above its equilibrium position on the windward side of the mountain and is directly proportional to the height of the barrier (Queney, 1948). Wavelength is proportional to wind velocity and increases in value when air stability decreases.

### **4.3 Methodology**

#### 4.3.1 Study area and data sources

Analyses were based on data from the La Encañada and Tambomayo watersheds in Peru, corresponding to an area of 160 km<sup>2</sup>. These watersheds are located between 7°0'21"S and 7°8'2"S latitude, 78°11'22"W and 78°21'31"W longitude and are at between 2950 and 4000 m above sea level.

Time-series data were used for rainfall and maximum and minimum temperatures (Table 4.1). Data were obtained from two automatic weather stations and four portable temperature and rainfall micro-loggers similar to the ones described by Lookingbill and Urban (2003). The climatic data were converted to the '\*.wth' format, the standardized format advocated by Hunt et al. (2000). The advantage of using this format is that it is widely used by crop modelers.

Images from the geo-stationary GOES-8 satellite were downloaded from Internet. The movements of clouds, determined using images taken at three-hourly intervals, were used to estimate wind direction at the cloud level. This wind direction is different to the one measured at surface level in weather stations, which is usually modified by the roughness and complexity of the terrain. A vector containing the daily wind direction was



**Table 4.1.** Location of weather stations and annual values of the main climatic variables during the evaluated period of time (1999-2000).

Weather station	Latitude (°S)	Longitude (°W)	Altitude (m a.s.l.)	Temperature (°C)		Rainfall (mm)
				Maximum	Minimum	
Asunción F.	7° 5.38'	78° 19.37'	3300	25.2	8.4	668
Calvario	7° 5.08'	78° 20.59'	3250	25.0	9.0	514
La Toma	7° 3.72'	78° 16.92'	3590	25.2	5.1	468
Paulino Rios	7° 4.64'	78° 19.90'	3250	24.9	7.9	974
Sogorón	7° 4.21'	78° 20.97'	3400	24.7	6.4	720
Usnio	7° 5.34'	78° 18.96'	3260	24.7	7.4	546

archived in a file for further use. Topographic data was derived from a Digital Elevation Model (DEM) 1:50 000 with a pixel size of 90 m x 90 m (De la Cruz et al., 1999).

#### 4.3.2 Mountain Wave Model

A digital mountain wave model is a digital representation of the three-dimensional cloud-route determined by the interaction between topography and wind direction. The DMWM establishes a displacement surface by where the bottom of an air mass displaces following a predetermined wind direction. The vertical movements caused by the topography thus modify the initial physical condition of the air mass leading in an interpolation model of rainfall. To produce the DMWMs, the DEM values were read, line-by-line (Figure 4.1a), in a direction determined by the eight main wind directions (every 45°).

An individual mountain wave (Figure 4.1b) was described using the following sine function:

$$MW_{i,j,k} = \alpha_i \sin(\lambda_i D_j) \quad (\text{m}) \quad (1)$$

Where  $MW_{i,j,k}$  equals the altitude of an individual mountain wave over the pixel  $j$  if the referential pixel  $i$  is the only elevation in the sequence of the line  $k$ ,  $D$  is the distance between the pixels  $i$  and  $j$  within the same line  $k$ , and  $\alpha_i$  and  $\lambda_i$  are the dimensionless amplitude and wavelength respectively of the wave for pixel  $i$  (both are functions of the altitude ( $H$ ) of the pixel  $i$ ).

According to Equation 1, the mountain wave peak should be located right above pixel  $i$ . Thus, any shift in the peak is characterized by the angle ( $\delta$ ), formed by the projections of those lines connecting the ideal and the shifted peaks to a bisecting point in pixel  $i$  when the altitude is equal to zero (Figure 4.1c). This angle ( $\delta$ ) produces a horizontal displacement ( $\Delta$ ) in each individual mountain wave in the direction of the wind, modifying  $MW_{i,j,k}$  to  $MW_{i,(j+\Delta),k}$ . The  $\delta$  angle can be positive or negative depending on the altitude and shape of the mountain (Queney, 1948; Carruthers and Choularton, 1982). According to Queney (1948), for more complex terrains the airflow can be computed by superimposing elementary solutions. Thus, the uppermost portions of all the sine functions for each line  $k$  are then calculated as the highest value for each pixel  $i$ , producing a composite wave for the line  $k$  (Figure 4.1d).

$$EMW_{i,k} = \text{Max}_{i,k} |MW_{i,(j+\Delta),k}| \quad (2)$$

Finally, all the lines are aggregated spatially, producing the matrix called the Digital Mountain Wave Model:

$$DMWM = \begin{vmatrix} EMW_{1,1} & \dots & EMW_{i,1} \\ \dots & \dots & \dots \\ EMW_{1,k} & \dots & EMW_{i,k} \end{vmatrix} \quad (3)$$

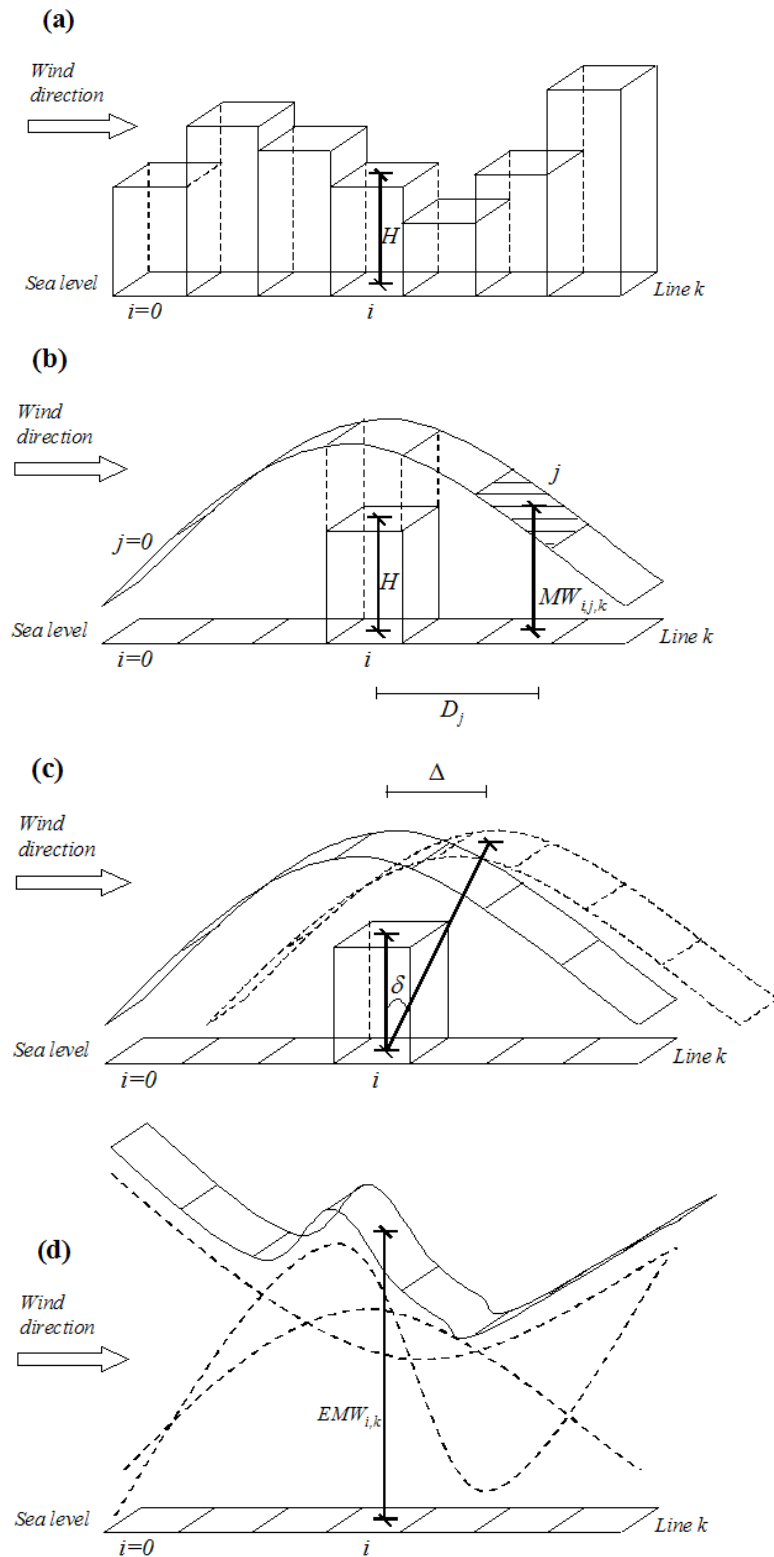


Fig. 4.1. Scheme representing generation of an individual mountain wave. (a) Pixel line isolation from the Digital Elevation Model (DEM), according to the wind direction. (b) Mountain wave generation, as a function of the altitude of only one pixel. (c) Horizontal displacement generated by angle  $\delta$ . (d) Composite wave.

The initial parameters  $\alpha$ ,  $\lambda$  and  $\delta$  were selected using an iterative procedure of different ranges of each parameter, assuring the smallest errors during the validation process. The values  $\alpha = 0.5$ ,  $\lambda = 1$  and  $\delta = 5^\circ$  were identified for the study area.

The analysis results in 8 DMWMs of which the rainfall model selects the most appropriate one according to the dominant wind direction on any specific simulation day.

#### 4.3.3 Rainfall interpolation model

The model assumes that the condensed water in the cloud falls immediately to the ground. However, approaches as those presented by Sinclair (1994) using formation time parameters, or Smith (2003) using time-delay functions between conversion of cloud water and its gravitational fallout, will be tested in future work.

The model was developed to function at daily basis, and the work comprised two consecutive steps: auto-calibration and the interpolation process *per se*. These steps are described below.

##### 4.3.3.1 Auto-calibration process

This process generates the initial conditions in the borderline of the grid every day when at least one weather station registers precipitation. The process begins by finding the pixels containing measured data and then using the information to characterize the atmospheric conditions through a backward tracking process, as conceptually described by Barros and Lettenmaier (1993). Four daily variables were obtained from each weather station: daily maximum temperature ( $^\circ\text{C}$ ), daily minimum temperature ( $^\circ\text{C}$ ), dew point ( $T_d, ^\circ\text{C}$ ), and rainfall (mm). The air temperature at surface level ( $T_{srf}$ ) was estimated as being the average of maximum and minimum temperatures ( $^\circ\text{C}$ ), and was in turn used to calculate the

saturation vapor pressure ( $e_s$ , hPa) using the Clausius-Clapeyron equation (Whiteman, 2000):

$$e_s = e_o \exp \left[ \frac{L}{R_v} \left( \frac{1}{T_o} - \frac{1}{T_{srf}} \right) \right] \quad (4)$$

Where,

$e_o$  = the saturation vapor pressure at  $T_o = 273^\circ\text{K}$ ,

$L$  = the latent heat of condensation of the water vapor,

$R_v$  = the gas constant for water vapor.

It is assumed that the air temperature at the bottom of the cloud equals the dew point at the surface level ( $T_{cld} = T_d$ ). Using these assumptions, the model estimates the actual vapor pressure ( $e$ , hPa) at the bottom of the cloud using the equation (5):

$$e = e_o \exp \left[ \frac{L}{R_v} \left( \frac{1}{T_o} - \frac{1}{T_d} \right) \right] \quad (5)$$

Temperature decline from the surface to the bottom of the cloud is thus estimated using:

$$\Delta T = T_{srf} - T_{cld} \quad (^\circ\text{C}) \quad (6)$$

Assuming a dry adiabatic lapse rate in the atmosphere under the cloud, and using the altitude of the weather stations ( $H$ , m) provided by the DEM, the altitude of the cloud ( $h$ , m) is estimated as (Peixoto and Oort, 1992):

$$h = \frac{\Delta T}{0.0065} + H \quad (7)$$

Under the assumption of hydrostatic conditions, the atmospheric pressure ( $P$ , hPa) at this level is estimated using:

$$P = 1014.78 \exp(-1.16852 \times 10^{-4} h) \quad (8)$$

The specific humidity ( $q$ ,  $\text{g g}^{-1}$ ), the potential temperature ( $\theta$ ,  $^{\circ}\text{C}$ ), and the equivalent potential temperature ( $\theta_e$ ,  $^{\circ}\text{C}$ ) are calculated as (Peixoto and Oort, 1992):

$$q = 0.622 \left( \frac{e}{P - 0.378e} \right) \quad (9)$$

$$\theta = T_{cld} \left( \frac{1000}{P} \right)^{R_d/C_p} \quad (10)$$

$$\theta_e = \theta \exp \left[ \frac{L q}{C_p (T_{cld} + 273^{\circ})} \right] \quad (11)$$

Where,

$R_d$  = the gas constant for dry air,

$C_p$  = the atmospheric specific heat at constant pressure.

$\theta_e$  = the potential temperature of an air parcel when all moisture is condensed, and the latent heat released is used to warm the parcel. Vertical variation in  $\theta_e$  is known as the saturated adiabatic lapse rate ( $\gamma_s$ ).

If data from the weather station has a rainfall datum that is not zero, the wind direction file is checked in order to find the altitude value of the backward tracking pixel from the DMWM ( $h_p$ ). From this backward tracked pixel, the difference in altitude is calculated as

$$\Delta h = h - h_p \quad (\text{m}) \quad (12)$$

Using  $\Delta h$  and  $\gamma_s$ , the temperature value for the backward tracked pixel ( $T_p$ ) is calculated using

$$T_p = T_{cld} - (\gamma_s \Delta h) \quad (^{\circ}\text{C}) \quad (13)$$

In addition, a new set of parameter values for this backward tracking pixel is calculated replacing  $h$  by  $h_p$  in the equations (8) to (11).

This vertical movement is responsible for the rainfall amount ( $PP$ ) over the pixels where the weather stations are located. This rainfall is an integration of the loss in specific humidity between these two points:

$$\Delta q = q - q_p \quad (\text{g g}^{-1}) \quad (14)$$

We assume wind velocity is uniform in space and in time, thus the model does not require an estimation of horizontal or vertical wind speed. Notwithstanding these wind velocities are important in the drop forming process, they are more related to the rainfall intensity. By assuming a constant velocity only the total amount of rainfall is estimated, which is the objective of the model.

Since water has a density equal to  $1 \text{ g cm}^{-3}$ , it is possible to express the rainfall values in  $\text{g}$  ( $1 \text{ mm} = 1000 \text{ g of water m}^{-2}$ ). Because the specific humidity is directly related to the amount of rainfall, the weight of the parcel ( $PW_m$ ) that produces rainfall can be calculated as:

$$PW_m = \frac{PP}{\Delta q} \quad (\text{kg of moist air m}^{-2}) \quad (15)$$

The value of  $PW_m$  is maintained as constant, and a backward  $PP$  calculation process is initiated. The model calculates  $PP$ , starting from the pixel where the weather station is located to the first line of the DMWM raster matrix (borderline pixel) and moving in the opposite direction with respect to the wind (Figure 4.2a and 4.2b).

#### 4.3.3.2 Interpolation process

Once the sets of values from all weather stations are projected onto the borderline pixels, the interpolation process is initiated. The values of the required parameters for all the pixels in the borderline are calculated first. The entire DMWM matrix, in the direction of the wind follows this process.

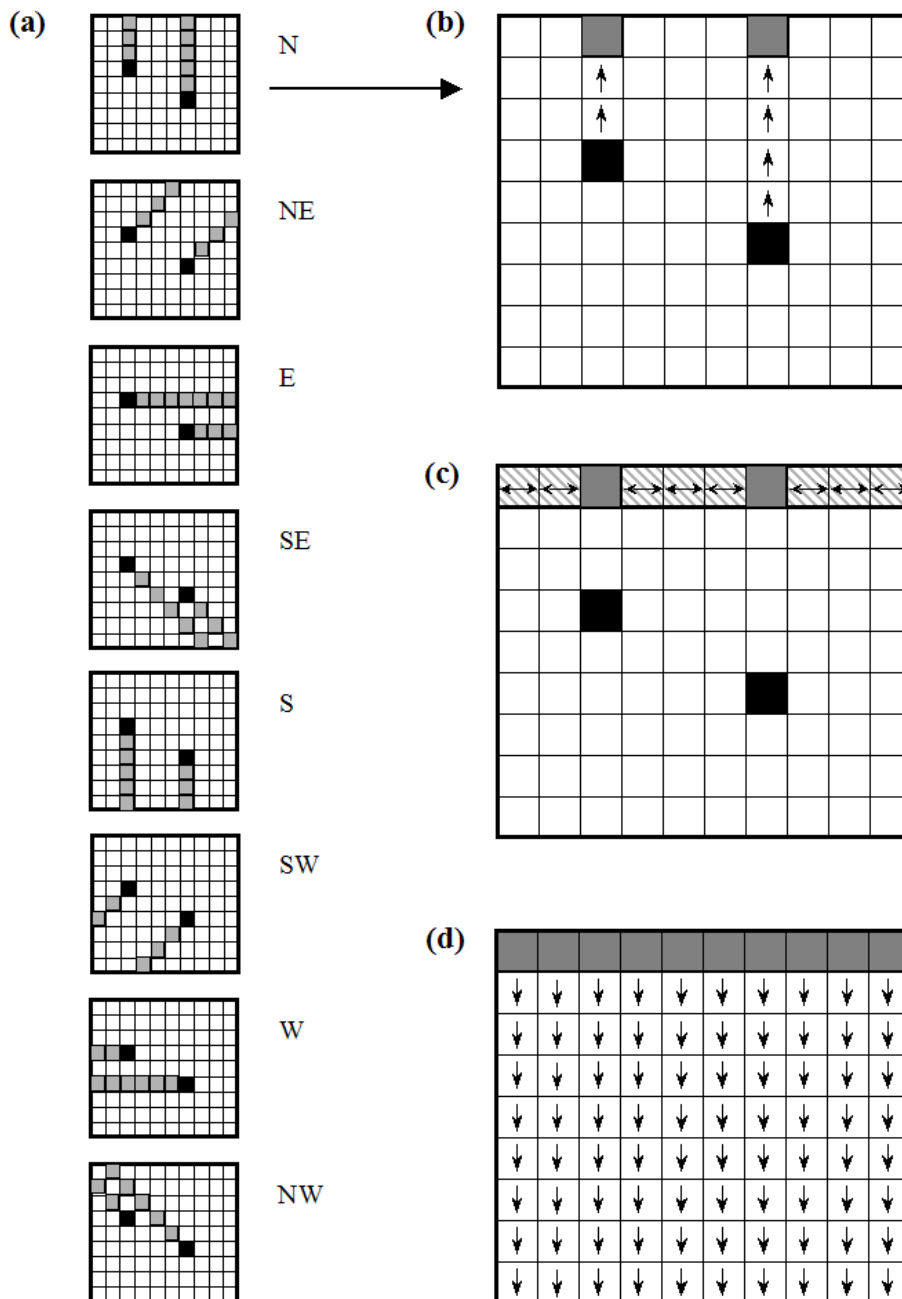


Fig. 4.2. Sequence of diagrams showing propagation of information from weather stations, represented in the grid as black pixels. (a) Directions of the backward tracking, according to the wind direction. (b) Direction of the auto-calibration process using winds from the north. (c) Interpolation within the borderline of the grid. (d) Interpolation within the entire grid of the study area.



a. Interpolation within the borderline of the grid

In the borderline of the grid (Figure 4.2c), there are five variables that need to be interpolated:  $T$ ,  $T_d$ ,  $h$ ,  $\gamma_s$ , and  $PW_m$ . The vertical gradient of temperature is calculated for each interval ( $i$ ) of available data as:

$$\left(\frac{\partial T}{\partial h}\right)_i = \left(\frac{T_{i+1} - T_i}{h_{i+1} - h_i}\right) \quad (\text{°C m}^{-1}) \quad (16)$$

In those pixels for which information is lacking, temperature is estimated using the following equation:

$$T = T_i + (Z - Z_i) \left(\frac{\partial T}{\partial h}\right)_i \quad (17)$$

Where,

$T$  = the estimated temperature in the interpolated pixel,

$T_i$  = the temperature at the beginning of the interval  $i$ ,

$Z$  and  $Z_i$  = the altitudes corresponding to these pixels.

In regards to the pixels for which there is no information, the altitude of the cloud ( $h$ ) and the weight of the parcel that produces rainfall ( $PW_m$ ) are estimated as a linear function of the altitude. The coefficients  $a$  and  $b$  for both equations are estimated using the information available in the borderline of the grid from the weather stations. The saturated adiabatic lapse rate ( $\gamma_s$ ) is also estimated as a linear function; however, in this case, the air pressure was estimated using equation (8).

Important issues in the interpolation process include the following: estimated  $T_d$  must be less than or equal to  $T$ ; and  $\gamma_s$  must be less than or equal to  $9.8 \text{ (°C km}^{-1}\text{)}$ .

b. Interpolation within the entire grid of the study area

Once the parameters for the borderline are generated, the program initiates a pixel-by-pixel interpolation for the entire DMWM matrix, following the direction of the winds (Figure 4.2d). The process is repeated daily during the pre-defined interpolation time. A 3 x 3 smoothing filter is applied to the discrete values to generate a continuous rainfall distribution.

#### 4.3.4 Validation

A cross-validation analysis was performed to assess the accuracy of the rainfall interpolation across space and time. Daily maps of a complete year were generated six times. In each run, data from one weather station was withdrawn from the calculation of the initial parameters. The data from the removed weather station were used to cross-validate the interpolation results. In order to facilitate the presentation of results, the interpolated daily results were aggregated into monthly maps. Regression analysis and regression diagnostic techniques (Rawlings, 1988) were used to assess the accuracy of the interpolation at monthly level.

## 4.4 Results and Discussion

### 4.4.1 Software

Version 2.1 of the Climate Interpolator software, programmed in Delphi, has been recently released. The software integrates all the components described in the methodology section, and also provides both numerical and map outputs.

#### 4.4.2 The Digital Mountain Wave Model (DMWM)

A visual representation of the DMWM is shown in Figure 4.3. The DEM and the wind direction are the main modifiers of the wave. The figure shows the shape of the DEM, the wind direction, and examples of how the interaction of these components might modify the appearance of the DMWM.

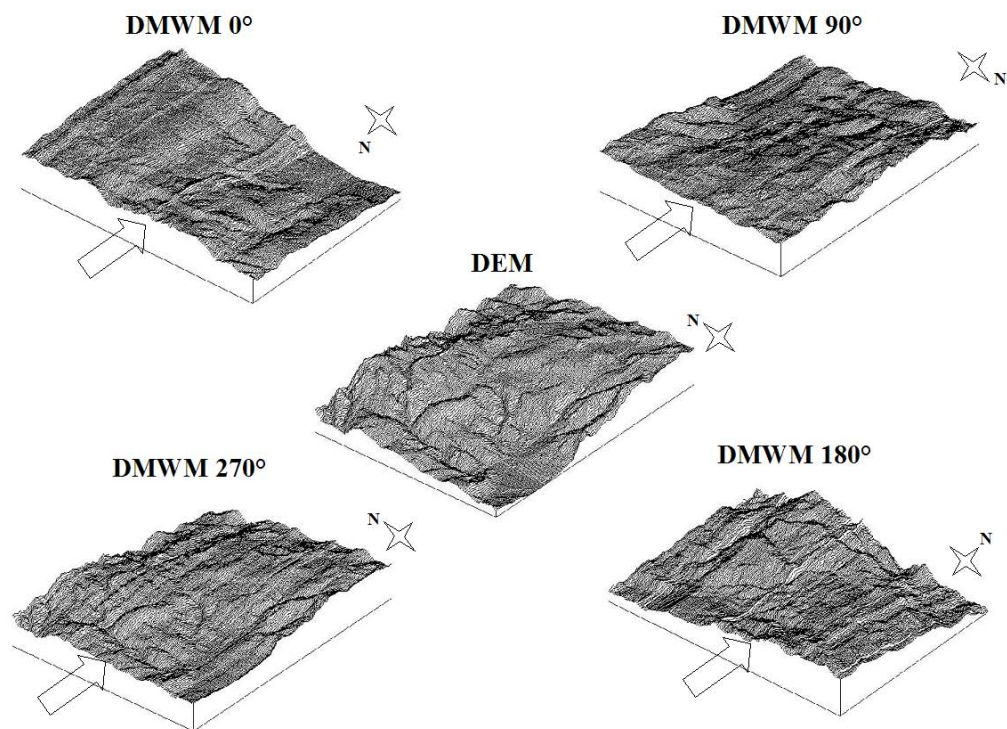


Fig. 4.3. Digital Elevation Model (DEM) and four Digital Mountain Wave Models (DMWMs) corresponding to wind directions of 0°, 90°, 180° and 270°.

Figure 4.4 shows the effect of the wave amplitude ( $\alpha$ ) on the DMWM. Two wind directions and three amplitudes are represented. The interactions between wind direction and amplitude are evident. The two other parameters – the wavelength ( $\lambda$ ) and peak shift ( $\delta$ ) – modify the DMWM and help determine rainfall distribution, particularly when the topography is highly irregular. So, for instance,  $\lambda$  smoothes the zones with

large altitude gradients thus providing a more accurate rainfall distribution across space. On the other hand,  $\delta$  allows the model to accurately simulate rainfall on the lee side of the crest.

The DMWM can be conceptualized as a smoothed projection of the DEM, modified by altitude, terrain roughness, slope, aspect, and wind direction. In this manner, it appears to be a better predictor of rainfall distribution than altitude alone. This phenomenon is shown by Daly et al. (1994), who demonstrated that the DEM was a better predictor of year-round rainfall than the altitude of the weather station.

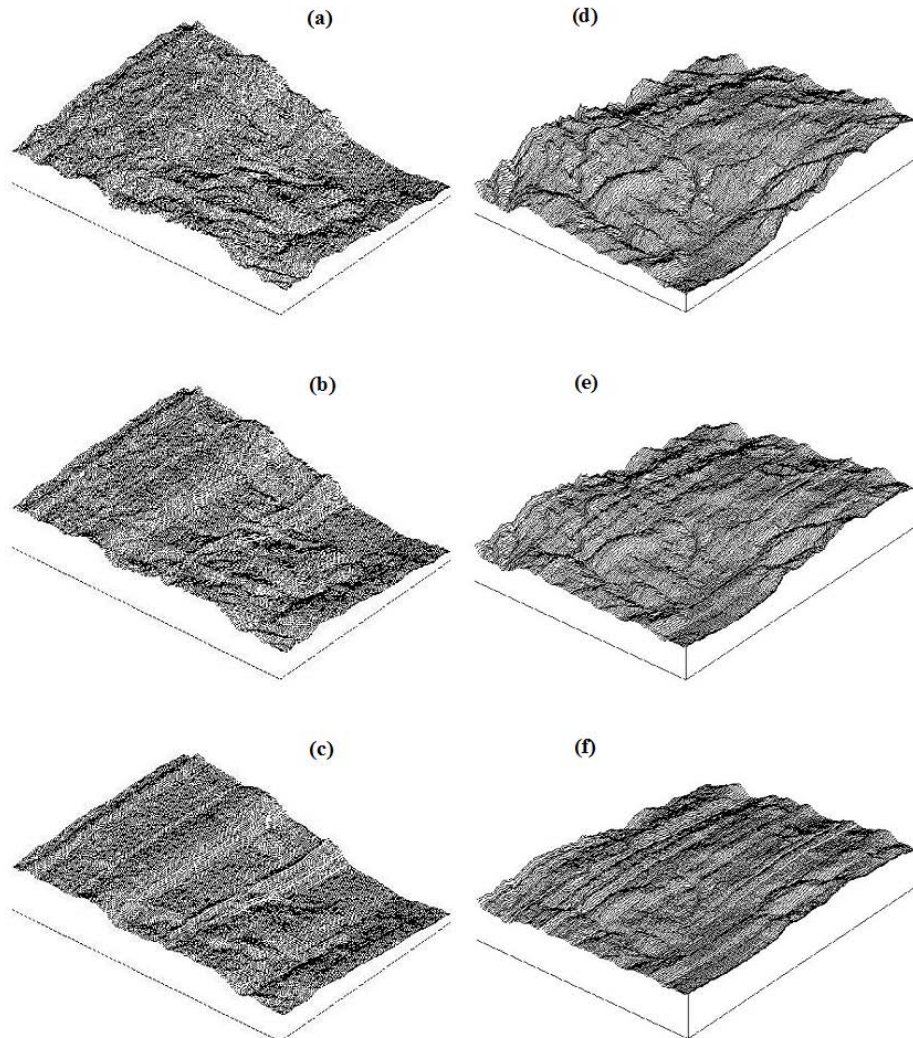


Fig. 4.4. Effect of changing the amplitude values in the DMWM: (a), (b) and (c) correspond to a DMWM of 0° with amplitudes of 0.25, 0.5 and 1.0 respectively; (d), (e) and (f) correspond to the same amplitude values for a DMWM of 270°.

#### 4.4.3. Rainfall interpolation

The variation in interpolated rainfall explained around 90% of the variation in measured rainfall in weather stations omitted in the validation exercise throughout a year (Figure 4.5). The deviations of the observations from the regression line were randomly distributed around zero, suggesting that there is no heterogeneity of variance. This finding is in agreement with the linear trend depicted in the half normal plot. As a result of the cross validation, Table 4.2 shows for each weather station the bias, median absolute error (MAE), and the coefficients of determination ( $R^2$ ) between observed and estimated rainfall aggregated monthly. The model underestimates the monthly aggregated rainfall with a maximum of 37 and 36 mm, corresponding to the weather stations of 'Paulino Rios' and 'Sogorón', respectively. Both weather stations have the highest annual rainfall among the stations used in the study (Table 4.1). Due to the scarce amount of weather stations in the study area, it was impossible to perform an autocorrelation analysis of the residuals to determine the spatial dependency of the model outcomes (Anselin and Griffith, 1988; Overmars et al., 2003). Potentially users could correct the model results for the total rainfall quantity.

**Table 4.2.** Bias, MAE and coefficient of determination between observed and estimated monthly rainfall after the cross-validation to each weather station.

Weather station	Bias	MAE	$R^2$
Asuncion F.	-15.3	16.0	0.936
Calvario	-6.0	15.3	0.910
La Toma	-11.3	14.6	0.861
Paulino Rios	-36.7	36.7	0.947
Sogorón	-35.6	36.9	0.713
Usnio	-13.8	18.2	0.666

The results of daily interpolations across the study area were aggregated to obtain the annual rainfall map. This process was repeated for five years. The average of these five years is shown in Figure 4.6. The first noteworthy aspect is the absence of a direct dependency between the DEM and the spatial distribution of rainfall: more rainfall at higher altitudes. Intermediate to large amounts of rainfall are ubiquitous distributed throughout the area, regardless of the altitude. The second noteworthy aspect is that no “bubble effect” (Hartkamp et al., 1999) was observed around the weather stations that provided the initial parameters for the model. This finding has at least two implications: first, it shows that the model does not bias the interpolation to “privileged” areas around the weather stations; second, it shows that the model is robust enough to make interpolations with a small number of initial parameters.

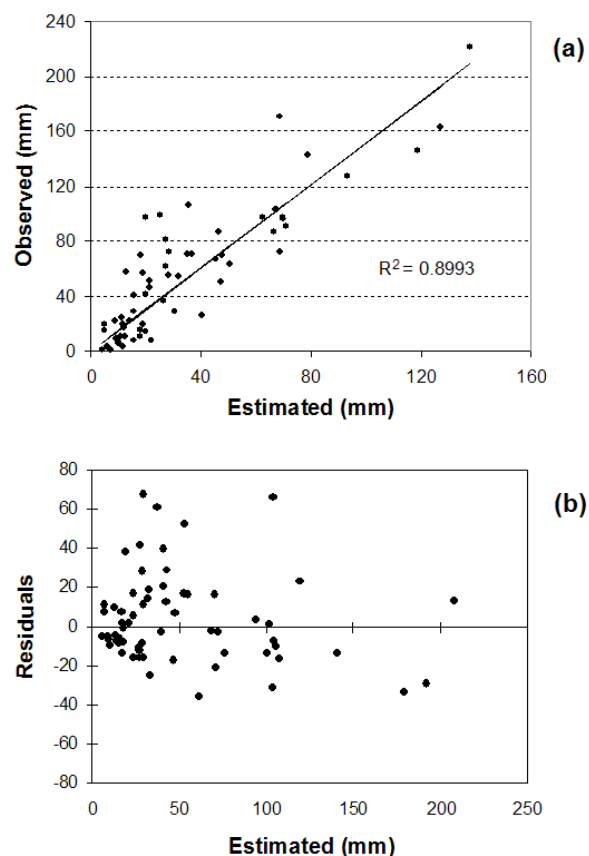


Fig. 4.5. Model validation through (a) observed versus estimated rainfall values, aggregated at monthly levels and (b) residuals analysis.

Despite the altitude decrease crossing the topographic division of one mountain in a mountain chain, the DMWM avoid the cloud decay or even increase in altitude because it can be influenced by the next individual mountain wave. As reported by Barros and Lettenmaier (1993), in moderately high and narrow mountains, this produces the intensification of preexisting precipitation. In contrast to other models, clouds do not follow the topography strictly, but they follow the different DMWM according to the wind direction. This phenomenon explains why rainfall does not decrease as soon as the topography division is reached. Therefore, the role of down slope regions in drying the air just crossing the crest (Barros and Lettenmaier, 1993) can be displaced or disappeared, according to the main wind direction (already included) and wind speed through the modification of  $\alpha$ ,  $\lambda$  and  $\delta$  at daily steps. Implementing this feature in the model is a logical refinement to improve the accuracy of the interpolated data. Although this improvement will enhance the capability of testing the impact of the DEM's resolution on the parameters  $\alpha$ ,  $\lambda$  and  $\delta$  and thus on the size and shape of the topography barriers, the demand of data might limit its use in data-scarce environments. The tradeoff between accuracy and data demand is critical for the target population, mountain environments in developing countries.

In terms of scale, we emphasize that in larger regions the wind fluxes are more complicated than in small ones where wind directions almost cross the area in only one direction. Therefore, a more complex approach of the DMWM must be applied to larger regions.

Areas with the highest estimated annual rainfall are clustered around the areas of the highest reported annual rainfall in the study region. In addition, when the interpolated data was analyzed using a daily time step, areas of high concentrations of rainfall were found to be related to the higher elevation parts of the DMWM and to windward faces of the mountains.

It is important to emphasize that data quality and quantity from weather stations are essential in the application of the described model. As a feedback, the model can be used to optimize the location of the weather stations, producing a network that really represents a study area so improving the function and effectiveness of each weather station.

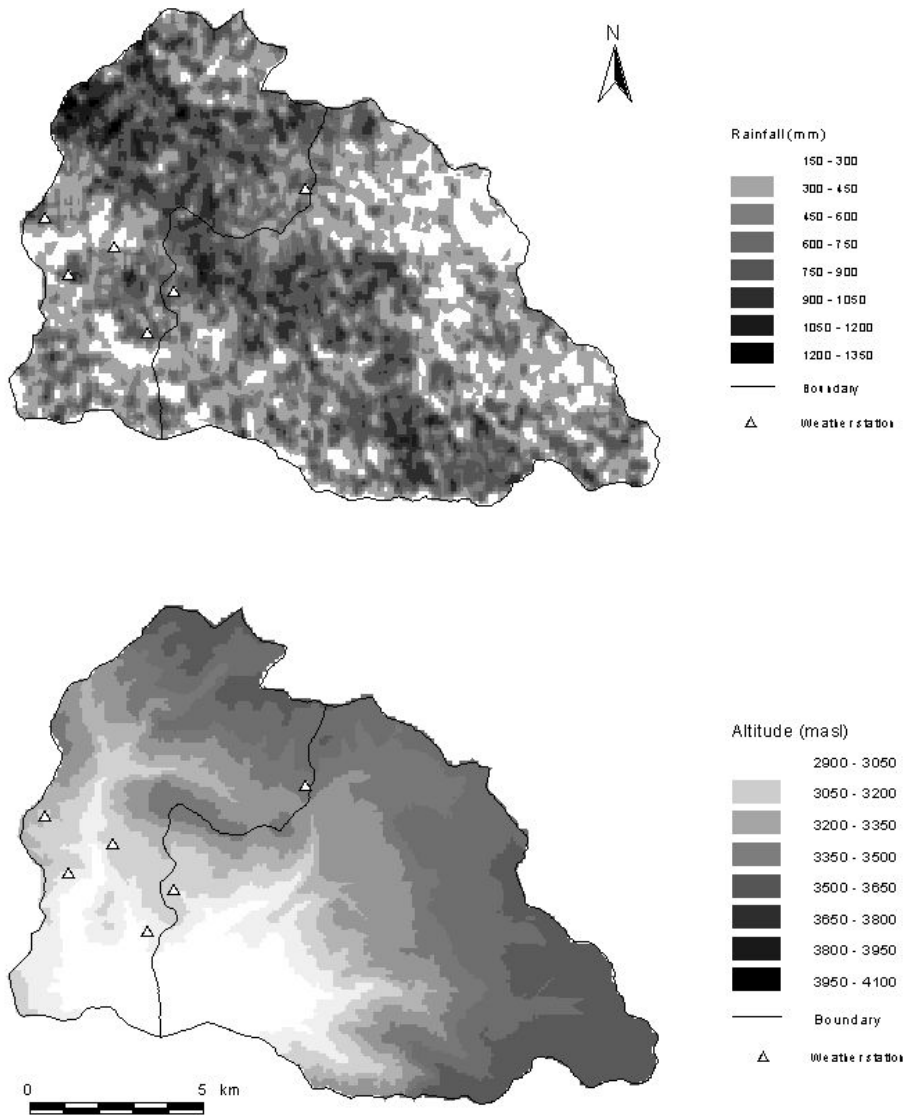


Fig. 4.4. Interpolated Rainfall Map in La Encañada and Tambomayo Watersheds (aggregated at an annual level) and the Map of Elevation.



#### **4.5 Conclusions**

The climate interpolation model described in this paper adequately simulated the spatial distribution of rainfall throughout a year. Up to 90% of the variation in the observed rainfall was explained by the interpolated data. Nonetheless, the model constantly underestimated the actual data by about 6 mm per month. The model could be improved by taking into account the variation over time of the  $\alpha$ ,  $\lambda$  and  $\delta$  parameters of the mountain waves. Each rainfall event should be considered as unique, and these parameters should be considered to be functions of wind speed. However, such improvement also increases the demand for input, thus requiring a re-assessment of the cost effectiveness of the model.

#### **Acknowledgements**

The authors acknowledge the constructive criticism of the two anonymous reviewers and the editor in chief. Their important inputs to this paper made it understandable and updated. The Grant # 291488 from USAID through its Soil Management Collaborative Research Program (SM-CRSP) supported the present work, financing the project 'Tradeoffs in Sustainable Agriculture and the Environment in the Andes: A Decision Support System for Policy Makers'.



## Chapter 5

---

### **Weather and seasonal-climate forecasts to support agricultural decision-making at different spatial and temporal scales**

Agricultural decisions deal with environmental impacts, investments, crop rotations, and day-to-day management decisions. These decisions are made within the context of available information in terms of *e.g.* natural resources, prices, and weather. In this paper, we discuss the need for weather and climatic data to support strategic, tactical, and operational decisions for a case study in the Peruvian Andes. Farmers base their decisions on risk experiences and their own weather and seasonal-climate forecast systems. Formal weather and seasonal-climate forecasts are used in only a small number of cases due to inadequate spatial scales and the lack of training to interpret the formal forecasting. This chapter analyzes the importance of the different sources of weather and seasonal-climate forecasts in current decision-making and the possibility of increasing its use following more quantitative and mechanistic approaches. Field workshops revealed information about (a) land allocation, planting dates, and fertilization rates; (b) local indicators for weather and seasonal-climate forecasts; (c) driving factors behind management decisions; and (d) current use of formal forecasts. In addition, climate forecasts produced by Global Circulation Models (GCM) were translated to the level of the weather stations in the watersheds using multiple regression models and weather generators. This weather data, together with soil maps, served as input in crop growth simulation models for potato (SUBSTOR) and cereals (CERES) to illustrate the use of the data in terms of yield forecasting. Maps of potato, wheat, and barley growth using two levels of N-fertilizer under the optimal planting-dates were produced for the 2003-2004 cropping season. The use of different sources of yield forecast at adequate spatial and temporal scales along with appropriate training is discussed as a tool to support agricultural decision-making for different stakeholders in the study area located in the northern Andean Highlands of Peru.

## 5.1 Introduction

Agricultural decisions deal with environmental impacts, investments, crop rotations, plant responses, and day-to-day management decisions. These decisions are made within the context of available information in terms of natural resources, prices, and weather. In this paper, the need for weather and climatic data to support agriculture at different levels (from farmer to policy maker) is investigated for a case study in the Peruvian Andes. Andean farmers plant their fields (usually under different agro-ecological conditions) before and during the initial months of the rainy season, avoiding planting all their fields on a specific date or with the same crop. This traditional technique reduces climatic risks that occur as a result of the high inter-annual climate variability and also assures a minimum production for self-consumption during years of poor production. Farmers make decisions according to their expectation and based on previous experiences of risk and have developed their own systems for weather and seasonal-climate forecast, based on meteorological and astronomical phenomena as well as biological behavior of wild species. However, these indicators are more related to operational decisions which include when to apply agro-chemicals, rather than tactical and strategic decisions (Bouma et al., 1999) such as what, when, where, and how to plant and crop. Although formal weather and seasonal-climate forecasts are available from the Peruvian National Service of Meteorology and Hydrology, these are used only in a few cases, due to the inadequate spatial resolution and the lack of training to interpret them properly. Similarly, extension offices and erosion control institutes, such as the National Service for Soil Conservation (PRONAMACHCS), provide general-purpose recommendations without using weather forecasts.

Historic weather data, as well as forecasts, can be used to evaluate different management options to support strategic and tactical decisions. For instance, a seasonal-climate forecast can support the application of tools such as crop and environmental simulation models by institutes to

provide refined recommendations for tactical decisions such as what, when, and how to crop. In addition, these forecasts enable institutes to evaluate dynamically the environmental impact of agricultural management and to take actions against environmental degradation. In this paper, we evaluate the use of weather and seasonal-climate forecasts for different decisions by farmers and institutions from three perspectives: 1) How are forecasts currently being used? 2) Can we downscale the forecasts to a scale appropriate for farmers and local institutions? and 3) What is the potential use of weather and climatic forecasts? An example of the latter may be the translation of a seasonal-climate forecast from Global Circulation Models (GCM) into a map with optimal planting dates for different crops. This requires downscaling the forecasts and applying crop growth simulation models to evaluate the impact of expected weather conditions and crop management on crop yields. These models give an extra value to the seasonal-climate forecast, making available this kind of information in appropriate agricultural terms to stakeholders not deeply involved in climatology.

The study focuses on two watersheds in the Northern Andean Highlands of Peru located at 7°4' Southern latitude and 78°16' Western longitude, at an elevation between 2950 meters and 4000 meters above sea level. The year can be subdivided into two main climatic regimes representing the rainy and dry season. Annual rainfall distribution in the watersheds is related to the Inter-Tropical Convergence Zone (ITZ) and has an inter-annual rainfall deep and intensity distribution affected by *El Niño* and *La Niña* phenomena (Romero, 2005).

Soils in the area are classified as Entisols, Inceptisols, and Mollisols following the Soil Taxonomy (USDA-NRCS, 1998). Romero and Stroosnijder (2001) determined that 35% of the area has a slope gradient steeper than 15% and slopes steeper than 65% can occur. Agriculture is dominated by pastures (31% of the area). Crop-land includes the cultivation of a number of Andean roots and tubers (e.g. potato, oca, and olluco),

wheat, barley, and natural and improved pastures (Tapia, 1995). Most commercial crops are planted under rain-fed conditions before the beginning of the rainy season (September), although it depends on the availability of water, seeds, crop varieties, the frost risk previously associated with some portions of land, and farmers' attitudes. Agriculture in the area is marginal with an income value per hectare and per year ranging from US\$ 400 to US\$ 3200 (Valdivia, 2002) and the average income is usually less than US\$ 1 per day (Baigorria et al., 2002).

## **5.2. Data and methods**

The study included three general phases:

1. Data collection and standardization:

Data describing the natural resources in the watershed were collected, including soil data, a digital elevation model, and long-term weather data. Surveys and workshops indicate current management practices and the use of weather data. Finally, the results of GCM's were downloaded (including actual data and forecasts).

2. Spatial and temporal downscaling of seasonal climate-forecasts:

Global circulation forecasts operate at a scale that makes them unusable for studies at the farm level. Methodology was developed to interpret seasonal-climate forecasts at the level of a single weather station.

3. Evaluation of land management:

The relevance of detailed seasonal-climate forecasts was evaluated by a number of scenario studies in which crop performances were evaluated using mechanistic simulation models.

### 5.2.1 Data collection and standardization

Tapia (1995) sub-divided the watersheds in three agro-climatic zones (ACZ) denominated as highlands, hillside, and valley. In each of these ACZs, a weather station is located: La Toma (3590 m.a.s.l.) in the highlands, Usnio (3260 m.a.s.l.) in the hillside, and Manzanas (3020 m.a.s.l.) in the valley. The oldest one is Usnio, with an historical record of 21 years, while the other two have nine years of recordings including daily time-series data of maximum and minimum temperatures, amount and intensity of rainfall, and incoming solar radiation.

A digital elevation model was available from De la Cruz et al. (1999) with a pixel size of 100 m x 100 m. Overmars (1999) created a 1:25.000 soil map providing quantitative high-resolution soil data suitable for modeling.

A two-year dynamic survey of agricultural management in the area was carried out in 1999-2000 (Antle et al., 2001; Valdivia, 2002). This survey monitored in detail agricultural practices of 30 farmers in the study area. In the context of this study, eight participative stakeholder workshops involving 339 farmers were held to obtain detailed information for the cropping season September 2003 – May 2004 and information about the current use of formal weather and seasonal-climate forecasts and the possibility to increase its utilization. Main goals were to evaluate: (a) crops, N-fertilization ranges, and planting dates during wet season; (b) local weather and seasonal-climate forecast indicators currently in use by farmers; (c) factors influencing crop decisions; and (d) current use of formal forecast by decision-makers. Each workshop was assigned to a different area of the watershed taking into account the hamlet boundaries as well as the varied access to natural and infrastructure resources.

Time-series data of observed Sea Surface Temperatures (SST) maps are available on the Internet<sup>1</sup> in a monthly step time and with a pixel

---

<sup>1</sup> <ftp://ncardata.ucar.edu/datasets/ds277.0/oi/mnly/data>

size of 2° latitude x 2° longitude. Monthly forecast maps of SST are also on the Internet<sup>2</sup> for a three-month moving average with a pixel size of 2° latitude x 1.5° longitude. Both sources of information were temporally and spatially aggregated standardized before they could be used in model development and model application. Observed SST were temporally aggregated as three-month averages and forecast maps were re-sampled to a pixel size of 2° latitude x 2° longitude using a weighted distance interpolation method (Isaaks and Srivastava, 1989).

### 5.2.2 Spatial and temporal downscaling of seasonal-climate forecast

The GCM's currently forecasts in terms of SST. However, agricultural decision making requires forecasts in terms of temperature, rainfall and incoming solar radiation at the level of the agro-ecological zone. In this chapter, each ACZ is represented by a weather station. Downscaling included three different steps:

1. Estimation of a multiple regression model describing meteorological variables for each weather station as a function of SST (Berri, 1998).
2. Application of the models to predict weather conditions in each ACZ on the basis of predicted SST.
3. Downscaling the weather predictions using the WGEN weather generator (Richardson and Wright, 1984).

Gilford et al. (1992) indicated that the SST of the Pacific Ocean between 20° N, 180° W to 26° S, 60° W strongly influences the climate of Northern Peru, including the study area. Using CLIMLAB2000 (Tourre, 2000), each pixel from the observed three-month average SST maps was correlated to the monthly time-series of maximum and minimum temperature and rainfall from weather stations. This analysis yielded monthly maps of correlation indexes between SST and weather conditions

---

<sup>2</sup> [http://www.emc.ncep.noaa.gov/research/cmb/sst\\_analysis/](http://www.emc.ncep.noaa.gov/research/cmb/sst_analysis/)



with a three month lag (e.g. SST in June – August versus Rainfall in September). Areas with the best correlation were selected visually from each map of correlation indexes. Each of the cell values belonging to a specific selected area was averaged, producing one value representing the SST of the water mass. Subsequently, a stepwise multiple regression analysis with a significance level of 0.05 was performed between the meteorological variable and the average SST. To perform this process, the first two-thirds of the-year of the historical record data available from each weather station was used. The remaining one-third of the-year corresponding to the last period of the historical record data was used in a validation and residual analyses.

The three multiple regression models (one for each ACZ) were used to generate a monthly seasonal-climate forecast for the cropping season September 2003 – May 2004.

Finally, a weather generator WGEN (Richardson and Wright, 1984) was used to downscale the monthly forecasts to the daily level. Inputs into the weather generator are:

- monthly forecasts,
- monthly standard deviation for maximum temperature and incoming solar radiation in dry and wet days, minimum temperatures, and rainfall (calculated using the time-series of each weather station),
- rainfall distribution scale parameter ( $\alpha$ ),
- the probability of dry-wet sequence, and
- the total number of rainy days.

Incoming solar radiation was estimated by inputting the monthly maximum and minimum forecasted temperatures in the model by Bristow and Campbell (1984), previously calibrated and validated for the region (Chapter 2).

To evaluate alternative management strategies, 99 different daily weather forecasts were generated for each ACZ for the files of the September 2003 - May 2004 season.

### 5.2.3 Evaluation of land management

Crop management obtained from the field workshops and the two-year dynamic survey (Antle et al., 2001; Valdivia, 2002) was characterized using three parameters: (a) main crops in the study area, (b) typical range of N-fertilization rates, and (c) planting-date ranges.

The SUBSTOR-potato model (Ritchie et al., 1995) and CERES-cereal model (Singh et al., 1991) are available within the Decision Support System for Agrotechnology Transfer (DSSAT) (Jones et al., 1998) and calibrated and tested under Andean conditions of DSSAT, described in Bowen et al. (1999) and Stoorvogel et al. (2004b). These models were used to simulate potato, wheat, and barley productivity under different management strategies.

Crop management scenarios and the geo-referenced information about the seasonal-climate forecast and soil were used for running the crop model (DSSAT). Each combination of ACZ, soil, and crop management was evaluated with 99 alternative outcomes of the WGEN software. Afterwards, averages and standard deviations from the 99 simulations for each scenario were calculated. Maps were generated assigning the simulated values according to the spatial distribution of ACZ and soil types. The next step was to produce the maps of optimal planting-date for each combination of crop and N-fertilization. For each combination crop and N-fertilization, an overlaying among the different planting-date maps was performed, selecting for each pixel across the maps the highest yield forecast. This ultimately led to a map with optimal planting-date for the different crops. Several sets of these maps were printed in size A0, and were used to train farmers from the different hamlets on methods of

interpreting the map. Maps were given to the respective authorities in order to make them available to people in the hamlets.

## **5.3 Results**

### **5.3.1 Data collection and standardization**

Figure 5.1 shows the monthly planting-date distribution (%) of potato, wheat, and barley during the rainy season. Table 5.1 summarizes the majority and more important local forecast indicators within the study area. In addition, the table presents information about the specific characteristics or processes observed in the indicator along with the observation time. These indicators are classified as Meteorological, Astronomical, and Biological. Biological indicators are sub-divided in plants, birds, and insects. Within each class, indicators are ranked according to the percentage of farmers who make use of the indicator, as a relative degree of importance in the local forecast process. Field surveys showed that radio is the means of media used by 100% of the farmers and that radio serves for farmers as the means of access to different sources of formal weather and seasonal-climate forecast. However, only five percent of the farmers in the watersheds had used this information before and only eight percent of the farmers had confidence in it.

Field surveys indicated that farmers already had established a year-by-year planting strategy. Thirty-six percent of the farmers use the same crop rotation and cropping area despite forecast indicators, while the remaining 64% change only the cropping area, trying to obtain benefits in good years or avoid losses in bad years. However, rainfall forecast around the established planting dates supports both groups in making their operational planting decisions. Crop yields have three general final destinations in the study area: self-consumption, seed production, and the

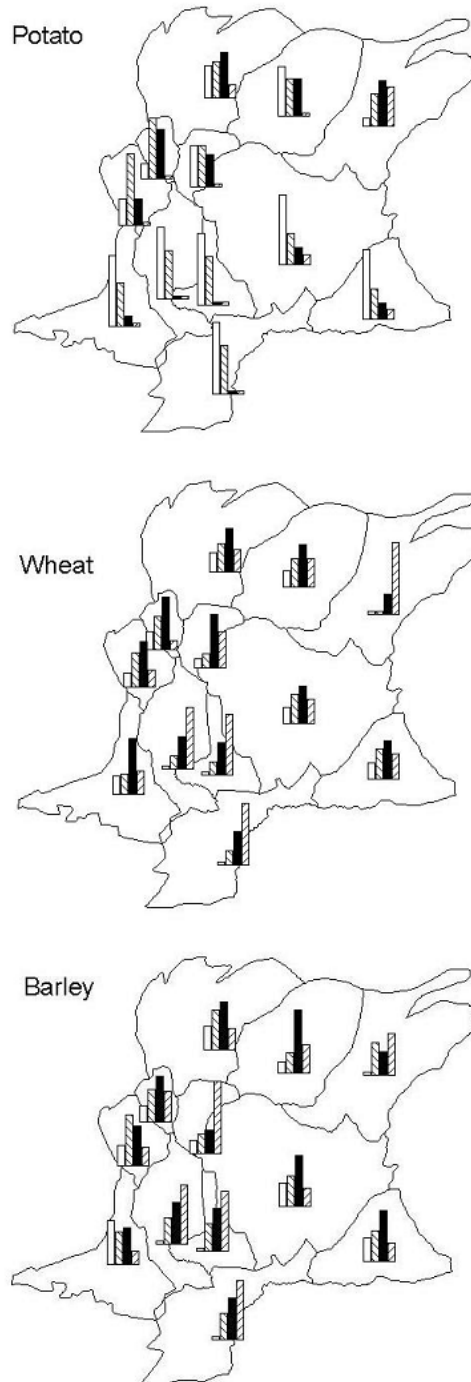


Fig. 5.1. Planting schedule during the rainfall season of the three main crops according to hamlets: □ October, ▨ November, ■ December, ▩ January.

**Table 5.1** Traditional weather forecast indicators and percentage of farmers using these indicators.

Indicator	Characteristic or process	Time of observation	Forecasts	Percentage of farmers use
<b>Meteorological indicators</b>				
Wind	direction	Jul. – Dec.	frosts, droughts	97
Whirlwind	formation	Jul. – Aug.	droughts	64
Cloud	form	Nov. – Dec.	frosts at night	31
3 clouds in clear sky	formation	no date	good year	26
Thunders	appearance	since Sep.	good year	24
Red clouds	appearance	Dec. – Jan.	droughts	21
First rainfall with hail	formation	no date	good year	9
<b>Astronomical indicators</b>				
New moon	green color	planting date	crop damage	98
New moon	inclination	phase of the moon	rainfall	47
Moon halo	appearance	no date	low yield	40
Sun halo	appearance	no date	low yield	37
Mon eclipse	appearance	no date	bad year	34
Sun eclipse	appearance	no date	bad year	14
Full moon	full view	phase of the moon	high yield	14
<b>Biological indicators (wild plants)</b>				
<i>Rubus sp.</i>	fruit production	Oct. – May	high/low yield	71
<i>Sambucus peruviana</i> HBK	fruit production	Oct. – May	high/low yield	50
<i>Agave americana</i> L.	fruit production	Aug. – Feb.	high/low yield	46
<i>Prunus serotina</i> Ehrb.	fruit production	Nov. – Mar.	high/low yield	32
<i>Passiflora mollissima</i> (HBK.) Bailey	fruit production	no date	high/low yield	29
<i>Opuntia ficus-indica</i> L. Müller	fruit production	Nov. – Mar.	high/low yield	18
<i>Agave americana</i> L.	inflorescence inclination	no date	high/low yield	12
'Lanche'	fruit production	no date	high/low yield	9
<i>Pernettya prostrata</i> (Cav.) Sleumer	fruit production	Oct. – May	high/low yield	7
'Perlas'	fruit production	Oct. – May	high/low yield	4
'Gualpañau'	fruit production	Oct. – May	high/low yield	4
<b>Biological indicators (wild birds and insects)</b>				
<i>Larus serranus</i> <sup>1</sup>	migration	previous planting	rainfall season	71
'Guyanas' <sup>1</sup>	migration	previous planting	rainfall season	51
<i>Cladosdes sp.</i> <sup>2</sup>	appearance	Oct. – Dec.	rainfall season	14
<i>Phalcobaenus albogularis</i> <sup>1</sup>	migration	Jun. – Jul.	low yield	14
<i>Ardeidae sp.</i> <sup>1</sup>	migration	previous planting	rainfall season	9

<sup>1</sup> birds<sup>2</sup> insects

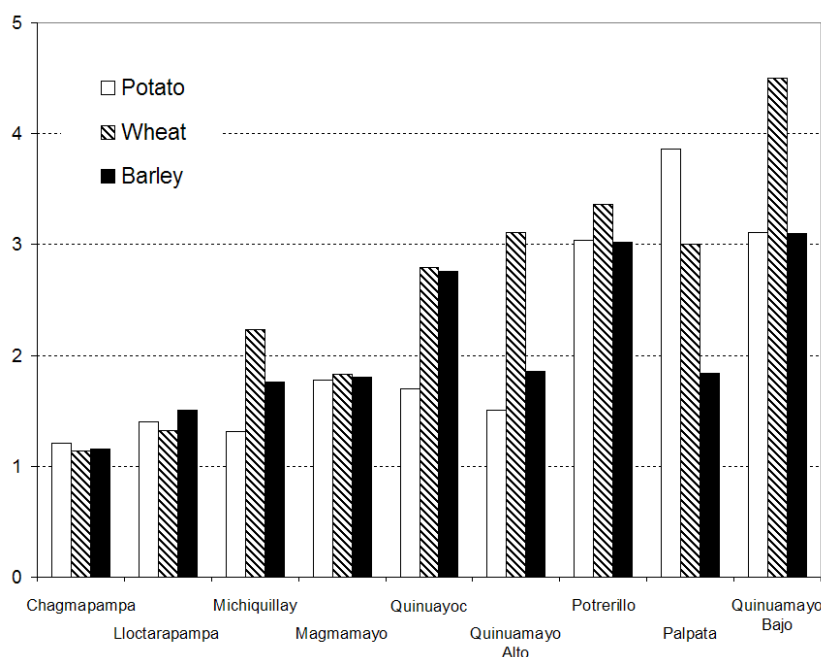


Fig. 5.2. Ratio between the production for self-consumption and allocated to the market of the four main crops across hamlets.

market. The percentage assigned to seeds is almost constant by year, except after extremely low-production years, when the seed is used for self-consumption. Considering the other two final destinations of the crop yields, a relationship is showed in Figure 5.2 as the rate between self-consumption and market use for the main crops. According to this relationship, the nine hamlets are ranked from highest market dependence (Chagmapampa) to lowest dependence (Quinuamayo Bajo). According to the results obtained from the workshops, the main factors influencing the decision of how much area to crop in the next cropping season are presented in Table 5.2, ranked by hamlet as in Figure 5.2.

These results from the field workshops were used as the reference to build the crop management strategies for simulating the cropping season of September 2003 – May 2004.

The identified crop management strategies were:

- Potato planted in October, November, and December. Wheat and barley planted in November, December, and January.

- Nitrogen fertilization rates named as low and high, corresponding to 25 and 100 kg ha<sup>-1</sup> for potato and 20 and 80 kg ha<sup>-1</sup> for wheat and barley.

### 5.3.2 Spatial and temporal downscaling of seasonal-climate forecast

Table 5.3 shows the correlation indexes for all the weather stations and for each meteorological variable at the time of calibration using the two-thirds of the year of the historical record. Figure 5.3 shows the tercile probabilities of the residuals during the validation process using the remainder one-third of the year of the historical record for maximum and minimum temperatures as well as rainfall during *El Niño* and *La Niña* years (IRI, 2003).

**Table 5.2** Factors influencing decision-makers in planting (%) by hamlet\*.

Hamlet	Market prices	Plagues & diseases	Seed availability	Rainfall delay after-planting	After-planting frost	
Chagmapampa	64	90	95	69	67	0
Lloctarapampa	0	44	44	44	0	0
Magmamayo	17	98	61	100	41	2
Quinuayoc	2	60	65	44	46	0
Quinuamayo Alto	36	100	100	100	100	0
Potrерillo	10	100	100	100	100	0
Palpata	3	100	100	67	50	0
Quinuamayo Bajo	36	100	100	100	100	0

\* Data from Michiquillay are not available

**Table 5.3** Monthly coefficient of determination ( $R^2$ ) to the three meteorological variables of each weather station. In parenthesis initials of the months aggregated in the seasonal-climate forecast of the sea surface temperature (SST).

Meteorological variable	Sep. (JJA)	Oct. (JAS)	Nov. (ASO)	Dec. (SON)	Jan. (OND)	Feb. (NDJ)	Mar. (DJF)
<b>La Toma</b>							
max. Temperature	0.57	0.85	0.96	0.86	0.77	0.78	0.96
min. Temperature	0.91	0.96	0.41	0.48	0.90	0.93	0.90
Rainfall	0.78	0.66	0.76	0.75	0.81	0.95	0.83
<b>Usnio</b>							
max. Temperature	0.35	0.45	0.65	0.48	0.68	0.42	0.56
min. Temperature	0.43	0.81	0.42	0.61	0.42	0.31	0.46
Rainfall	0.52	0.51	0.26	0.54	0.27	0.55	0.40
<b>Manzanas</b>							
max. Temperature	0.97	0.87	0.96	0.78	0.90	0.88	0.77
min. Temperature	0.79	0.84	0.68	0.78	0.94	0.86	0.84
Rainfall	0.75	0.52	0.45	0.82	0.95	0.42	0.45

Table 5.4 shows a comparison between the monthly climatic values versus the monthly forecasted values (cropping season September 2003 – May 2004) of the three meteorological variables and for each weather station. The forecasted values are those used as inputs to the weather generators to produce the 99 files of daily-weather distribution, according to the specific forecast.

### 5.3.3 Yield forecast and risk evaluation

Figure 5.4 shows the optimal planting-date maps and the forecasted yield ranges of potato (a, b), wheat (c, d), and barley (e, f). High N-fertilization scenarios across the crops are shown in (a, c, and e) respectively, while the low N-fertilization scenarios are shown in (b, d, and f) respectively. These maps optimize the planting-date of each crop and N-fertilization combination according to the downscaled forecast to the



cropping season of September 2003 – May 2004 in La Encañada and Tambomayo watersheds. Maps indicate the highest yield of each pixel among the simulated months. Figure 5.5 shows the risk of potato production as a coefficient of variation due to both the errors in downscaling process of seasonal-climate forecast and uncertainties of the crop simulation process because of the use of different daily-weather distributions. Scenarios of low and high N-fertilization are presented as Figure 5.5a and 5.5b respectively.

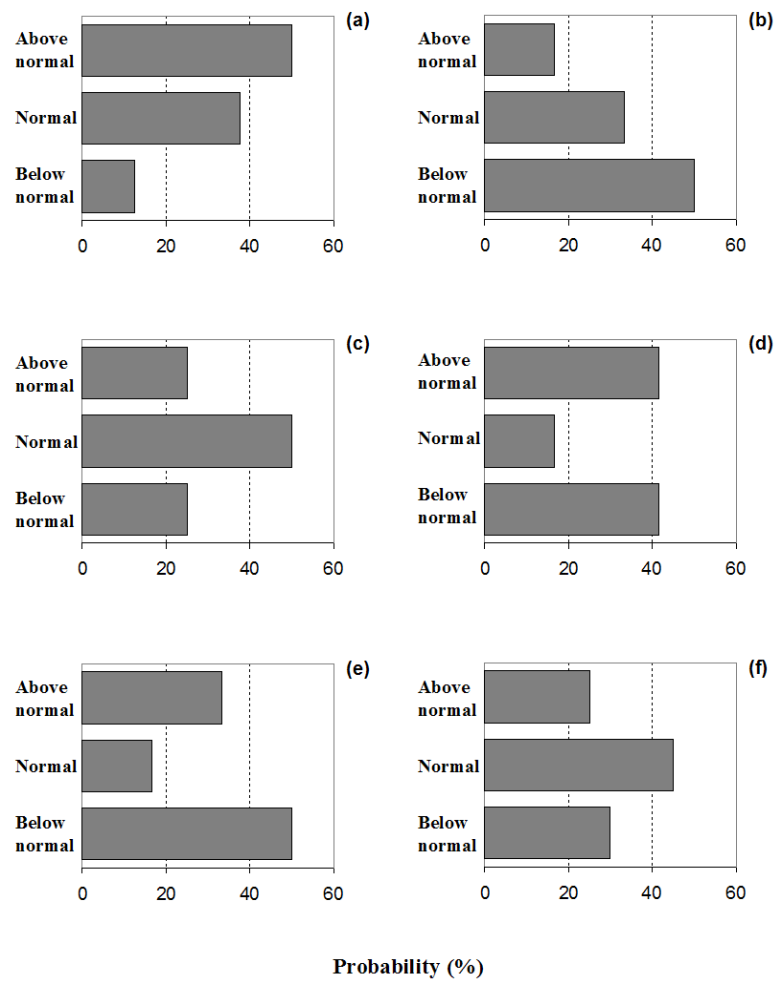


Fig 5.3. Tercile probabilities of the residuals at the time of validation during the events of *El Niño* (a, c, and e) and *La Niña* (b, d, and f). Variables correspond to (a) and (b) Maximum temperature, (c) and (d) Minimum temperature, and (e) and (f) Rainfall.

**Table 5.4** Monthly climate and forecast values of maximum and minimum temperature and rainfall for each weather station in the period of work.

Month	Temperature (°C)				Rainfall (mm)	
	maximum		minimum		climate	forecast
	climate	forecast	climate	forecast		
<b>La Toma</b>						
September	12.0	12.0	3.1	3.0	68.6	88.8
October	12.3	11.8	3.6	3.2	45.7	45.2
November	11.9	11.3	3.1	3.0	69.4	68.6
December	10.8	10.8	3.1	2.7	128.7	132.3
January	10.7	10.6	2.7	2.4	92.7	88.2
February	10.4	11.3	3.9	2.0	143.1	103.2
March	9.8	12.0	2.5	1.6	102.5	199.1
<b>Usnio</b>						
September	14.7	15.0	6.3	6.4	40.0	39.3
October	14.9	14.5	6.7	6.4	62.6	65.3
November	14.7	14.7	6.1	6.1	67.4	65.4
December	14.2	14.5	6.4	6.6	75.0	68.6
January	14.5	14.7	5.9	5.7	92.8	94.9
February	14.2	14.5	6.9	5.7	108.0	110.3
March	14.0	13.4	6.5	5.8	105.3	86.9
<b>Manzanas</b>						
September	16.7	15.6	5.8	3.7	53.9	65.4
October	17.5	16.0	6.4	4.8	45.1	51.0
November	17.9	16.7	5.6	5.8	63.2	62.7
December	17.0	16.6	7.3	6.5	52.9	64.3
January	16.2	17.5	6.5	6.3	63.4	85.2
February	15.9	17.1	6.9	7.6	147.7	147.4
March	16.1	16.1	6.6	6.5	105.5	106.7

## 5.4. Discussion and conclusions

### 5.4.1 Current decision-making processes

Observations of many local forecast indicators in the study area are done by farmers who translate them into weather forecasts rather than seasonal-climate forecasts. As a result, farmers use the indicators for operational decisions rather than tactical decisions. As a result, farmers incorporate their local forecast to assist in operational decisions on water, nutrient, and crop protection management according to their conceptual models. According to Table 5.1, seasonal-climate forecast indicators are

evaluated right before, during, or following the planting dates, making it difficult to use them to assist in tactical decisions such as planning in advance which crop will be planted or planting dates. However, from a tactical point of view, indicators are useful for farmers in order to have an idea about the crop yield at the end of this season; thus, they can take actions at an earlier time such as emigrating for temporal work.

Farmers from La Encañada produce under different agro-ecological conditions and with large differences in market accessibility. The order imposed to the hamlets in Figure 5.2 shows high correspondence between the accessibility to resources and markets. There is also a variation across the crops due to the accessibility to better lands for valuable crops. Farmers who have the highest number of factors affecting their planting decision (Table 5.2) are the ones directly related with the highest values of the self-consume/market ratio in Figure 5.2. After-planting frost does not influence the decision to plant because farmers have the possibility to replant. Market prices have a variable importance as a factor influencing the planting area, the more market dependable hamlet (Chagmapampa) presents the largest number of farmers influenced by market conditions. The importance of market prices as a factor influencing the planting area is explained because a high number of farmers belong to a subsistence economy (Baigorria et al., 2002), there is an imperfect market (Antle et al., 2001), and the price expectation at the moment of harvesting is insecure. Plagues and diseases in the potato crop are highly related to seed availability and are both dependent on the weather and the management conditions of the previous cropping season. The first rainfall events during the wet season ultimately determine the planting date; however, farmers do not take into account the forecast of total rainfall and rainfall distribution during the beginning season. In this case, local forecast of weather is being used to assist tactical decisions that in fact require middle-term forecast.

The seasonal-climate forecast is available from the National Service of Meteorology and Hydrology and most of the farmers have access to it

mainly by radio. However, the field survey shows that they can't change their tactical decisions due to the impossibility to understand the forecast presented by the media, as well as its translation in terms of agricultural impact. Weather forecast, as well as seasonal-climate forecast, is useful mainly if it addresses a real necessity, and viable decision options can be taken by the decision makers (Hansen, 2002). In the study area, agricultural related institutes either support farmers by providing translated-forecast information; yet, they lack the capabilities to do proper jobs on the strategic and tactical level.

#### 5.4.2 Downscaling the GCM's forecast to the field level

The international scientific community makes efforts to predict weather, seasonal-climate, and climate. However, because of complexity of the models, the number of atmospheric and oceanic variables involved, and the global scale, these predictions are often inappropriate for decision-making at field level and even at the watershed level. Some efforts in the last years focus on how to downscale this information in space and time so that it is useful for stakeholders from regional to parcel scales. This paper made use of techniques to downscale the seasonal-climate forecast from September 2003 to March 2004 and to test the possibility of supporting farmers in the decision-making process.

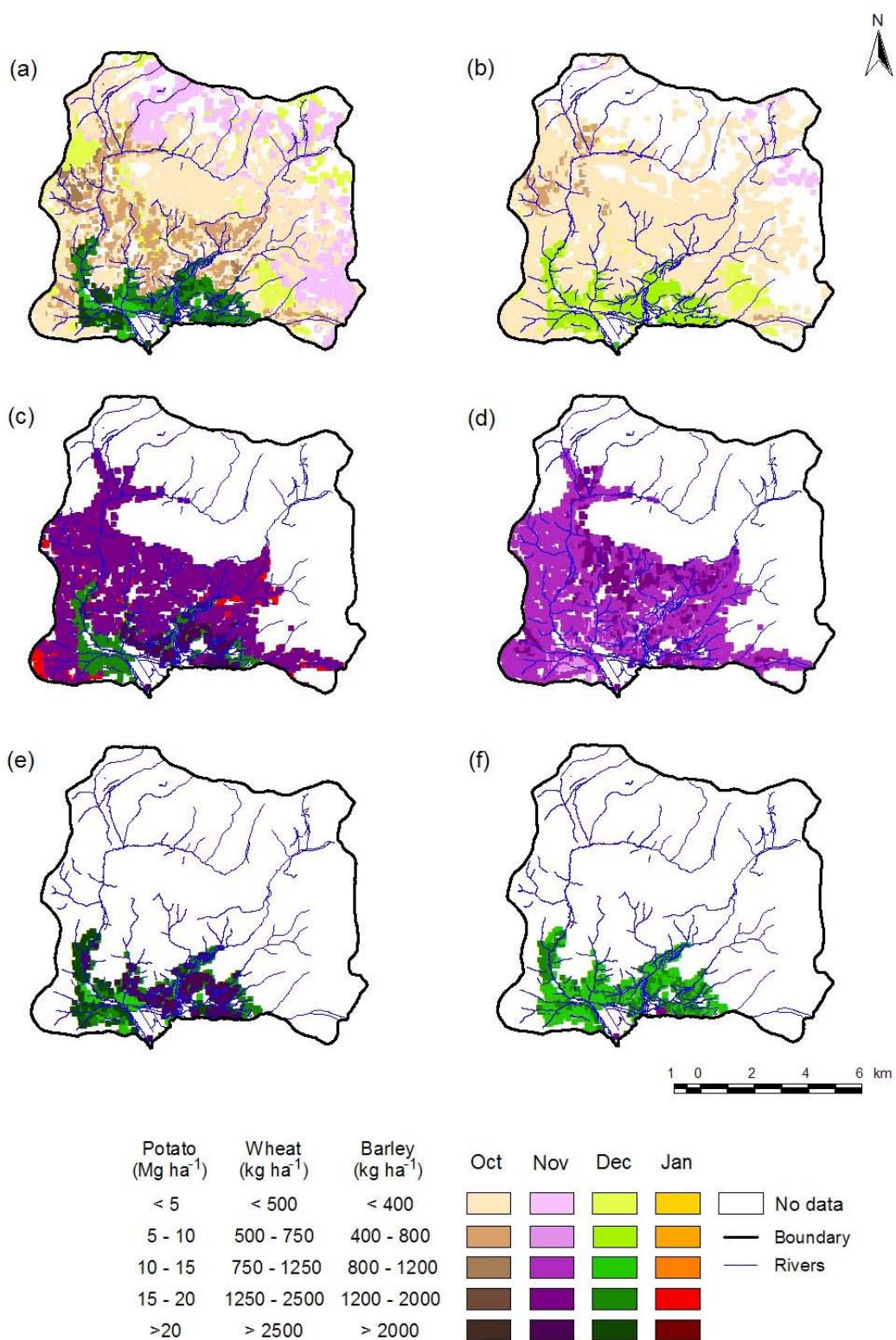


Fig. 5.4. Optimal planting-date maps of potato, wheat, and barley under high and low N-fertilization levels. (a) Potato – High N, (b) Potato – Low N, (c) Wheat – High N, (d) Wheat – Low N, (e) Barley – High N, and (f) Barley - Low N.

According to the multiple regression models, maximum and minimum temperatures, as well as rainfall, are expected to be close to normal conditions in the cropping season September 2003 – May 2004 within the study area. This prediction is also confirmed by the seasonal-climate forecast made in December 2003 (during the preparation of the present chapter) by the International Research Institute for Climate Prediction (IRI, 2003). Forecast from IRI is presented such as tercile-probability to temperature and rainfall in general terms around the study area.

Residual analysis suggested that the developed multiple regression models are quite appropriate for normal years. However, for maximum temperature (Figures 5.3a and 5.3b), the largest positive residuals belong to *El Niño* years while the largest negative residuals belong to *La Niña* years. These results are interpreted as the multiple regression model, under-estimating the maximum temperature during *El Niño* and over-estimating during *La Niña*. In the case of minimum temperature (Figures 5.3c and 5.3d), the tercile probabilities show that residuals are well distributed during *El Niño*; however, during *La Niña* years the tercile probabilities of the residuals demonstrate a large noise in the predicted values. In the case of rainfall (Figures 5.3e and 5.3f), results show that during *El Niño* years the multiple regression models produce the largest noise.

The downscaling process presented here is based on the forecast of monthly averages of maximum and minimum temperatures and rainfall. However, when the daily weather conditions are produced, the monthly climatic variability of these variables is applied, which cannot be generalized for all kinds of seasonal-climate conditions (*i.e.* Normal, *El Niño*, and *La Niña* years). Romero (2005) demonstrates that variability of rainfall is affected seriously during *El Niño* and *La Niña* events in La Encañada and Tambomayo watersheds. Thus, in areas affected by some extreme meteorological events, it is recommended to make a previous

characterization analysis about the variability of the meteorological variables. Different values of standard deviation, rainfall distribution scale parameter, and probability of dry-wet sequence can be used as input in weather generators according to the general forecast of the extreme event. Generation of several daily weather files, as presented in this paper, also support the variability analysis of each kind of event, with the advantage that it captures the probabilistic normal distribution of the meteorological variables and not only absolute values.

It is necessary to explore multiple regression models in a more dynamic way and based on a physic explanation of the involved process. Results obtained in the present research using a more empiric approach of those multiple regression models indicate the necessity of in-depth analysis, whether to generate multiple regression models in general climatic terms as the presented here or multiple regression models to normal conditions and to each specific extreme meteorological event. Models involving physic explanation can better represent a total variety of meteorological behaviors of an entire area.

#### 5.4.3 Yield forecast, risk evaluation, and training

Yield forecast maps under different scenarios of crop production (Figure 5.4) support farmers to interpret the effects of the formal seasonal-climate forecast on their lands under the different crop management options. Risk maps (Figure 5.5) support farmers with quantitative information about the risk of each crop management scenario under the seasonal-climate forecasted conditions. Thus, both low-yield fields and high-yield fields can be related to a low or high percent of coefficient of variation. Farmers with the highest economic portfolios can rent lands with better response to N-fertilization (Figure 5.4a) and lower risk (Figure 5.5). High-yield fields with a high risk typically have investments of valuable crops and N-fertilization, according to the risk preference or risk aversion of

the owners. However, in low-yield fields, often related to marginal areas or natural pastures opened as new fields, yield forecasts support poorest farmers to make better investments of the low resources they have in an attempt to assure food security.

After a training process, farmers understood how to use the maps (same as presented in Figures 5.4 and 5.5), and they began to interpret the yield forecast in the areas corresponding to their own fields to analyze the feasibility of the information and more rapidly incorporate the information into their own conceptual models. The first observed response from farmers at the time of information dissemination was a desire to increase the percentage of planting area within the optimal proposed planting-date, attempting to take advantage of the yield forecast. However, the farmers never wanted to risk the entire planting area, neither in a single planting date nor for one crop. Also notable is that only a small percentage of farmers considered changing the predetermined crop, despite the fact that the information was proportioned one month before the first evaluated planting-date. In this way, adoption of the findings by farmers would finally depend on the destination of their harvest products, which varies according to the hamlet and crop (Figure 5.2), and the economic portfolio, and also to farmers' risk preferences (Materer, 2001). However, best crop yields are not necessary related with the highest net incomes, especially in the more market-dependable hamlets. Thus, the use of this information is to translate forecasts to support decision-making and not to make the actual decision.



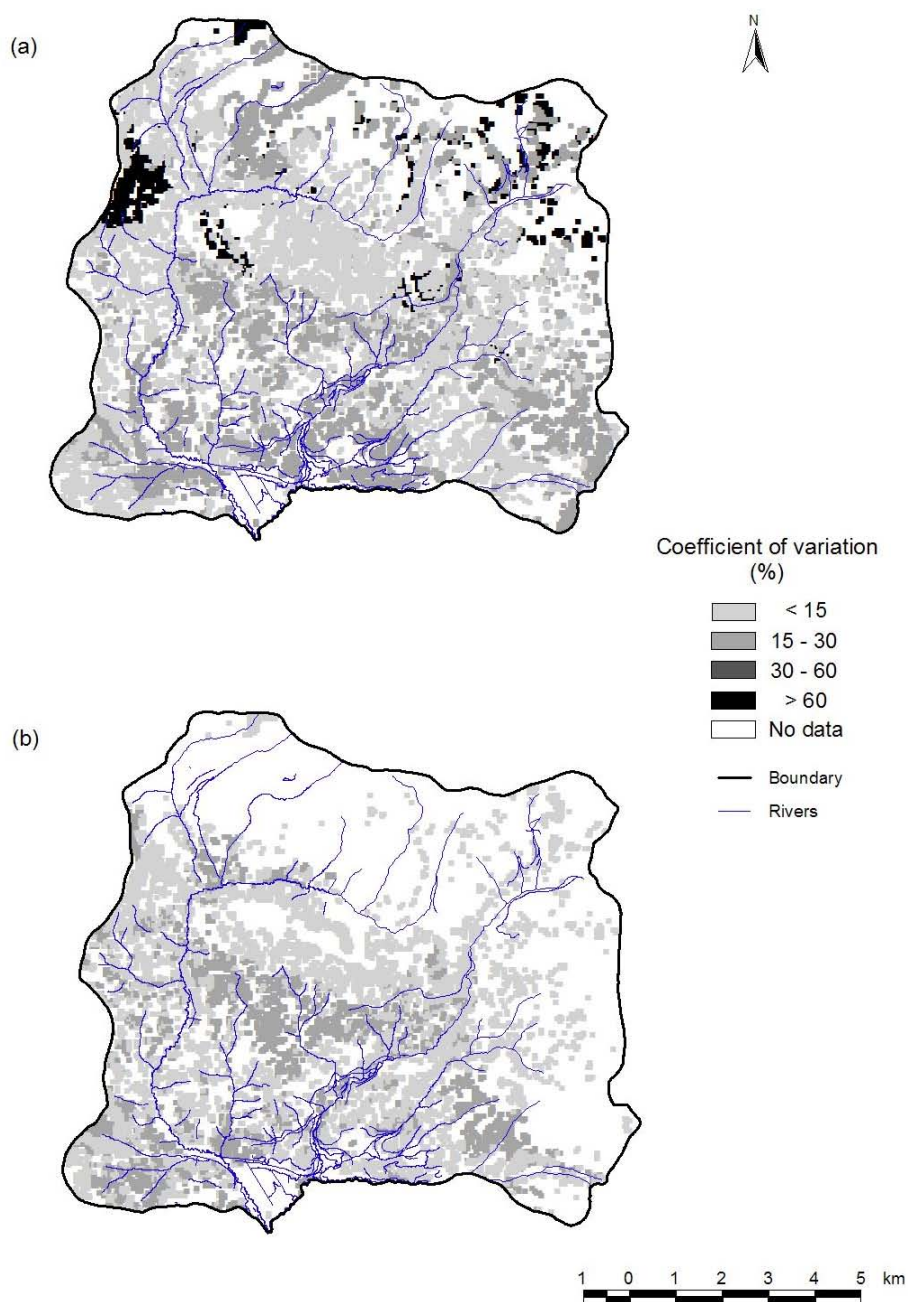


Fig. 5.5. Maps of coefficient of variation (%) of potato yield under different levels of N-fertilization. (a) High and (b) Low.

#### 5.4.4 Improving decision-making at different levels

During the decision-making process, farmers evaluate all available information to make the best decision according to their conceptual models, traditions, and capabilities. It is not easy to translate the formal forecasts regarding the total amount of rainfall during the cropping season or the monthly average temperatures, to how they will impact crop yields. Crop growth simulation models make it possible to dynamically assess the impact of forecasts in combination with other variables such as soil, cultivars, and crop management.

Availability of more detailed spatial information of climate, soil, and topography, in combination with tools with a more quantitative and mechanistic approach, provides the possibility to make a deep and complex analysis similar to the real world situation, describing the maximum spatial and temporal variability in complex terrains such as the Andean Highlands. Higher levels of complexity can be reached in the analysis, including more variables within the distinct scenarios. These variables can include cultivars into each crop (*i.e.* native potatoes, winter wheat, short photoperiod cultivars, etc.), irrigation systems, and crop rotations, etc. However, this information must be used as a support system such as in the case of the farmers of La Encañada, and not as a final recommendation.

Uncertainty analysis regarding soil loss, for example, allows the estimation of the potential impacts of different crop managements across an area. However, when this analysis is geo-referenced in a map, highly sensible areas can be identified, analyzed, and taken into account to make decisions to a proper scale (Romero, 2005). National Soil Conservation Programs can use the information to plan in a more quantitative and mechanistic approach, including where to install which soil conservation practice to optimize resources in order to obtain the best impacts. Sometimes, changes in crop managements can be enough to drastically reduce soil loss. Usually, farmers in the study area do not have access to

high levels fertilizers because of high costs and the aversion to the risk due to the high level of climate risk. However, it is necessary to know the potential risks originated by the use of these due to possible changes in agricultural policies. Similar to soil loss, pollution can be analyzed from point specific to regional levels, with the possibility to identify fields with a high risk of pollutant leaching and to analyze total amounts of these pollutants accumulated as the effect of a whole watershed (Stoorvogel et al., 2004a; Crissman et al., 1998). Spatial variation of combinations of ACZs, soils, and slopes can produce different rates of soil loss under the same crop yield. However, in this case, temporal effect will show decreasing rates of crop yields under high rates of soil loss.

Seasonal-climate forecast can support not only tactical decisions exploring the different alternatives of farmers to decrease or take advantage of some extreme event (*i.e.* climatic, economic, or political), but also to estimate possible extreme impacts on the environment, such as soil loss or water pollution.

Dissaggregation of some generalizations of information, such as the ACZ, in higher spatial resolutions and for each of the different meteorological variables, still can make more robust the spatial and temporal analysis. However, it is important to take into account the necessity of more intensive calculations to perform the process.

The possibility to analyze high-resolution maps allows different stakeholders to better make decisions, from investing in N fertilization at farmer level to decreasing taxes in N fertilizers at political level (Crissman et al., 1998). The pixel – parcel analysis supports the strategic decision making of a farmer, drawing the actual versus potential harvest of different crops, effectively reducing the uncertainty of the next seasonal weather and its influence on the crops. This valuable information, together with market prices, seed availability, information of plagues and diseases, and economical portfolios as the principal factors, constitute the total framework

for the final decisions made by the stakeholders at different spatial and temporal levels.

### **Acknowledgements**

The authors express their gratitude to the Secretariat of the “Global change SysTem for Analysis, Research and Training – START” for co-funding the research, the International Research Institute for Climate Prediction – IRI for the training at ATI (especially to Dr. J. Hansen and Dr. N. Wards), to Dr. C. Valdivia for supporting the field-workshop, the “David and Lucille Packard Foundation” for supporting ATI, to the field team L. Sanchez, J. Pizarro, L. Chavez, and E. Regalado and to the farmers of La Encañada and Tambomayo. The present work is supported by the United States Agency for International Development (USAID), through its Soil Management Collaborative Research Program (SM-CRSP) financing a project entitled, “Tradeoffs in Sustainable Agriculture and the Environment in the Andes: A Decision Support System for Policy Makers” (Grant # 291488).

## Chapter 6

---

### **Climate variability explaining soil variability in volcanic ash soils in the Ecuadorian Andes**

Young Andisols in the Carchi region in the Ecuadorian Andes present limited spatial variation in parent material and age. The high infiltration capacity of the volcanic ash soils prevents runoff and consequently limits topography (in terms of slope and curvature) as an important soil forming factor. Land use can be described by a rotation of potato and pasture and also presents limited variation in the study area. On the other hand, climatic differences are large in the steeply dissected mountainous region. Given the limited variation in the above soil forming factors one can expect that soil variation is strongly correlated to climatic differences. Typically, little is known about the spatial variability in climate (except through proxies like altitude and aspect). In regions like Carchi, the possibilities for digital soil mapping are, therefore, limited. In digital soil mapping, the spatial variation in soils is described as a function of auxiliary information providing insight on the soil forming factors. To apply this technique in the Carchi region requires insight in the spatial variation in climatic conditions. The lack of reliable climatic data at high-resolutions has stimulated the use of climatic indexes based on topography such as the wetness index and altitudinal relationships. Recently new process-based interpolations techniques of meteorological variables with emphasis in mountainous areas have developed. In this chapter we test their applicability to explain the distribution of soil properties in the Carchi region. Soil organic matter and other soil properties are mapped using stepwise multiple regression models (SMRM) using soil mapping units, topography, and climate parameters as independent predictors. Validation was performed using cross-validation, residual analysis, and the median square error. The outcomes were compared with mapping units; stratified linear regression results using altitude as predictor, and SMRM results using DEM's related parameters as predictors. Comparisons demonstrated a significant contribution of climate in predicting the spatial distributions of all soil characteristics. Different meteorological variables explain the variations within the soil units, demonstrating the potential to use interpolated climatic maps for digital soil mapping.

Based on: Baigorria, G.A., J.J. Stoorvogel, and A.Veldkamp. Climate variability explaining soil variability in volcanic ash soils in the Ecuadorian Andes.

© Submitted. Geoderma. January 2005.

## 6.1 Introduction

In 1898, Dokuchaev identified five main soil-forming factors: parent material, topography, climate, organisms, and time (Jenny, 1941). The combination of these factors determines the type of process (physical, chemical, and biological), the duration, and the rate of soil development at a given location (van Breemen and Buurman, 1998). Parent material and topography define the initial state where climate and organisms initiate the physical, chemical, and biological soil forming process resulting over time in the current pedon. In this conceptual model of soil formation, climate is an important driving factor as it influences weathering rates, but also, indirectly through the type and quantity of organisms affecting soil organic matter dynamics. The effect of climate has been studied for a long time but mostly at large scales to explain major differences between zonal soils (Baldwin et al., 1938). At more detailed scales, however, the lack of insight in climatic variability forced researchers to use proxies for climate like altitude (Zehetner et al., 2003; Lopez, 2000) and the wetness index (Jenson and Domingue, 1988; More et al., 1993) for which the spatial variability was known or could be assessed. The attention for climate variability as a driving factor behind soil variability was already apparent by the definition of soil moisture and soil temperature regimes for pedological research (FAO and UNESCO, 1998; USDA and NRCS, 1998). Recently it received renewed attention in the field of digital soil mapping using reproducible, quantitative methods that make extensive use of auxiliary information (Bogaert and D'Or, 2002; McKenzie and Ryan, 1999; Florinsky et al., 2002). If successful, digital soil mapping may be an interesting addition to the well accepted methods as described in the soil survey manual (Soil Survey Staff, 1993; Schoeneberger et al., 1998) and resolves some of the resource constraints of soil surveys (Bouma et al., 1999). New techniques are rapidly being developed ranging from geostatistical techniques, geographical information systems (GIS), topographic analysis and remote sensing (Mueller and Pierce, 2003; Bell et al., 2000).

Nevertheless, high resolution input data remain a serious constraint for many cases. Recently, process-based interpolations models estimating the spatial and temporal distribution of maximum and minimum temperatures, incoming solar radiation and rainfall have been developed for mountainous areas (Chapter 2,3 and 4). These methodologies produce high-resolution maps of the meteorological variables based on daily weather data from a few weather stations and digital elevation models (DEMs). The maps provide a new basis for digital soil mapping using climatic variability, a factor that has often been neglected due to limited data availability. Climate as a soil forming factor can now be studied at larger scales and may help us to predict exact values of soil properties at a particular site by disaggregating soil mapping units and incorporating secondary climate information.

In this study we use the interpolation techniques for climate and analyze the relations between climate and soil properties. The 95 km<sup>2</sup> study area is located in Carchi province in the Ecuadorian Andes. The volcanic ash soils in the area have a high inherent soil fertility that makes them very suitable for the cultivation of potato and the production of milk. Consequently, Carchi is one of the major potato growing areas of the country. The area is highly suitable for a first exploration of the relations between soil properties and short-distance variability since climatic variability is probably one of the main driving factors behind soil differences. In the study area, a blanket of highly porous volcanic ash has been deposited 1600 years before present. With the deposition of this ash sheet the time factor in soil formation became constant, all soils started to develop since the last ash falls. Secondly, the highly porous ash layers have high infiltration rates preventing significant runoff of rainwater and thus limiting topography related erosion processes. The current paper explores climate induced soil variability within the units of an existing 1:100.000 soil survey (MAG and ORSTOM, 1980).

## 6.2. Data and methods

### 6.2.1 Study area

The study area is located in the Ecuadorian Andes (Figure 6.1) between 0°42' N, 78°30' W and 0°32' N, 77°30' W. The area includes the Chitan and San Gabriel watersheds range between 2700 and 3840 meters a.s.l. From an ecological point of view, Troll (1968) named the study area as 'Páramo-Andes' describing equatorial regions of the Northern Andes with possible rainfall throughout the year. The temperature regime typically corresponds to an equatorial climate with a small variation in average monthly temperature but with a daily temperature swing of over 10°C. This large swing is caused by the complex mountainous topography, even allowing for radiative frost events during clear skies at night.

According to Zebrowski (1997), the observed soils in the study area are composed by two sources of volcanic ashes and pyroclastic products, the first from 50,000 to 11,000 before present and the second from 8,000 to 1,600 before present. Soil surveys made by MAG and ORSTOM (1980) classified the young soils as Andepts (Anidisols in the recent, updated classification by USDA-NRCS, 1998). The main soil units in the study area are presented in Figure 6.1 and described as (MAG and ORSTROM, 1980):

- (a) Cf-Hf: Duriudoll (silty ashy halloysitic montmorrillonitic isothermic) - Andic Argiudoll (silty ashy isothermic)
- (b) Hf: Andic Argiudoll (silty ashy isothermic)
- (c) Ck-Cf: Duriudoll (silty isothermic) - Duriudoll (silty ashy halloysitic montmorrillonitic isothermic)



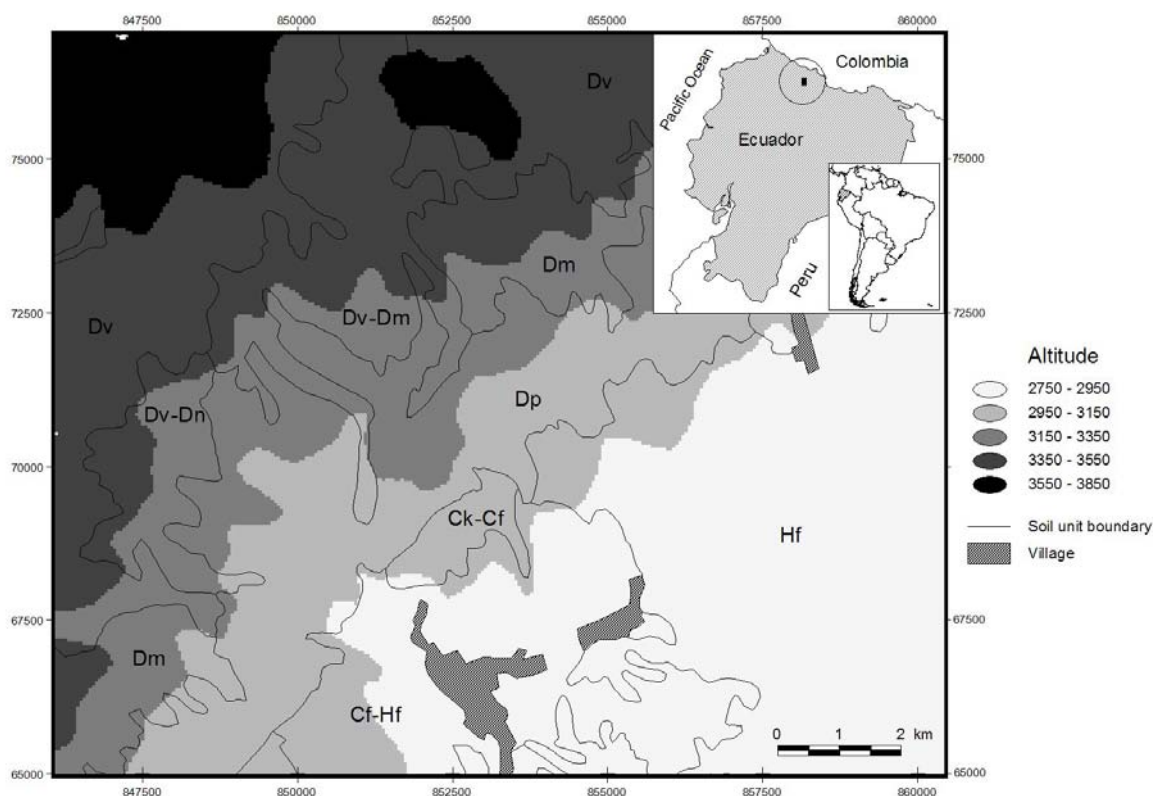


Fig. 6.1. Map of the study area, including the digital elevation model (DEM) and soil units

- (d) Dp: Typic Dystrandept (pseudo-silty medial isothermic)
- (e) Dv-Dm: Typic Hydrandept (pseudo-silty thixotropic isomesic) - Typic Dystrandept (pseudo-silty medial isomesic)

The Ck and Cf soils include the typical compound soils below the Páramo that exhibits the typical 'Cangahua' (Zebrowski, 1997). Quantin (1997) defines 'Cangahua' as volcanic soils hardened by atrophic erosion limiting seriously the agricultural production. In the study area the 'Cangahua' is usually found at 70 cm in Cf soil unit and at 40 cm in Ck soil units. In general terms, the area has highly fertile soils resistant to soil erosion and is one of the major potato growing areas of the country. The Hf soil unit corresponds to buried soils deeply altered without significant restrictions for agricultural activities. Crissman et al. (1998) described in

detail the agricultural system dominated by the production of potatoes and milk, which are developed on steep hillsides. However, crops like wheat, maize, beans, faba beans, barley, peas and some Andean root crops are also components of the cropping systems. Part of the highest elevations constitute part of the El Angel Ecological Reserve since 1992 with no agricultural or livestock activities and mostly undisturbed soils.

### 6.2.2 Data collection

Four automatic weather stations registering maximum and minimum temperatures, rainfall, and incoming solar radiation were installed in the study area operating for 3 years. These weather stations were located at: Capuli bajo (0°35'07" N, 77°49'44" W, and 2831 meters a.s.l.), Cristobal Colon (0°36'59" N, 77°48'24" W, and 2821 meters a.s.l.), Chutan alto (0°37'59" N, 77°51'27" W, and 3181 meters a.s.l.), and Chicho (0°39'13" N, 77°49'51" W, and 3261 meters a.s.l.). Monthly variation of minimum and maximum temperatures and rainfall for each weather station are shown in Figure 6.2. Sequences of infrared images from the GOES satellite were used to derive the main wind direction in the study area at daily time steps (based on cloud movement).

Soil data from two previous soil studies in the study area (van Soest, 1998 and Lopez, 2000) were used. During these studies, 190 geo-referenced soil samples were collected and analyzed in 1997, 1999, and 2000. Table 6.1 present summary statistics of these soil samples (MAG and ORSTOM, 1980).

A digital elevation model (DEM) has been derived from the 1:50,000 topographic maps with a cell size of 20 x 20 m. (Figure 6.1). From this DEM, maps with topographic indicators were generated for further analysis including slope, aspect, profile and plane curvature (Pellegrini, 1995) and the topographic wetness index (TWI) (Jenson and Domingue, 1988; More et al., 1993) to serve as input for further analysis. The aspect was

transformed into two indicators. The sinus of the aspect expresses the east-west (longitudinal) effect and the co-sinus expresses the north-south, latitudinal effect. A database was established that includes the soil observations and the topographic variables for the respective locations.

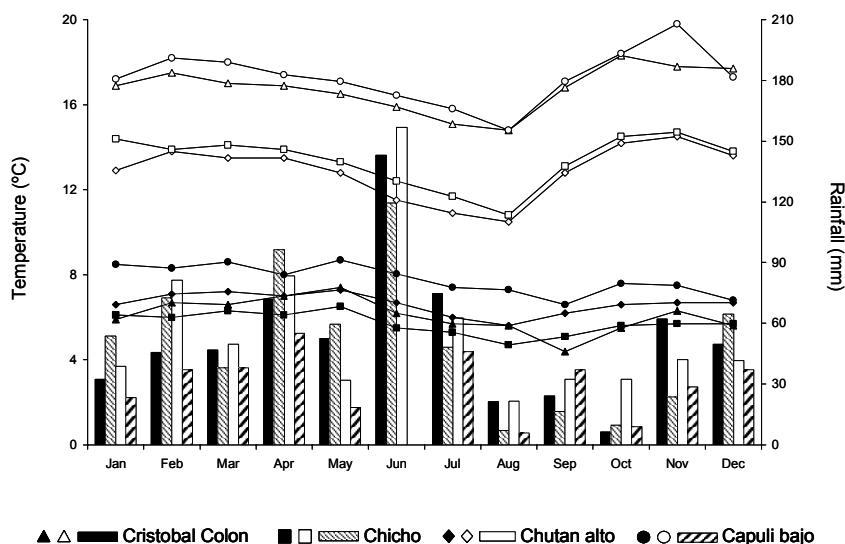


Fig. 6.2. Variation in minimum and maximum temperatures and rainfall for the four weather stations. Solid and empty marks correspond to minimum and maximum temperatures respectively while bars correspond to monthly rainfall.

**Table 6.1:** Summary statistics of soil properties across the 190-geo-referenced samples, stratified according to the soil units in the study area

	Organic matter (%)	pH	Al <sup>+++</sup> +H <sup>+</sup>	P (ppm)	K (meq/100mg <sup>-1</sup> )	Total N (%)	Sand (%)	Clay (%)	Silt (%)
<b>Cf-Hf (n=45)</b>									
Avg.	6.3	5.5	1.1	65	0.86	0.37	44	28	28
Stdev.	3.0	0.4	0.7	50	0.60	0.15	7	9	8
<b>Ck-Cf (n=9)</b>									
Avg.	10.3	5.4	0.8	39	0.99	0.53	39	40	21
Stdev.	1.9	0.2	0.2	22	0.53	0.09	6	8	8
<b>Dp (n=57)</b>									
Avg.	10.7	5.2	1.3	56	0.65	0.59	41	34	25
Stdev.	3.7	0.4	0.6	50	0.36	0.20	8	14	11
<b>Dv-Dm (n=13)</b>									
Avg.	14.7	5.0	1.8	32	0.28	0.81	36	40	23
Stdev.	2.1	0.4	0.7	22	0.19	0.21	7	17	13
<b>Hf (n=65)</b>									
Avg.	9.2	5.5	1.1	63	0.81	0.54	44	35	21
Stdev.	3.8	0.6	0.7	51	0.40	0.23	9	11	9

### 6.2.3 Weather data interpolation and climate maps

Incoming solar radiation and minimum and maximum temperatures were used to calculate the Bristow-Campbell coefficients to the study area. The Bristow-Campbell model (1984) estimates incoming solar radiation ( $H_i+h_i$  in  $\text{MJ m}^{-2} \text{ day}^{-1}$ ) on the basis of extraterrestrial incoming solar radiation ( $H_o$  in  $\text{MJ m}^{-2} \text{ day}^{-1}$  calculated as a function of the ratio between actual and mean sun–Earth distance, latitude, solar declination and solar angle at sunrise) and the difference between maximum and minimum temperatures  $T$  ( $^{\circ}\text{C}$ ):

$$(H_i + h_i) = H_o a_B [1 - \exp(-b_B \Delta T^{c_B})]$$

In Chapter 2 this model was selected for an application in the central Andes with similar meteorological and topographic conditions. Calibration of this model allows us to interpolate incoming solar radiation on the basis of topographic differences. Because of the equatorial location of the study area, there is a low variation of the incoming solar radiation in the upper part of the atmosphere. As a result clouds in the atmosphere will cause the largest differences in the incoming solar radiation at the earth surface. Therefore, the Bristow-Campbell coefficients  $a_B$ ,  $b_B$  and  $c_B$  were estimated separately for dry and wet conditions.

DEM, slope, and aspect maps were reduced in resolution to a pixel size of 100x100 m according to the previous experiences of the interpolation process performed in a similar area located in the northern Andes of Peru. Using the interpolation model developed in Chapter 3 to interpolate maximum and minimum temperatures and incoming solar radiation and Chapter 4 to interpolate rainfall in mountainous areas, daily maps of these four variables were generated at the same resolution of the aggregated DEM.

The interpolation of maximum and minimum temperatures is based on the fact that net radiation is zero twice a day (Peixoto and Oort, 1992). Taking into account the variation in topography across weather stations, functions of atmospheric transmissivity ( $\tau$ ) and atmospheric irradiation ( $F_{LW}^{\downarrow}$ ) are determined (Chapter 2). These functions are applied spatially to estimate maximum and minimum temperatures according to the topography of each pixel after a new radiation balance on each. Rainfall interpolation is based on the Digital Mountain Wave Model (DMWM) describing the three-dimensional cloud-route, determined by the interaction between topography and the main wind direction, and the processes involved in the formation of rainfall. Parameters of the DMWM were setting as: wave amplitude ( $\alpha = 0.5$ ), wavelength ( $\lambda = 1$ ) and shift peak angle ( $\delta = 5^{\circ}$ ).

On the basis of the daily interpolations of the four meteorological variables, average monthly and yearly maps were calculated. In addition maps with monthly temperature swing, variation in monthly variables, the square and square root of the variables (to deal with non-linearity) were calculated.

#### 6.2.4 Development and validation of stepwise multiple regression models

An overlay of the soil sampling locations with the climate maps provide a new database containing soil, topographic, and climatic data. The database was stratified on the basis of the five main soil units. Correlation matrices for each soil unit were calculated as a first approach to establish relationships between the soil characteristics and potential predictors. Two sets of stepwise multiple regression models (SMRMs) between the soil characteristics and the topographic and climatic were generated using a stepwise analysis. The first one was developed using only DEM related parameters as predictors, while the second one was performed including the interpolated climate data. Given the goal of the study to explore the

effect of high-resolution climate data, interaction factors among the predicting variables were not included.

The validation was done on the basis of a cross validation analysis comparing each individual value estimated by the SMRM after being extracted from the sample with the observed one. The coefficient of determination ( $R^2$ ), bias, and the median square error (MSE) were calculated and a residual analysis was performed. Comparisons among the performances of the stratified linear regression models using altitude as predictor and the two sets of SMRMs constitute the added value of including the new high resolution climate data instead of using the more traditional methods to estimate spatial distribution of soil properties. Effects of spatial autocorrelation were analysed to determine the spatial dependency of the SMRMs outcomes (Anselin and Griffith 1988; Overmars et al. 2003).

### **6.3 Results and discussion**

#### **6.3.1 Weather data interpolation and climate maps**

The validated values for the Bristow-Campbell are presented in Table 6.2. Figure 6.3 shows the four interpolated climate maps of average annual minimum and maximum temperatures, incoming solar radiation and rainfall. The relatively flat areas in the south-east (corresponding to the soil units Cf-Hf, Hf, Ck-Cf and the lower parts of Dp) exhibit little variation in temperatures and radiation. Most variation occurs in the steeply dissected areas (the soil units Dv, Dv-Dn, Dm and Dv-Dm). The highest parts of the

**Table 6.2:** Monthly coefficients of the Bristow-Campbell model (Bristow and Campbell, 1984) for Carchi under dry and wet conditions.

Month	Dry conditions			Wet conditions		
	$\alpha_B$	$b_B$	$c_B$	$\alpha_B$	$b_B$	$c_B$
January	0.56	6.35	0.56	0.32	4.69	0.30
February	0.68	9.72	0.47	0.49	7.34	0.42
March	0.63	8.82	0.31	0.58	8.44	0.37
April	0.85	10.57	0.38	0.55	7.48	0.48
May	0.80	8.34	0.34	0.52	7.20	0.55
June	0.72	7.74	0.18	0.50	6.06	0.33
July	0.78	8.34	0.36	0.63	6.52	0.38
August	0.63	6.67	0.33	0.52	5.70	0.41
September	0.75	9.23	0.32	0.61	7.87	0.36
October	0.82	10.29	0.42	0.79	9.34	0.43
November	0.73	10.00	0.53	0.58	8.34	0.29
December	0.69	8.53	0.32	0.56	6.78	0.48

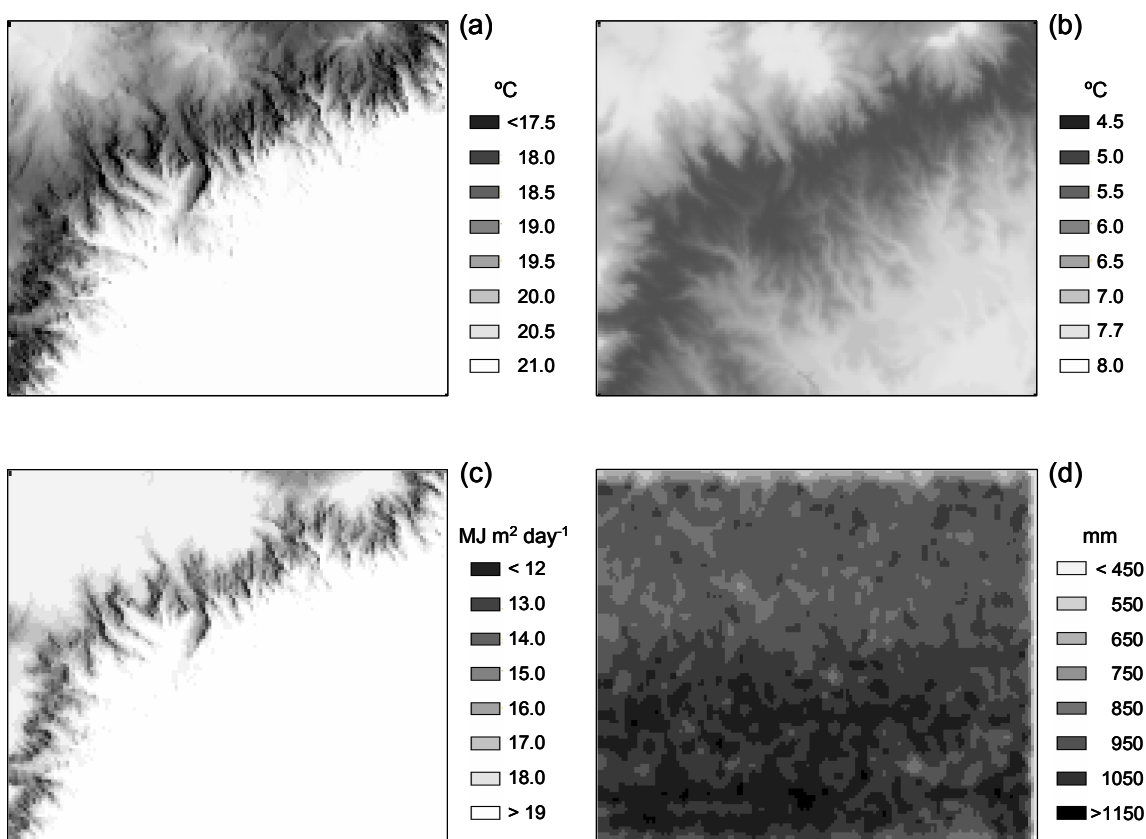


Fig. 6.3. Interpolated maps of climate. (a) annual average of maximum temperature, (b) annual average of minimum temperature, (c) annual average of incoming solar radiation, and (d) total annual rainfall.

watershed show a large temperature swing that can probably explained by the lower water vapor contents. The spatial variability in weather conditions increases during the solstices in summer and winter (June and December respectively in the northern hemisphere) due to the farthest position of the sun from the equatorial line. The opposite effect is found during the equinoxes where the sunbeams are perpendicular to the equatorial line producing the lowest spatial variation of the maximum temperature. Average annual rainfall (Figure 6.3d) does not show a clear relationship with the digital elevation model. Despite some boundary effects outside the actual watershed, a general north-south trend seems to exist. During the year dominant wind directions changes between the north, north-east, east, south-east, and south. Although, with every wind direction a specific DMWM correlates strongly with the digital elevation model, the effect averages out in the mean annual rainfall.

Table 6.3 shows the summary statistics for the different soil units. The table confirms the earlier observations with respect to the correlation between topographic variation, incoming solar radiation and temperature. They also indicate large differences in both topography and climatic conditions between the soil units. Given the importance of climate and topography as soil forming factors in combination with the relatively small differences in parent material and age this is not surprising. Key question that remains is whether the variation in climate and topography explains the soil differences within the different soil units.



**Table 6.3:** Summary statistics of topographic and climatic variables for the 190 geo-referenced samples stratified according to the soil units in the study area

	Soil unit									
	Cf-Hf		Ck-Cf		Dp		Dv-Dm		Hf	
Altitude (m.a.s.l.)	2897	(59)	3100	(47)	3126	(99)	3268	(97)	2878	(103)
Slope (degree)	12	(7)	14	(10)	13	(6)	19	(9)	8	(7)
Sine (Aspect)	0.1	(0.7)	0.2	(0.5)	0.2	(0.7)	0.3	(0.7)	0.4	(0.6)
Cosine (Aspect)	-0.1	(0.7)	-0.3	(0.9)	-0.3	(0.6)	-0.5	(0.4)	-0.3	(0.6)
Profile curvature	0.02	(0.05)	0.03	(0.07)	0.01	(0.03)	0.02	(0.04)	0.02	(0.04)
Plane curvature	-0.02	(0.05)	-0.03	(0.07)	-0.01	(0.03)	-0.02	(0.04)	-0.01	(0.04)
Wetness index	5.4	(4.1)	8.9	(12.8)	6.0	(5.5)	19.9	(31.7)	151.0	(965.3)
Inc. solar radiation	19.2	(24.5)	19.2	(25.0)	19.0	(0.9)	18.0	(1.8)	19.1	(0.4)
Max. temperature	24.5	(1.4)	25.0	(1.6)	23.5	(1.8)	21.5	(2.9)	24.5	(1.4)
Min. temperature	6.7	(0.2)	6.1	(0.2)	6.0	(0.2)	5.8	(0.1)	6.8	(0.3)
Annual rainfall	825	(54.8)	807	(55.2)	767	(72.9)	710	(88.1)	757	(76.6)

\* Altitude in meters above sea level, incoming solar radiation in  $\text{MJ m}^{-2} \text{ day}^{-1}$ , temperature in  $^{\circ}\text{C}$  and rainfall in  $\text{mm yr}^{-1}$ .

### 6.3.2 Soil organic matter

Table 6.4 shows the correlation coefficients between soil organic matter and the topography and climate variables stratified by soil unit. For climate we analyzed average annual figures (both average, standard deviation, maximum and minimum) as well as the correlations with the individual months. In the table we only present the highest correlation coefficient that was obtained for these monthly figures. Although general relations between soil organic matter contents in relation to temperature, rainfall, aspect and altitude are known, the different soil units seem to react very differently. Altitude is found to be especially important in Dp whereas in the other units aspect and curvature are more important. In addition, monthly climatic variables generally give better results than the average annual values.

**Table 6.4:** Correlation coefficients of soil organic matter versus topographic and climatic variables. Highest correlations are emphasized in bold.

	Soil unit				
	Cf-Hf	Ck-Cf	Dp	Dv-Dm	Hf
<b>Topographic variables</b>					
Altitude	0.217	0.071	<b>0.532</b>	-0.061	0.215
Slope	-0.027	-0.228	-0.182	-0.043	-0.049
Aspect	0.027	<b>-0.729</b>	-0.007	-0.180	0.214
Profile curvature	0.235	-0.373	0.060	-0.106	0.036
Plane curvature	-0.176	0.373	-0.007	<b>-0.413</b>	0.092
Topographic wetness index	0.032	0.556	0.145	-0.109	-0.022
Easting	0.080	0.508	0.116	0.055	0.144
Northing	<b>0.510</b>	0.016	0.364	-0.285	<b>0.255</b>
<b>Climatic variables</b>					
Incoming solar radiation					
Annual average	0.359	-0.351	-0.293	-0.031	0.101
Standard deviation	-0.302	0.655	0.262	0.032	0.000
Maximum	0.000	0.000	0.073	-0.101	0.074
Minimum	0.237	0.000	-0.290	-0.036	0.083
Max correlation for month*	<b>0.449</b>	-0.610	-0.375	-0.101	0.218
Maximum temperature					
Average	-0.125	-0.617	-0.129	0.263	-0.199
Standard deviation	0.125	-0.117	0.072	0.024	-0.189
Maximum	-0.125	-0.637	-0.009	0.528	-0.198
Minimum	-0.125	-0.594	-0.150	0.209	-0.196
Max correlation for month*	-0.125	-0.647	-0.397	0.582	-0.236
Minimum temperature					
Average	-0.325	0.300	-0.502	0.269	-0.229
Standard deviation	-0.291	0.250	-0.505	0.327	-0.158
Maximum	-0.305	0.271	-0.489	0.110	-0.244
Minimum	-0.344	0.270	0.355	-0.243	-0.148
Max correlation for month*	-0.445	0.417	<b>-0.527</b>	0.321	-0.261
Rainfall					
Total annual rainfall	0.136	0.046	-0.094	0.105	-0.256
Standard deviation	0.308	0.062	-0.020	0.039	-0.229
Maximum	0.229	0.090	-0.043	0.016	-0.204
Minimum	0.026	0.156	-0.120	0.127	-0.236
Max correlation for month*	0.229	0.175	-0.250	0.189	<b>-0.347</b>
Temperature swing					
Average	0.158	0.540	-0.501	0.166	0.150
Standard deviation	-0.278	-0.048	-0.359	0.092	-0.205
Maximum	-0.100	-0.599	-0.353	0.431	-0.203
Minimum	-0.048	-0.660	-0.029	0.195	-0.093
Max correlation for month*	-0.100	<b>-0.702</b>	-0.399	<b>0.598</b>	-0.208

\* The maximum correlation indicates the highest correlation coefficient that was found of all months

Table 6.5 shows the SMRMs resulting from the performed stepwise analysis to predict soil organic matter with a 5% and 10% as significance level. Despite the fact that the number of samples plays an important role in the significance estimation, the coefficients of determination levels (higher in the Ck-Cf and Dv-Dm unit soils with a lower number of soil samples), the  $R^2$  demonstrate that relations to predict soil organic matter have all increased when adding the climate predictors to the more traditional methods. Specifically in the unit Dp, altitude has the best correlation compared with other predictors, this relationship is improved with a 10% level of significance by a relationship using swing temperature as predictor. In all cases, the standard error of the estimate is lower to the standard deviation of the soil organic matter on each soil unit (Table 6.1). It is relevant to notice that for all relationships in Table 6.5, a climatic variable is used as an independent predictor.

The coefficients of determination, bias, and MSE at different significance levels ( $\alpha = 0.05$  and  $0.10$ ) as a measurement of the validation and the cross-validation are presented in Table 6.6. The results show that the regression models perform well for most soil units.

Table 6.7 shows the evolution of the coefficient of determination from the stratified linear regression model to the SMRMs including climate data. Changes in  $R^2$  can be interpreted as the gain in explanatory power due to the additional information involved as well as the importance of the predictors as soil forming factors. The residuals of the SMRMs including climate data were tested for spatial autocorrelation, obtaining a pure nugget model corresponding to a total lack of spatial dependency and spatial structure. This confirms the good performance of the SMRMs in explaining the spatial variation in SOM contents in the study area.

**Table 6.5:** Significance level, coefficient of determination, standard error of the estimation, standardized coefficients, and list of independent variables included in the SMRMs stratified according to the different soil units.

Significance Level ( $\alpha$ )	Coefficient of determination ( $R^2$ )	Std. Error of the estimate	Standardized coefficients ( $\beta$ )	List of topographic and climatic variables
<b>Cf-Hf</b>				
0.05/0.10	0.661	1.8782	0.279	Northing
			0.804	Standard deviation of rainfall
			-0.487	Rainfall – Nov.
			0.582	Incoming solar radiation – Dec.
			-0.333	Incoming solar radiation – Apr.
			0.206	Profile curvature
<b>Ck-Cf</b>				
0.05	0.833	0.9009	-0.927	Aspect
			0.583	Minimum temperature – Dec.
0.10	0.942	0.5959	-1.123	Aspect
			0.549	Minimum temperature – Dec.
			0.391	Incoming solar radiation – Sep.
<b>Dp</b>				
0.05	0.283	3.1460	0.532	Altitude
0.10	0.410	2.9071	0.673	Swing temperature – Aug.
			-0.611	Ann. aver. swing temperature
<b>Dv-Dm</b>				
0.05/0.10	0.829	0.9850	-7.563	Swing temperature – Oct.
			1.745	Altitude
			9.413	Maximum temperature – Oct.
<b>Hf</b>				
0.05	0.306	3.2621	0.760	Incoming solar radiation – Aug.
			-0.328	Slope
			0.340	Easting
0.10	0.656	2.4177	0.854	Incoming solar radiation – Aug.
			0.538	Easting
			-3.800	Minimum temperature – Jun.
			2.719	Minimum temperature – Jan.
			0.520	Standard deviation of swing temperature
			1.548	Minimum temperature – Apr.
			-1.190	Minimum temperature – Oct.
			-0.462	Incoming solar radiation – Apr.

**Table 6.6:** Summary statistical parameters during the validation stratified according to the soil units

	<b>Significance level of the model (<math>\alpha</math>)</b>	<b>Coefficient of determination (<math>R^2</math>)</b>	<b>Bias</b>	<b>Median square error (MSE)</b>
<b>Cf-Hf</b>	0.05/0.10	0.510	0.32	4.4
<b>Ck-Cf</b>	0.05	0.565	-0.68	1.4
	0.10	0.837	-0.10	0.5
<b>Dp</b>	0.05	0.233	0.12	<b>10.2</b>
	0.10	0.330	-0.11	<b>9.0</b>
<b>Dv-Dm</b>	0.05/0.10	0.653	-0.77	1.4
<b>Hf</b>	0.05	0.152	0.40	<b>12.3</b>
	0.10	0.447	-4.30	<b>8.4</b>

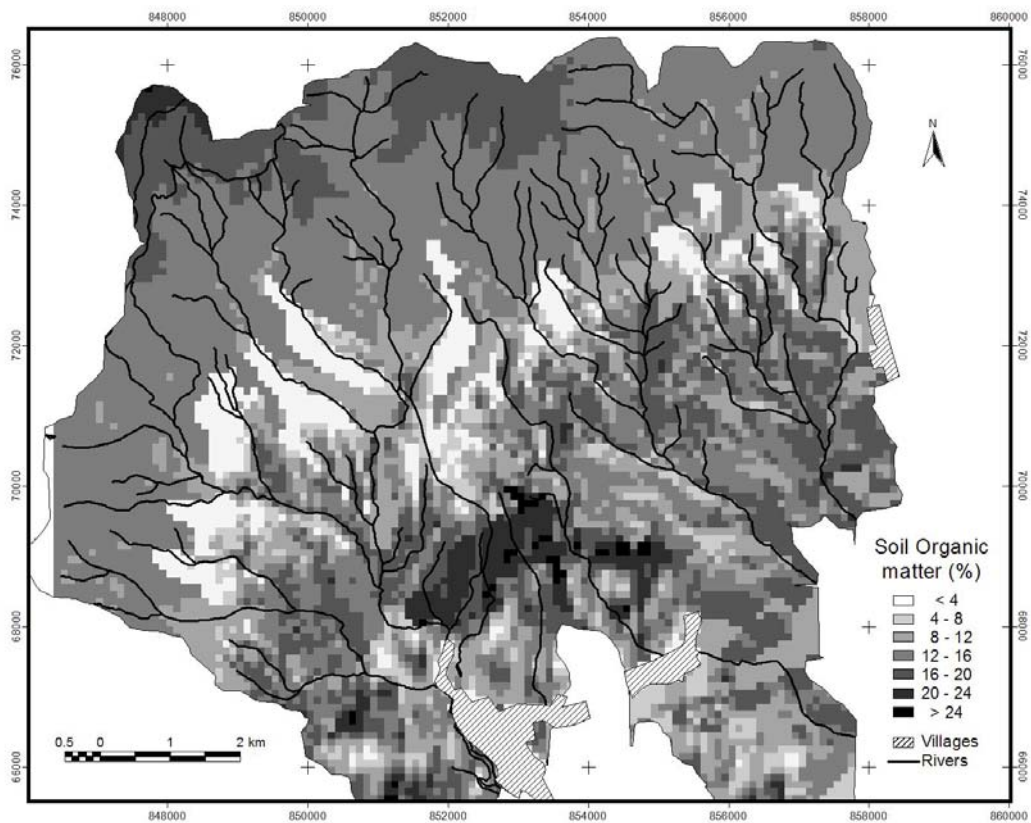
**Table 6.7:** Changes in the coefficient of determination according to the independent variables used to predict the spatial distribution of SOM

<b>Soil unit</b>	<b>Altitude</b>	<b>Topographic</b>	<b>Topographic and Climatic</b>
<b>Cf – Hf</b>	0.047	0.321	0.661
<b>Ck – Cf</b>	0.005	0.532	0.942
<b>Dp</b>	0.283	0.283	0.959
<b>Dv – Dm</b>	0.004	0.004	0.829
<b>Hf</b>	0.046	0.108	0.961

The models for the different soil units can now be applied to finalize our digital soil mapping exercise. The model application resulted in the map of SOM for the study area presented in Figure 6.4. Throughout the study area high soil organic matter contents are presented corresponding to the Andic character of the soils in the region. The few locations that showed relatively low SOM values (<2%) are found in the Dp soil unit close to the boundary with the Dv-Dm soil unit. In this area very steep slopes (>25°) are found on the sides of the rivers. This has resulted in land slides that removed all the topsoil exposing the sub-soil with lower SOM contents. As described in section 6.3.1, the steeply dissected character in the Dp and Dv-Dm soil units also played an important role in maximum temperatures caused by differences on incoming solar radiation. Table 6.5 shows that these soil units are the only ones using maximum temperature as predictor

variable to estimate SOM. The maximum levels of SOM are found in the highest area of the watershed where temperatures are relatively low and rainfall is high. The low temperature results in low mineralization rates of soil organic matter. In addition, there are no agricultural activities in this area. The lack of tillage conserves even more the SOM pool. The humid conditions throughout the year result in a constant vegetative production. In few locations even organic soils are found.

Fig. 6.4. Map of soil organic matter obtained because of the application of the findings SMRM's in the study area.



### 6.3.3 Other soil characteristics

SOM is probably the textbook example to illustrate the role of climate as a soil forming factor. Typically, the role of climate on other soil properties is less apparent. The results of the methodology to other soil characteristics (pH, P, K, Total N, soil texture) with the topographic and climatic predictors are presented in Table 6.8. The results are expressed in terms of significance levels of the developed SMRMs, the coefficient of determination and the standard error of the estimation.

Different soil properties are explained by different topographic and climatic variables. Admittedly we have to realize that the different explanatory variables are not independent. Nevertheless, we see that several models explain very well the variation in the different mapping units. Different predictors have different relative levels of importance according to the soil unit, what might be explained by the different physical, chemical, and biological processes involved in the actual evolution of each soil unit. Weathering is likely to explain most of the relationships between climate and the pH, P, K, and texture (Jongmans et al., 1991). Ecopedological processes, on the other hand are likely to explain the relationships between climate and soil organic matter and total N. Especially the effects of rainfall, minimum temperature, and swing temperature are important for the latter (van Breemen and Buurman, 1998; Zehetner et al., 2003). In the past, the lack of detailed spatial and climatic information made it virtually impossible to demonstrate these relationships at detailed scale levels. The importance of the climatic variables in the different regression models demonstrates the relative importance of these variables to explain the soil forming processes in general terms. It is important to notice that incoming solar radiation is also included in this relation because of the high altitude of the study area (low optical thickness) and the low water vapor contents in the atmosphere, which mostly explains daily changes in temperature and soil moisture regimes at high altitudes. If we aggregate the results of the different regression models

for the study area we see that climatic factors explain 41% of the total variation in soil properties whereas 19% is accounted for by topographic factors. These relative percentages will change under different soil orders depending on the different sources of spatial and temporal variations taking into account during soil classification (USDA & NRCS, 1998). Nevertheless they underline the importance of the analysis.

Time as a soil forming factor, can not be only understood as a cumulative factor, but also must be viewed in the context of the seasonal-cycles within the same solar cycle. Soil moisture and temperature regimes described by USDA & NRCS (1998) can be disaggregated using more detailed information as presented in this chapter. As an example, total rainfall is not enough to describe the spatial variability of processes effects involving soil forming. Rainfall events due to different climate systems in different seasons are characterized by different amounts and intensities of available water. Several times, the directions from where the storm is coming are relevant as well. Especially in mountainous areas, the interaction between the exposition degree of determined slope and from where the rainfall event is coming on, it is an important issue. These interactions increase the predictability of topographic indexes like the topographic wetness index and profile and plane curvatures.



**Table 6.8:** Results for SMRMs explaining different soil properties on the basis of the topographic and climatic variables

	$\alpha$	R <sup>2</sup>	MSE	Explanatory variables
<b>Cf-Hf</b>				
pH	0.10	0.08	0.43	Slope
Total N	0.10	0.53	0.11	Profile curvature, radiation, rainfall
P	0.05	0.14	47.10	Minimum temperature
K	0.05	0.11	0.58	Radiation
Sand	0.10	0.53	5.28	Slope, Minimum temperature, rainfall
Clay	0.10	0.38	7.38	Wetness index, radiation, rainfall
Silt	0.05	0.34	6.52	Altitude, minimum temperature, temperature swing
<b>Ck-Cf</b>				
pH	0.05	0.82	0.11	Rainfall
Total N	0.10	0.32	0.08	Minimum temperature
P	0.05	0.58	15.39	Maximum temperature
K	0.10	0.90	0.20	Profile curvature, rainfall
Sand	0.05	0.71	3.49	Maximum temperature
Clay	0.10	1.00	0.00	Slope, wetness index, minimum temperature, rainfall
Silt	0.05	0.99	0.63	Aspect, profile curvature, wetness index, maximum temperature
<b>Dp</b>				
pH	0.05	0.15	0.36	Swing temperature
P	0.10	0.37	41.04	Altitude, plane curvature, rainfall
K	0.10	0.39	0.29	Plane curvature, temperature swing, rainfall
Total N	0.05	0.31	0.17	Swing temperature
Sand	0.10	0.54	6.09	Minimum temperature, rainfall
Clay	0.10	0.73	8.06	Curvature, minimum temperature, rainfall
<b>Dv-Dm</b>				
pH	0.05	0.90	0.15	Aspect, plane curvature, rainfall
P	0.10	0.93	7.58	Aspect, curvature, minimum temperature
K	0.05	0.48	0.14	Plane curvature
Total N	0.05	0.99	0.03	Plane curvature, minimum temperature rainfall
<b>Hf</b>				
pH	0.05	0.51	0.38	Profile curvature, rainfall
P	0.05	0.21	44.43	Aspect, temperature swing, rainfall
K	0.10	0.64	0.26	Aspect, wetness index, radiation, minimum temperature, rainfall
Total N	0.10	0.18	0.21	Radiation
Sand	0.05	0.27	8.48	Profile curvature, radiation, maximum temperature
Clay	0.10	0.29	10.30	Profile curvature, maximum temperature, rainfall

## **6.4 Conclusions**

The use of spatial and seasonal disaggregated information of climate significantly improves the spatial predictability of soil organic matter and other soil characteristics in volcanic ash soils in the Andes demonstrating that soil variability within soil units can be explained by climatic differences. The use of these secondary data supports the refinement of the usually applied altitude-temperature or altitude-rainfall relationships. The combined use of different soil forming factors can easily explain most of the spatial variability in soil organic matter and related soil characteristics. This is supported by the rapid advances in the field of pedometrics and digital soil mapping. Increased predictability of climate variables as well as the related soil characteristics will give a new approach to environmental modelers often facing general data paucity. Finally, one should realize that the study area was an ideal case where climate is likely to govern soil variation. In other regions, one may have to include other soil forming factors as well.

## **Acknowledgements**

The present work is supported by the United States Agency for International Development (USAID), through its Soil Management Collaborative Research Program (SM-CRSP), financed a project entitled 'Tradeoffs in Sustainable Agriculture and the Environment in the Andes: A Decision Support System for Policy Makers' (Grant # 291488).

## Chapter 7

---

### **The effect of the resolution of climate and soil data on a land use study in the Ecuadorian Andes**

Researchers in agricultural production systems often have to face a lack of climate and soil data, especially when in areas with high spatial variability. Traditional approaches like agro-climatic zones governed by *e.g.* relations with altitude, and soil maps with large delineated areas ignore a large part of the existing variability. The effect of generalizing weather station data as well the effect of using representative soil profiles for large mapping units in land use studies is not very well known. Advances in interpolation models of climate and soil offer new opportunities to the researchers using detailed information and derive more detailed results. However, the generation of more accurate inputs of climate and soil is time consuming and represents a big investment in resources if we rely on traditional inventorization techniques. Ideally, the relationship between the level of detail of the input data with the quality of output data is known and a threshold can be set by the researcher. The objective of this paper is to measure the effects of different spatial resolution of climate and soil on modeling agricultural production systems. We used the Tradeoff Analysis System to model agricultural systems in the Ecuadorian Andes. Climate and soil data are key inputs into the Tradeoff Analysis System to model the expected or, so-called, inherent productivity of potatoes and the effect of management on carbofuran leaching. Traditional agro-climatic zones and soil units were confronted with new methods of interpolation producing continuous surfaces of climate and soil characteristics. Histograms of inherent productivity, tradeoff curves between net returns and carbofuran leaching, cumulative probabilities of carbofuran leaching at different policy potato-price, and maps of carbofuran leaching using different levels of input data were performed. Climate and soil used as inputs to modeling agricultural production systems in the study area shows different effects on the different outputs. Aggregated tradeoff curves are not significantly affected by increasing the spatial input resolution, however when site-specific outputs are analyzed, quality in the outputs increased significantly.

Based on: Baigorria, G.A., J.J. Stoorvogel, and A.Veldkamp The effect of the resolution of climate and soil data on a land use study in the Ecuadorian Andes.

© Submitted. Agriculture, Ecosystems & Environment. March 2005.

## 7.1 Introduction

In every decision and every choice, there is a tradeoff between benefits and cost. In the case of agriculture this could reflect the benefit of food production against the environmental impacts. The Tradeoff Analysis System (Stoorvogel et al., 2001, 2004a) is developed implementing the integrated analysis of tradeoffs between different sustainability indicators dealing with the *e.g.* economic, environmental and health effects of agricultural systems. A recent application of the Tradeoff model in the Ecuadorian Andes forms the basis of this study (Stoorvogel et al., 2004b).

The application of regional land use models coincides with a tremendous demand for high quality data. Especially in mountain areas it is essential to get a description of the spatial variation in the growing conditions in terms of climate and soil data. Many efforts to capture the spatial variability of these inputs were performed (*e.g.* Van Soest, 1998; Lopez, 2000). However, these approaches were always based on traditional agro-climatic zones and soil units that are considered homogeneous and described by representative weather stations and representative soil profiles. New process-based interpolation models to estimate maximum and minimum temperatures, incoming solar radiation and rainfall distribution have been developed (Chapter 2,3, and 4). In addition, maps of soil organic matter (SOM), as well as other soil characteristics, have been developed to the study area using stratified stepwise multiple regression models using topography and climate as a predictors (Chapter 6).

All this new available information opens the possibility to explore in depth the effect of including higher resolution data into the tradeoff analysis model. Ideally one would come up with thresholds for the resolution of input data for a specific application of the Tradeoff Analysis Model. The objective of this paper is to measure the effects of using high spatial resolution of climate and soil in comparison to the traditional use of agro-climatic zoning

and soil mapping units. The comparison analysis is performed using two biophysical models: the SUBSTOR-potato (Ritchie et al., 1995) to estimate potato production and the PEARL model (Tiktak et al., 2000) to estimate carbofuran leaching. These models are integrated with econometric-process simulation model under the framework of the Tradeoff Analysis Model.

## **7.2. Study area**

The study area is located in the Ecuadorian Andes between 0°42' N, 78°30' W and 0°32' N, 77°30' W (Figure 7.1). The area ranges between 2700 to 3840 meters above sea level and covers a total area of 95 km<sup>2</sup>. From the ecological point of view, Troll (1968) classified the study area as 'Paramo-Andes' describing the equatorial regions of the northern Andes with rainfall throughout the year. The temperature regime typically corresponds to an equatorial climate with a small range in average monthly temperature but a daily swing of over 10°C. This large swing is due to the high altitude as well as its complex mountainous topography, even allowing for radiative frost events during clear night skies.

Zebrowski (1997) described the soils in this area as composed by two sources of volcanic ashes and pyroclastic products deposited until 1600 years BP. According to MAG and ORSTOM (1980), these young soils are classified as Andepts, suborder of Inceptisols (USDA-NRCS, 1998).

Crissman et al. (1998) provides a detailed description of the agricultural system developed on the steep hillsides and dominated by a potato-pasture rotation. Crops like wheat, maize, peas, barley, beans, broad beans, and some Andean root crops are components of the cropping systems. The highest parts in the watershed include the 'Paramo' area, constitutes part of the El Angel Ecological Reserve.

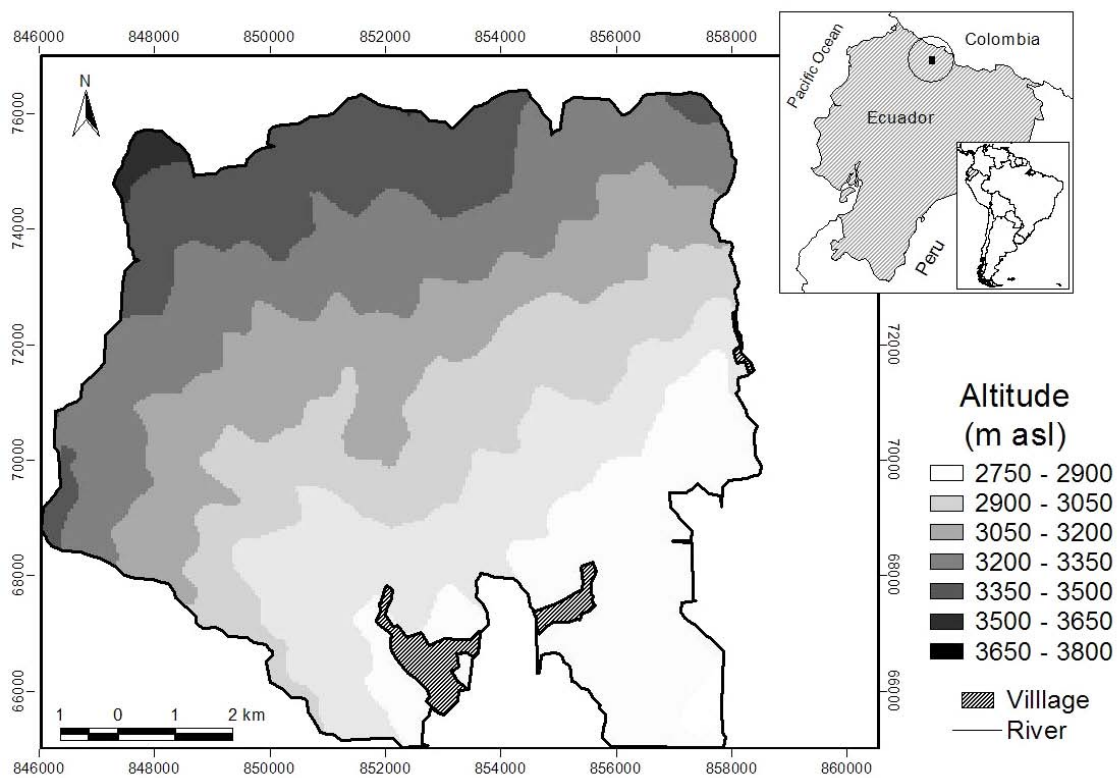


Fig. 7.1. Location map of the study area, including the digital elevation model (DEM).

### 7.3 Data and methods

#### 7.3.1 The Tradeoff Analysis System

The core of the tradeoff analysis is an economic simulation model based on supply and demand functions. Production economist typically specify these production functions in the general form  $q=f(x,z,e)$  where  $x$  is a vector of variable inputs,  $z$  is a vector of fixed inputs, and  $e$  is a vector of bio-physical factors. Vector  $e$  usually includes *ad hoc* indicators for climate and soil quality such as dummy variables for average rainfall during the growing season and soil types. The TOA system takes an alternative approach to econometric modeling that exploits the scientific knowledge embodied in biophysical process models. Climate and soils define the potential agricultural productivity of a specific location and crop

management (crops, cultivars, fertilization, irrigation, etc.) that determines the final output. Crop growth simulation models can be represented in stylized form as  $q=g(x,e)$  (Antle et al., 1998, Stoorvogel et al., 2004a). Defining an expected or average input use as  $x^*$ , it is possible to use the crop growth simulation models to estimate an expected or inherent productivity  $q^*$  for a specific location on the basis of weather and soil data as  $q^*=g(x^*,e)$ . Replacing the vector  $e$  in the production function including the calculated inherent productivity:  $q=h(x,z,q^*)$ . Substituting  $q^*$  we obtain  $q=h(x,z,g(x^*,e))$ , showing that this procedure yields a special case of the production function  $q=f(x,z,e)$  in which the biophysical variables  $e$  are weakly separable from the variable and fixed inputs  $x$  and  $z$ . Details of the economic simulation model are described by Antle et al. (1998) and Antle and Capalbo (2001). In this way, crop growth models are used to systematically transform site-specific biophysical data into an estimate of the spatial and temporal variation in expected or inherent productivity. Because of this site-specific information, the production functions are capable to simulate the relationships between land quality and management decision by the farmer.

The Tradeoff Analysis System goes one step further including also environmental impact models (Stoorvogel et al., 2004a). In previous studies the effect of the application of a commonly applied pesticide, carbofuran, on the environment and human health was studied (Antle et al., 1998, Crissman et al., 1998; Yangen et al., 2002, Stoorvogel et al., 2004b). Tax policies and different levels of integrated pest management (IPM) technologies were evaluated, analyzing the changes between potato and milk production, and its impacts on health because of agro-chemical leaching.

### 7.3.2 Farm survey data

Farm survey data for the Tradeoff Analysis Model are collected to estimate the land use and management decisions of farmers in the study region. A two-year dynamic survey was conducted for a sample of 40 farmers with 187 fields in the study area (Crissman et al., 1998). The survey includes site-specific production, planting, sprays, fertilization, and harvest dates, agro-chemical inputs (quantity and frequency), and price data. To ensure accuracy in measurement of farm management information, data need to be collected frequently enough to minimize farmer recall error to the degree possible. The survey for those fields was collected through a series of interviews not exceeding a month between visits during the production period being measured. Data registers for each field in cultivation were designed for the collection of labor, equipment and supplies data based on date-linked activities.

### 7.3.3 Climate and soil data

For both, climate and soil data, two spatial resolution levels were used. Combination of these levels generated the four input levels evaluated in the present paper:

- Low-resolution maps of climate and soil;
- High-resolution maps of climate and low resolution maps of soil;
- Low-resolution maps of climate and high resolution maps of soil; and
- High-resolution maps of climate and soil.



### 7.3.3.1 Low-resolution maps

The first work performed in the study area by Crissman et al. (1998) divided the region in four agro-climatic zones based mainly in the altitude (Figure 7.2<sup>a</sup>). Three weather stations around the study area (Table 7.1) were assigned to the different agro-climatic zones, using its daily data as representatives to all the polygon area that constitutes each agro-climatic zone. The weather stations are located at: San Gabriel (0°36'11" N, 77°49'11" W, and 2815 meters above sea level), El Angel (0°37'34" N, 77°56'38" W, and 3000 meters above sea level), and Voladero (0°41'00" N, 77°52'00" W, and 3620 meters above sea level).

**Table 7.1:** Main parameters ranging the weather stations in the study area

Weather station	Temperature (°C)		Rainfall (mm)	Incoming solar radiation (MJ m <sup>-2</sup> d <sup>-1</sup> )
	maximum	minimum		
Capuli bajo	17.5 <sup>c</sup>	7.8 <sup>c</sup>	no data	17.4 <sup>c</sup>
Chicho	13.4 <sup>c</sup>	5.7 <sup>c</sup>	910 <sup>c</sup>	14.6 <sup>c</sup>
Chutan alto	12.9 <sup>c</sup>	6.6 <sup>c</sup>	831 <sup>c</sup>	22.3 <sup>b,c</sup>
Cristobal Colon	16.8 <sup>c</sup>	6.1 <sup>c</sup>	875 <sup>c</sup>	22.4 <sup>b,c</sup>
El Angel <sup>a</sup>	16.3	7.0	976	23.3 <sup>b</sup>
San Gabriel <sup>a</sup>	17.2	7.0	944	22.8 <sup>b</sup>
Voladero <sup>a</sup>	no data	no data	1313	no data

<sup>a</sup> Belonging to the main weather station network

<sup>b</sup> Estimated by Bristow-Campbell model (1984) calibrated to the study area (Chapter 6)

<sup>c</sup> From three-year average measurements

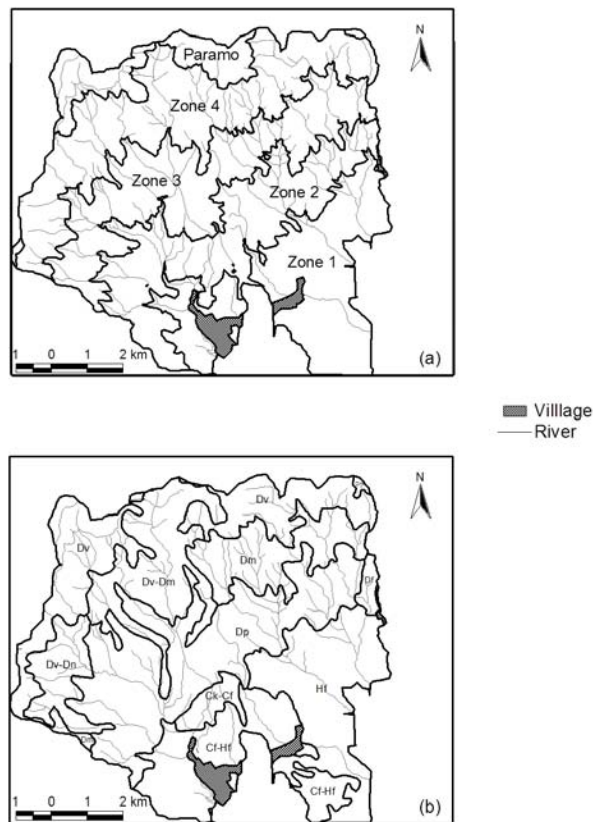


Fig. 7.2. Low resolution input maps for (a) climate and (b) soils.

A soil map performed by MAG and ORSTROM (1980) describe the main soil units in the study area (Figure 7.2b). These soil units are described as:

- Cf-Hf: Duriudoll (silty ashy halloysitic montmorillonitic isothermic) - Andic Argiudoll (silty ashy isothermic)
- Hf: Andic Argiudoll (silty ashy isothermic)
- Ck-Cf: Duriudoll (silty isothermic) - Duriudoll (silty ashy halloysitic montmorillonitic isothermic)
- Dp: Typic Dystrandept (pseudo-silty medial isothermic)

- Dv-Dm: Typic Hydrandept (pseudo-silty thixotropic isomesic) - Typic Dystrandept (pseudo-silty medial isomesic)

Physical and chemical descriptions of each soil unit (Table 7.2) were used as representative soil profiles to the area represented by the soil unit.

**Table 7.2:** Main soil characteristics ranging the different soil units in the study area.

Soil unit	Organic matter (%)	pH	P (ppm)	K (meq 100mg <sup>-1</sup> )	Total N (%)	Sand (%)	Clay (%)
Cf-Hf	6.3	5.5	65	0.86	0.37	44	28
Ck-Cf	10.3	5.4	39	0.99	0.53	39	40
Dp	10.7	5.2	56	0.65	0.59	41	34
Dv-Dm	14.7	5.0	32	0.28	0.81	36	40
Hf	9.2	5.5	63	0.81	0.54	44	35

### 7.3.3.2 High resolution

With the validated process-based interpolation models for maximum and minimum temperatures, incoming solar radiation, and rainfall (Chapter 2-4), daily maps of these four meteorological variables were created (Figure 7.3a and b). The interpolation of maximum and minimum temperatures are based on the fact that net radiation is zero twice in a day during these temperatures occurs. Taking into account variation in altitude, slope, and aspect (azimuth) across weather stations, functions of atmospheric transmissivity ( $\tau$ ) and atmospheric irradiation ( $F_{LW}^{\downarrow}$ ) are found. These functions are applied spatially to estimate maximum and minimum temperatures according to the topography of each pixel after a new radiation balance on each. Incoming solar radiation was estimated by the Bristow and Campbell model (1984) based on the incoming solar radiation in the top of the atmosphere, maximum atmospheric transmissivity for wet and dry conditions, and the difference between maximum and minimum

temperatures calculated on the step before. Rainfall interpolation is based on the Digital Mountain Wave Model (DMWM) describing the three-dimensional cloud-route determined by the interaction between topography and wind direction (obtained from sequences of infrared images from the GOES satellite) and the processes involved in the formation of rainfall. Parameters of the DMWM were setting as: wave amplitude ( $\alpha = 0.5$ ), wavelength ( $\lambda = 1$ ) and shift peak angle ( $\delta = 5^\circ$ ). After performed the interpolation of the four meteorological variables at daily steps, the obtained maps were aggregated at monthly and yearly level. The pixel size of these meteorological variables was set in 100 m x 100 m.

To produce these maps, four new automatic weather stations (Table 7.1) registering maximum and minimum temperatures, rainfall, and incoming solar radiation were added to the previous network during 3 years. These weather stations were located at: Capuli bajo ( $0^\circ35'07''$  N,  $77^\circ49'44''$  W, and 2831 meters above sea level), Cristobal Colon ( $0^\circ36'59''$  N,  $77^\circ48'24''$  W, and 2821 meters above sea level), Chutan alto ( $0^\circ37'59''$  N,  $77^\circ51'27''$  W, and 3181 meters above sea level), and Chicho ( $0^\circ39'13''$  N,  $77^\circ49'51''$  W, and 3261 meters above sea level).

The monthly aggregated maps of the four meteorological variables were joined to topographic variables as altitude, slope, aspect, profile and plane curvature and the topographic wetness index to predict the spatial variability of the soil characteristics (Chapter 6). Using stepwise multiple regression models stratified by the different soil units, new maps of soil characteristics were generated to the study area. The soil organic matter content map presented in Figure 7.3(c) was used as input in the present paper. Pixel size of the map was 100 m x 100 m.

#### 7.3.4 Model simulations

The inherent productivity of potatoes is simulated by the SUBSTOR model (Ritchie et al., 1995) previously calibrated to the Andes by Bowen et al. (1999). In this paper environmental impact is reflected by carbofuran leaching based on the LEACHP model (Wagenet and Hutson, 1989). In the study area, field experiments revealed site-specific data on pesticide degradation and sorption (Stoorvogel et al., 2004b).

The tradeoff curves represent the joint distribution of economic or environmental indicators and how they respond to changes in prices or other parameters (Stoorvogel et al. 2001). The tradeoff points were constructed by varying mean potato prices to change the incentives of farmers to produce potatoes or pasture for dairy cows. For comparing previous works of Crissman et al. (1998) and Stoorvogel et al. (2004a), with the present work, the same five tradeoff points were defined: reflecting changes in the mean potato prices: two with a 50% and 25% decrease, one with the observed potato prices, and two with a 25% and 50% increase.

The scenarios are defined in a way that represents the effect of certain changes in the socio-economic environment (possibly initiated by policy interventions) and the introduction of an alternative technology. Two scenarios were used in the present paper corresponding to a base scenario and the integrated pest management (IPM) technology. The base scenario is the current land allocation, land use management and prices. The IPM scenario is implemented as a lower probability that Carbofuran will be applied at a certain crop development stage and the number of farmers adopting this alternative technology. To each scenario, the econometric-process model was used to simulate land use management decisions and land allocation for five crop cycles. The simulations yielded data on inputs and outputs and the timing of pesticide application decision.

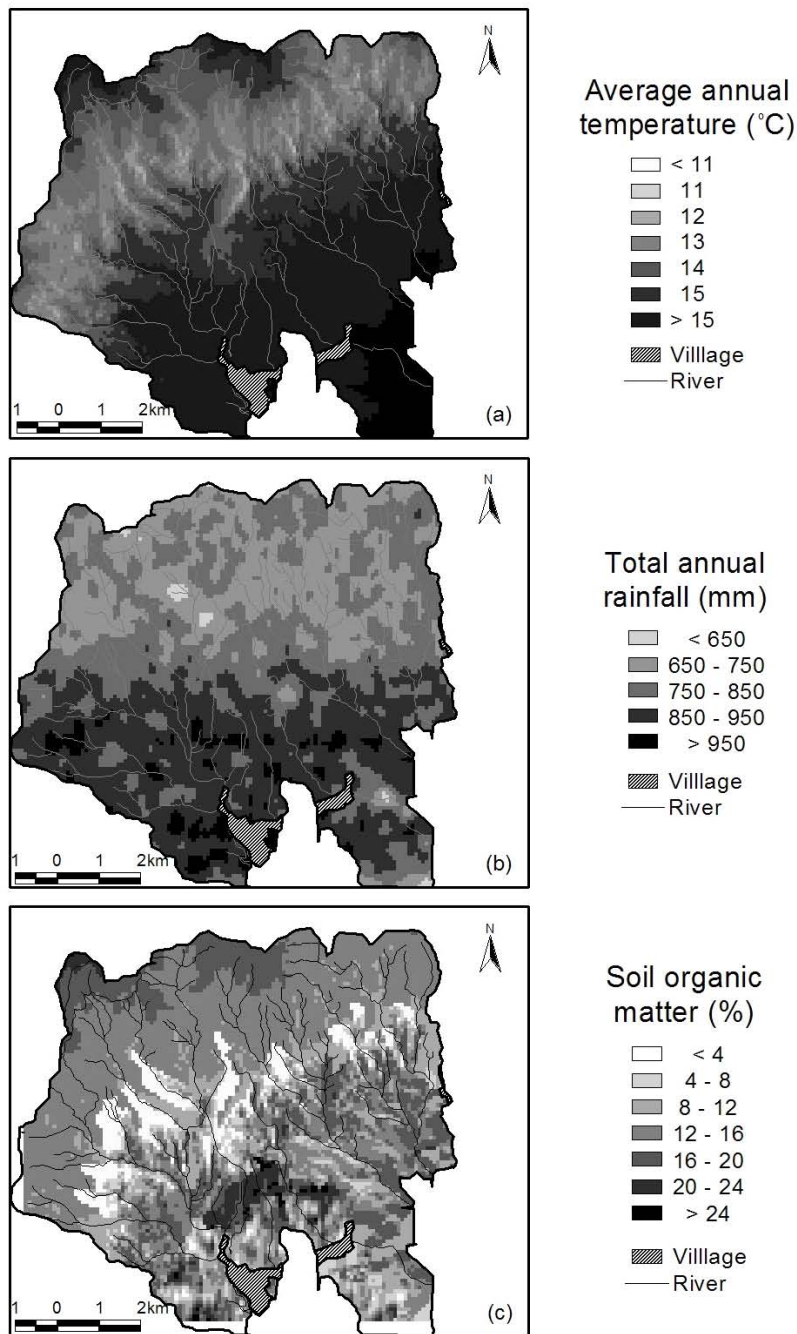


Fig. 7.3. High resolution input maps for (a) Average annual temperature, (b) Total annual rainfall, and (c) soil organic matter.

The analysis of the present paper is based on the comparison of different levels of spatial resolution of climate and soil, measuring the impacts on the estimation of the inherent productivity, but also on the tradeoff curves between leaching and net returns. Because the tradeoff curves represent certain levels of aggregation, also the raw data provided by the environmental models are analyzed in terms of cumulative probabilities and by mapping the results of decreasing carbofuran leaching due to change in scenarios at different input spatial resolutions.

#### **7.4 Results and discussion**

Figure 7.4 shows the most direct effect of the different spatial resolution of climate and soil on the expected or inherent productivity of potato production. Increasing the resolution of soil data (Figure 7.4c), produced a more homogeneous distribution of the dry matter than the base case, *i.e.* the case where we use low resolution soil and climate data (Figure 7.4a). Increasing the climate resolution (Figure 7.4b) generated an increased area with high potato dry matter; however, it also generated an increment in the areas with low inherent productivity. Figure 7.4(d) shows the intense effects in the increment of areas with low inherent productivity, as well as a better homogeneous distribution compared with Figure 7.4(b). Table 7.3 shows the main statistics of the inherent productivity, net returns and carbofuran leaching distributions around the survey fields. Table 7.3 is disaggregated by both scenarios and by the four-resolution level each. In all cases, the standard deviation of using high-resolution of climate and soil is larger than the standard deviations of using agro-climatic zones and soil units. However, using only climate interpolated or soil interpolated with soil units and agro-climatic zones respectively, does not show any general behavior.

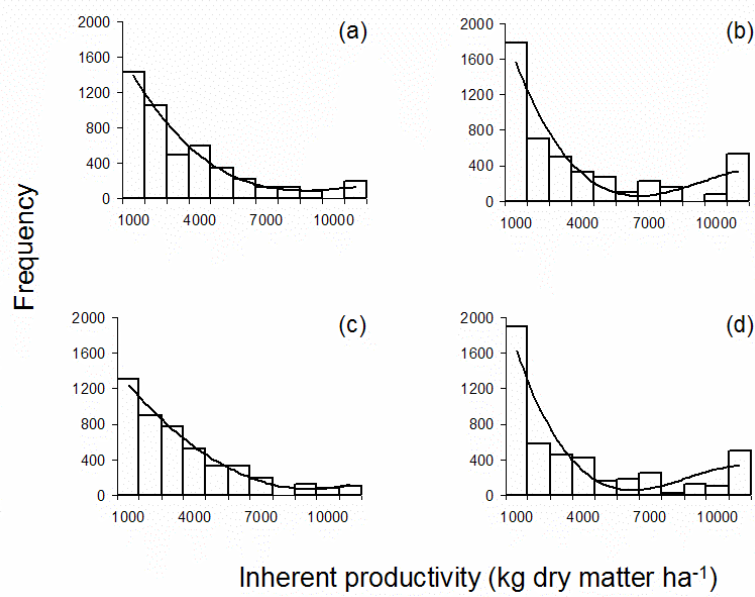


Fig.7.4. Histograms of inherent productivity simulated under different inputs levels of climate and soil. (a) Low resolution of climate and soil, (b) High resolution of climate and Low resolution of soil, (c) Low resolution of climate and High resolution of soil, and (d) High resolution of climate and soil.

**Table 7.3:** Summary of statistics of different evaluated parameters stratified by spatial resolution and scenarios.

Resolution level		Inherent productivity (kg dry matter ha <sup>-1</sup> )		Net returns (Sucres ha <sup>-1</sup> )		Carbofuran leaching (g ha <sup>-1</sup> )	
climate	soil	avg.	stdev	avg.	stdev	avg.	stdev
<b>Base scenario</b>							
Low	Low	3071	4049	1632	2403	277	535
High	Low	3866	5558	1575	2667	273	610
Low	High	2886	2748	1752	2453	287	529
High	High	4134	7232	1530	2524	254	527
<b>IPM scenario</b>							
Low	Low	3071	4049	1383	1917	160	342
High	Low	3866	5558	1443	2134	168	359
Low	High	2886	2748	1411	1686	177	365
High	High	4134	7232	1421	2120	161	352



The aggregated tradeoff curves between net returns and carbofuran leaching under the studied scenarios are shown in Figure 7.5. It is clear that there is not a major shift in the Tradeoff curves. As a result one could conclude that users of the Tradeoff Analysis System that are only interested in the aggregated tradeoff curves do not have to bother in this particular case with high resolution weather and/or soil data. However, it is necessary to realize that there is a large variability among the simulated outcomes across the fields. Variation in the simulated outcomes is induced by differences in the land use management and environmental characteristics of the sampled fields, especially related to climate and soil. The spatial variation is shown in Figure 7.6 representing the difference between the base and the IPM scenario under the observed potato price. The effect to disaggregate agro-climatic zones and soil units in the spatial variability of the outcomes can be observed among the different tested level resolution. From Figure 7.6(a) to Figure 7.6(d), different patterns of changes in carbofuran leaching can be appreciated. The difference between Figure 7.6(d) and the other figures can be considered as the error due to the aggregation of input information.

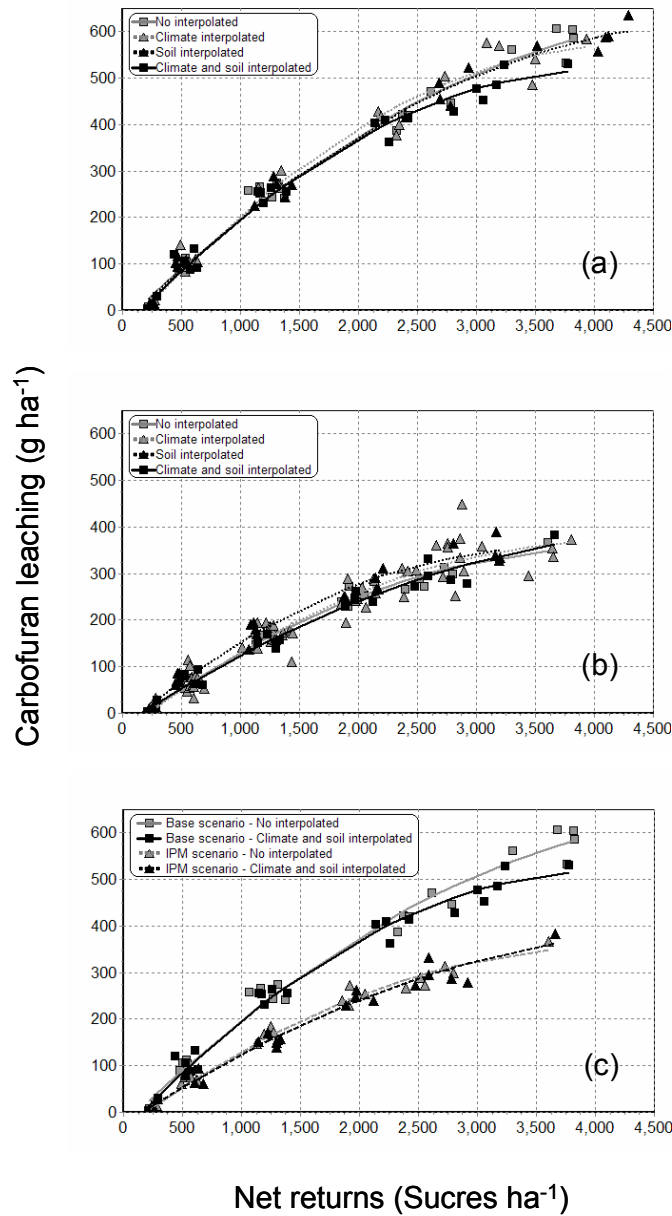


Fig. 7.5. The relation between net returns and carbofuran leaching. (a) Tradeoff curves under the base scenario comparing the different levels of inputs resolution. (b) Tradeoff curves under the integrated pest management (IPM) technology scenario. (c) Tradeoff curves comparing base and IPM scenarios using Low resolution of climate and soil and High resolution of climate and soil.

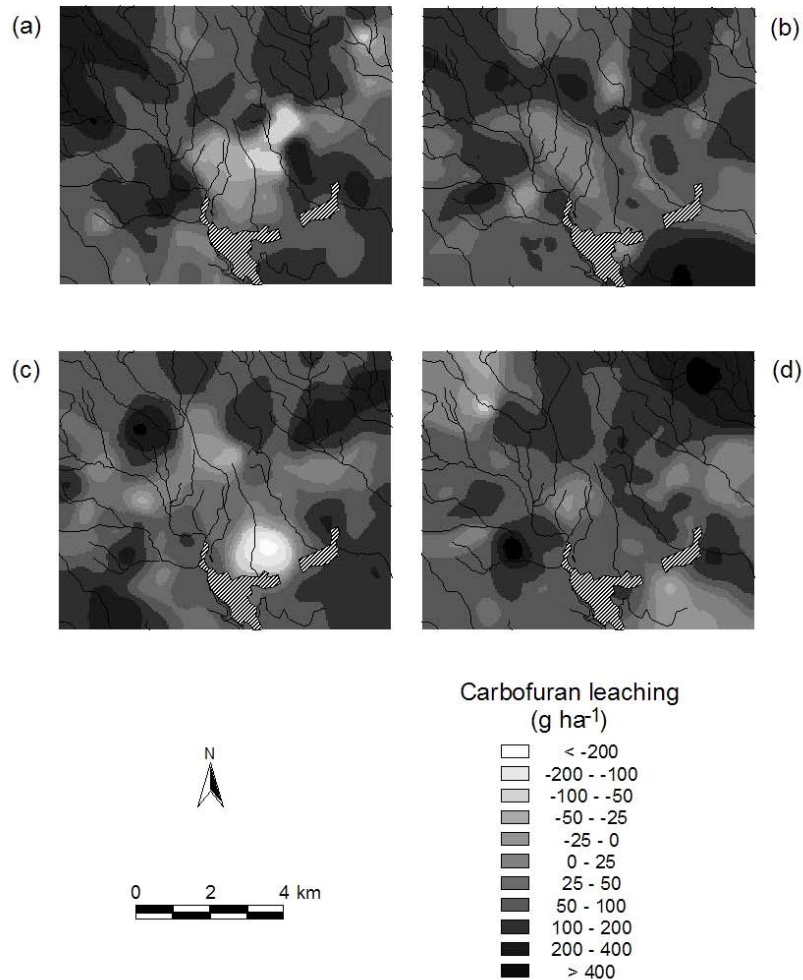


Fig. 7.6. Maps of decreasing carbofuran leaching between the base and the IPM scenarios using different spatial resolution of climate and soils used as inputs during the modeling process. (a) Low resolution of climate and soil, (b) High resolution of climate and Low resolution of soil, (c) Low resolution of climate and High resolution of soil, and (d) High resolution of climate and soil.

As mentioned by Stoorvogel et al. (2004b), it is often useful to provide to different decision makers information in terms that express the risk of environmental contamination or human health risk. In the case of risk by using pesticides like carbofuran, thresholds for a significant risk need to be defined with comparison purposes. According to the United States Environmental Protection Agency (USEPA, 1988), the maximum contaminant level of carbofuran in drinking water is set at 40 ppb. Given an

average drainage in the study area, this concentration corresponds to approximately 160 g of carbofuran per hectare (Crissman et al., 1998). Table 7.4 shows the cumulative probability that the EPA threshold for carbofuran leaching is not exceeded under the aggregated potato price regimes to the four input levels of climate and soil. In general, the values for each scenario tend to correspond to the same ranges without a significant variation among the four input levels. However, a significant difference between the base and the IPM scenarios is noticed for the four input levels. Comparison of the aggregated relative difference (%) of carbofuran leaching between scenarios among the four inputs levels does not have an important impact to decision makers. However, when the same differences are shown in absolute terms (*i.e.* hectares in the present case), big consequences in environmental damage can be appreciated. Using high-resolution data of climate and soil indicates an overestimation of 246 ha crossing the EPA threshold for carbofuran leaching. Although the application of IPM scenarios is 246 ha less than the ones previously estimated using aggregated climate and soil unit information, it is also easy to detect and to monitor these particular areas to implement specific land allocation and/or land use management to decrease potential health risks. Figure 7.7 shows the cumulative probability of areas crossing the EPA threshold this time disaggregated by tradeoff points previously established as potato price changes. As higher the tradeoff point of the potato price, higher the changes in the cumulative probability curves. This is due to an increment of the potato price in the market; make the farmers to increase the inputs in the crop to protect their investments and to increase the importance of potato in the crop rotation. Low potato prices decrease the amount of area cultivated with potato.

**Table 7.4:** Percentage of area under the EPA threshold for carbofuran due to changes in scenarios according to the different spatial resolution.

Resolution level		Area (%)		Difference between scenarios	
Climate	Soil	Base	IPM	(%)	(ha)
Low	Low	60.19	72.02	11.83	1124
High	Low	62.69	71.85	9.16	870
Low	High	58.80	69.72	10.92	1037
High	High	62.70	71.94	9.24	878

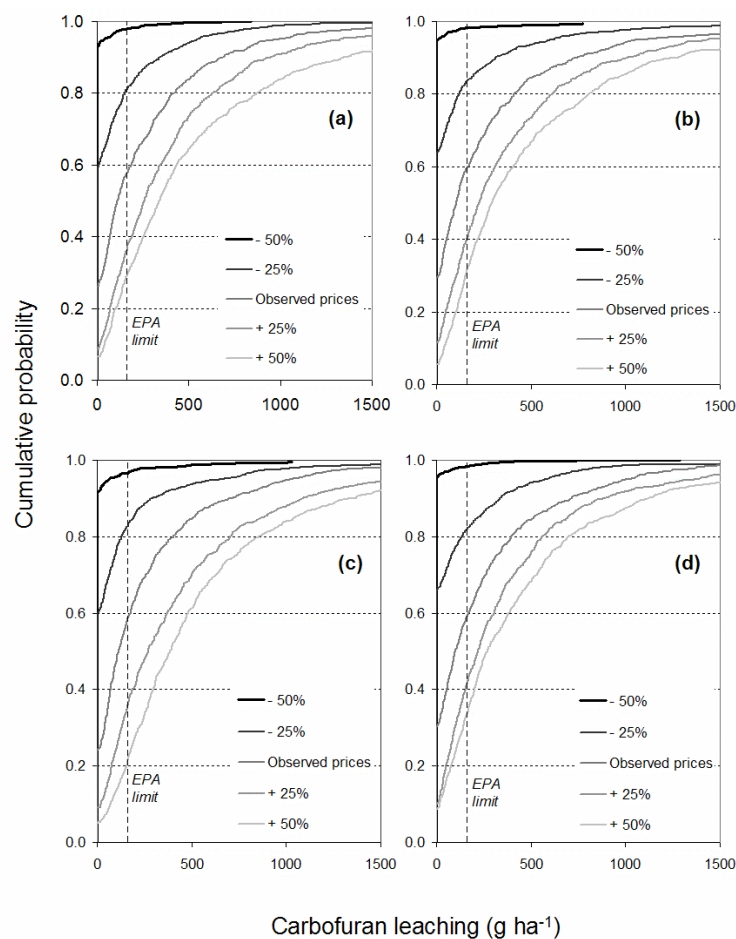


Fig. 7.7. Cumulative probability that threshold values for carbofuran leaching are met. (a) Low resolution of climate and soil, (b) High resolution of climate and Low resolution of soil, (c) Low resolution of climate and High resolution of soil, and (d) High resolution of climate and soil.

## **7.5 Conclusions**

There is not a unique spatial resolution level of climate and soil when an agricultural production system is studied. Depending on the objective of the research, different levels of inputs data are necessary to get a good balance between the effort to produce quantity and quality of inputs and the desired outputs. In the present case study, the aggregated tradeoff curves do not show a significant change according to the increasing spatial resolution inputs of climate and soil. However, from the site-specific point of view, an increase in the spatial resolution of climate and soil data generates a more accurate approach to deal with spatial patterns and risks.

## **Acknowledgements**

The present work is supported by the United States Agency for International Development (USAID), through its Soil Management Collaborative Research Program (SM-CRSP), financed a project entitled 'Tradeoffs in Sustainable Agriculture and the Environment in the Andes: A Decision Support System for Policy Makers' (Grant # 291488).

## Chapter 8

---

### Synthesis

This final chapter addresses the most important issues and conclusions of the previous chapters. It is important to notice that although the first three chapters have a strong disciplinary character dealing the development and calibration of climatic tools, the important added value of the research is their implications to other disciplines as illustrated in the other chapters. This is a matter of hierarchy with climate being an important soil forming factor and, subsequently, climate and soils being important driving factors of agricultural production systems. This is illustrated through the added value of seasonal-climate forecasts for agriculture. The temporal variation in potential crop production is the result of the dynamics in weather conditions (assuming similar management practices) and seasonal-climate forecasts give insight in this variation. However, one should realize that the maximization of agricultural production is not the main objective of farmers. Other objectives like income, food security and risk may be much more important. As a result it is necessary to have a more holistic approach towards the farming system through integrated multi-disciplinary research. An analysis of the sustainability of the production systems *per se* through, for example, the tradeoffs between agriculture and environment is one of the options. Although smallholder farmers are mainly dealing with the short term effects of their agricultural production, the long term effects should not be forgotten. This is an important role for the national agricultural research institutes.

### **8.1 Generalization: taking care**

Proxies are often used as an alternative to solve the lack of information. Generalization of values, indexes and/or coefficients to large areas without take into account climatic controls, topography as well as other factors, as demonstrated in the first chapter, could largely affect the expected results. The lack of insight in the use of these proxies does not mean that we can ignore it: 'The absence of evidence is not the evidence of absence' (Sagan, 1997). Nevertheless, environmental sciences tend to use relationships observed at small scales at implement them at large scales at the watershed or even farm level. Especially in complex mountainous terrain this may result in major errors.

All this does not mean that empiric approaches do not work or that process-based models perform better than the empiric ones. It rather means that before applying any methods, it is necessary to calibrate, validate and if possible to perform an uncertainty analysis of the models as well as the effect of the data resolution. From a scientific point of view, process-based models are more appreciated than the empiric ones. However, process-based models are complex to develop, usually require detailed inputs and have inherent problems in their operation related to their complexity. Although they contribute to the cumulative process of scientific understanding, they do not always perform better than simple empiric procedures. Perhaps the best approach is to disaggregate the empiric analysis in components with a biophysical significance.

### **8.2 Modeling spatial and temporal distribution of meteorological variables**

Two process-based, spatial interpolation models have been developed to the present thesis. The first one is to interpolate maximum and minimum temperatures based on the radiation balance at specific hours when those



temperatures occur. The second one is to interpolate rainfall based on the cloud movements over complex terrains, incorporating the physical processes driving rainfall events. A Digital Mountain Wave Model (DMWM) is defined during chapter 4, making easy the comprehension of how a modified topography, just because of different wind directions, alters the rainfall patterns. The model not only introduces the effects of aspect and altitude, but also disaggregates its effects with wind directions. Figure I.1 and I.2 of Annex I, shows these relationships. With dominant wind directions during storms from the northeast to north. NE and N, hillsides facing these directions receive more rainfall than hillsides facing other directions at the same altitude. Rainfalls coming in different seasons from other directions can be less erosive producing for instance less soil loss, so affecting the land degradation processes in different ways.

The models have been proved work in the study areas. However, despite their mechanistic character, an application in other regions will require intensive testing. Much more research is needed to make these tools generic and applicable in other environments and scale levels. An example of their application under different climatic conditions, at country level (pixel size of 500x500 m) and used as a tool to decision makers to design photovoltaic panels can be found in the Peruvian Atlas of Solar Energy (SENAMHI-MEM, 2003).

### **8.3 Supporting decision makers**

Decision support systems have to face scales, resolution, and especially important: language. A positive anomaly of three-Celsius degrees in the *El Niño 3.4* zone has different meanings to different stakeholders in the same area. On one side, meteorological and hydrological national services, which usually work in that issue, can be in red-alert. On the other hand, farmers knowing something will happen (because everybody is running) have no idea about the impacts on their

own economies. Sometimes, their local indicators show a totally opposite behavior of the next season-climate. Two possible explanations, errors in the forecasting models or decreasing accuracy of the local indicators due to externalities as for instance climate change. Forecasting models are improved year-by-year and local indicators will adapt to the new conditions at a slower pace. It is therefore important that local forecasters will keep up and are learned to read the national forecasts instead of relying on the local indicators.

In chapter 5 of this thesis it is demonstrated that seasonal-climate forecast at global scales can be downscaled to watershed levels using empiric relations. However, the key point in the study is the possibility to link time-dimension dominated by climate during a cropping season with the spatial-dimension dominated by soils and microclimates. Another key point is the possibility to translate seasonal climate forecast from Celsius degrees to production in tons per hectare; from science language to farm language. Interdisciplinary approaches in this chapter, give support to make better tactical decisions under different land use management performed by farmers. However, farmers need time to incorporate this new information in their decision frameworks. Translated seasonal yield forecast information must be taken as one of the many components of the systems and not as the unique. For instance, information of local indicators within a setting of national policies is needed to make operational and strategic decisions. The possibility to make risk maps available to farmers and institutes give pieces of advices to farmers and researchers of how to incorporate risk in the decision-making framework. On the other hand, feedbacks from stakeholders on the research and scales is similarly important.

#### **8.4 Explaining spatial and temporal distribution of soil characteristics**

Soil forming factors are the components of a very simple algorithm developed by Jenny in 1941. When this simple algorithm is disaggregated in order to model the development of different soil profiles, very complex physical, chemical and biological processes appear. Despite the fact that the effect of climate in the equation was only demonstrated at large scale, lack of detailed climate data hampered its validity at small scales. Chapter 6 demonstrates the availability to produce more detailed maps of soil characteristics in the volcanic ash soils of the study area. The availability of detailed climate information demonstrates that Jenny's equation can be applied also at small scales. It is only a first approximation in an area where soil differences are likely to be dominated by climate, nevertheless it provides exiting results for future research in other areas. The approach can be very useful dealing with, for instance, carbon sequestration maps. In other applications, as illustrated in chapter 7, the increase of resolution in the information of climate and soil can affect seriously the spatial distribution of the crop production and the environmental impacts. Better resolution of the inputs result in an increased resolution of the outputs making it possible to identify particular hot spots.

#### **8.5 Measuring the effects of an interdisciplinary approach**

How much detail in input data is necessary to represent the real world as much as possible? How much input is possible to manage? How much output can we generate and how much is relevant? All these questions are related with the resources and efforts necessary to support in a better way the clients of scientific research. New, high-resolution databases require the development of new tools capable not only to integrate disciplines but also the capacity to manage it. New levels of data quantity and quality give a new spatial and temporal perspective.

Chapter 7 stresses the fact that different disciplines, applications and objectives require different levels of input information. In our study case, the aggregated TOA curves are just little affected by the resolution of the input information. However, the different levels of inputs largely affected the spatial variability of all the analyzed variables. The study faced the problems of different levels of aggregation of information by different disciplines, but the results are very specific and not possible to be extrapolated. It is important to develop methodologies in a forward-looking perspective. Serendipity may have given excellent results in the past, but in development oriented research we have to listen to our clients and the input that they require.

## **Síntesis**

Este capítulo sintetiza los aspectos más importantes de los capítulos previos. Es importante notar que a pesar de que los tres primeros capítulos enfatizan el desarrollo y calibración de herramientas meteorológicas, lo más importante son las implicancias de estas herramientas sobre otras disciplinas, lo que es presentado en los capítulos siguientes. Es solo cuestión de jerarquía el tomar el clima como un importante factor de formación de suelos, y posteriormente, el uso de clima y suelos como factores importantes en el manejo de los sistemas de producción agrícola. Esto se demuestra a través del valor del pronóstico climático-estacional en la agricultura. La variación temporal en la producción potencial de un cultivo es el resultado de la dinámica de las condiciones meteorológicas (asumiendo prácticas de manejo similares); y un pronóstico climático-estacional reduce la incertidumbre de esta variación. Sin embargo, uno debe darse cuenta que la maximización de la producción no es el objetivo de los agricultores. Otros objetivos como ingresos, seguridad alimentaria y riesgo pueden jugar un papel más importante. Como resultado es necesario tener una aproximación más holística dirigida hacia los sistemas agrícolas a través de investigaciones multidisciplinarias. Un análisis de sostenibilidad de los sistemas de producción *per se* a través, como por ejemplo las relaciones de intercambio entre agricultura y medio ambiente es una de estas opciones. Aunque pequeños agricultores principalmente se enfrentan con efectos a corto plazo en cuanto a la producción agrícola, efectos a largo plazo no deben ser olvidados, y este es un importante rol que deben cumplir los institutos de investigación agrícola.

### **Teniendo cuidado con las generalizaciones**

Diferentes aproximaciones se utilizan como alternativas para solucionar el problema de la falta de información en las ciencias ambientales. La generalización de valores, índices y/o coeficientes en

grades áreas sin tener en cuenta los controladores climáticos, topografía entre otros factores, pueden afectar grandemente los resultados. El no conocer estas relaciones no significa que deban ser ignoradas: 'La ausencia de evidencia no es evidencia de ausencia' (Sagan, 1997). Sin embargo, las ciencias ambientales tienden a utilizar relaciones observadas en pequeñas escalas e implementarlas a mayores escalas, lo que causa grandes errores en los resultados, especialmente en terrenos complejos como las montañas.

Todo esto no significa que los métodos empíricos no funcionan o que los modelos basados en procesos funcionan mejor que los empíricos. Esto significa que antes de aplicar cualquier método, es necesario calibrar, validar y si es posible hacer análisis de incertidumbre de los modelos y de sus efectos en la resolución de los datos. Desde el punto de vista científico, los modelos basados en procesos son mas complejos para desarrollar, usualmente requieren de información mas detallada y además tienen problemas inherentes en cuanto a su operatividad relacionada con su complejidad. Aunque ellos contribuyen al proceso acumulativo del conocimiento científico, no siempre funcionan mejor que simples procedimientos empíricos. Quizás la mejor aproximación es el desagregar los análisis empíricos en componentes con significancia biofísica.

### **Modelando la distribución espacio-temporal de variables meteorológicas**

En la presente tesis se desarrollaron dos modelos de interpolación espacial basados en procesos. El primero interpola las temperaturas máximas y mínimas basado en el balance de radiación en horas específicas a las que estas temperaturas ocurren. El segundo, un modelo para interpolar precipitación y que esta basado en el movimiento de las nubes sobre terrenos complejos y en los procesos físicos que producen los eventos de lluvia. El Modelo Digital de Ondas de Montaña (MDOM) que se

define en el capítulo 4, hace más fácil la comprensión de cómo la topografía, modificada solo por la dirección del viento, altera los patrones de lluvia. El modelo no solo incorpora el efecto del aspecto y altitud, sino que también desagrega los efectos de estos con la dirección del viento. Las Figuras I.1 e I.2 del Anexo I muestran estas relaciones. Con vientos dominantes del noreste a norte durante las tormentas, las laderas que encaran estas direcciones de viento, reciben más lluvia que aquellas laderas hacia otras direcciones pero que sin embargo se encuentran a la misma altitud. Por otro lado, lluvias en diferentes épocas del año pueden provenir de diferentes direcciones y a su vez pueden variar en su grado de erosividad. Esto provoca por ejemplo, una mayor o menor erosión de suelo afectando así directamente los procesos de degradación del paisaje en diferentes maneras en el tiempo y espacio.

La funcionalidad de estos modelos han sido probadas en las áreas de estudio. Sin embargo, debido a su carácter mecanístico, su aplicación en otras regiones requiere una previa validación. Mucha mas investigación es necesaria antes de que estas herramientas puedan ser de aplicación general para otros ambientes y escalas. Un ejemplo de su aplicación bajo diferentes condiciones climáticas, a nivel país (tamaño de píxel 500x500 m) y utilizadas como herramientas para tomadores de decisiones en la construcción de paneles fotovoltaicos puede ser encontrada en el Atlas de Energía Solar del Perú (SENAMHI-MEM, 2003).

### **Ayudando a tomadores de decisiones**

Muchos de los sistemas de ayuda en la toma de decisiones encaran temas de escalas, resolución, y especialmente lenguaje. Una anomalía positiva de tres grados centígrados en la región *El Niño 3.4* tiene diferentes significados para diferentes tomadores de decisiones en la misma área. Por un lado los meteorólogos e hidrólogos de los servicios nacionales, quienes monitorean este tema constantemente, pueden estar en alerta

nacional. Por otro lado, los agricultores saben que algo va a pasar (porque todo el mundo esta corriendo) pero no tienen la menor idea sobre los impactos de esto en sus formas de vida. Algunas veces, sus indicadores locales muestran comportamientos totalmente opuestos a los 'oficiales' correspondientes a la próxima estación climática. Dos posibles explicaciones, errores en los modelos numéricos y/o estadísticos de pronóstico o la disminución del grado de acierto de los indicadores locales debido a externalidades como por ejemplo cambio climático. Los modelos numéricos y/o estadísticos de pronóstico son mejorados año tras año, paralelamente los indicadores locales también se van adaptando a estos cambios, pero a un paso un poco mas lento, siendo mas difícil su interpretación por los pronosticadores locales. De esta manera es importante que los pronosticadores locales mantengan sus indicadores pero que a la vez incorporen los pronósticos 'oficiales' a sus indicadores.

El capítulo 5 de esta tesis demuestra como el pronóstico climático-estacional a escala global puede ser desagregado a nivel de cuenca utilizando relaciones empíricas. Sin embargo , el punto clave en el estudio es la posibilidad de ligar la dimensión temporal dominada por el clima durante la estación de siembra con la dimensión espacial dominada por la variación de suelos y microclimas. Otro punto importante es la posibilidad de traducir el pronóstico climático-estacional dado en grados centígrados a producción en toneladas por hectárea; de lenguaje científico a lenguaje de los agricultores. En este capítulo, el análisis interdisciplinario es el punto clave para ayudar a una mejor toma de decisiones tácticas bajo los diferentes manejos en el uso de la tierra típica de los agricultores. Sin embargo, la incorporación de esta nueva información en su modelo conceptual no es inmediata. La traducción del pronóstico climático-estacional debe ser tomada como un componente más del sistema y no como única herramienta. Así, la información obtenida por los indicadores locales para la toma de decisiones operacionales y estratégicas, debe ser vista dentro de un conjunto de políticas nacionales. La posibilidad de tener



mapas de riesgo disponibles para los agricultores e instituciones, da consejos a agricultores e investigadores de cómo incorporar el factor riesgo en el marco conceptual de toma de decisiones. Asimismo, la retroalimentación por parte de tomadores de decisiones tiene que ser incorporada en los procesos de investigación.

### **Explicando la distribución espacial y temporal de las características de los suelos**

Los factores de formación de suelo son los componentes de un algoritmo simple desarrollado por Jenny en 1941. Cuando este algoritmo se desagrega para modelar el desarrollo de los diferentes perfiles de suelo, salen a la luz la interacción de muchos complejos procesos físicos, químicos y biológicos. A pesar de que el efecto del factor clima en la ecuación fue solamente demostrada a grandes escalas, la falta de información detallada de clima ha dificultado su validez a escalas menores. El capítulo 6 muestra que la posibilidad de producir mapas de información de características de suelo mas detallada para los suelos volcánicos correspondientes al área de estudio. La disponibilidad de información detallada de clima demuestra que la ecuación de Jenny puede ser aplicada también a escalas menores. Esta es por supuesto una primera aproximación en un área donde las diferencias en el suelo son probablemente dominadas por el clima, sin embargo esto genera expectativas para futuras investigaciones en otras áreas de estudio. Esta aproximación puede ser muy útil en por ejemplo, el mapeo de secuestro de carbono. En otras aplicaciones, tal como se muestra en el capítulo 7, el incremento de la resolución en la información de clima y suelo pueden afectar seriamente la distribución de la producción de cultivos y los impactos en el medio ambiente. Una mejor resolución en los datos, incrementará la resolución de los resultados haciendo posible la identificación de áreas específicas de gran interés.

### **Midiendo el efecto de un enfoque interdisciplinario**

¿Cuánto detalle en los datos es necesario para representar el mundo real lo mas preciso posible? ¿Cuántos datos son posibles de manejar? ¿Cuántos resultados podemos generar y cuántos son realmente relevantes? Todas estas preguntas están relacionadas con los recursos y esfuerzo necesarios para ayudar de una mejor manera a los usuarios de una investigación científica. Nuevas bases de datos de alta resolución requieren también del desarrollo de nuevas herramientas capaces no solo de integrar disciplinas sino que también la capacidad de manejarlas. Nuevos niveles de cantidad y calidad de datos dan una nueva perspectiva espacial y temporal.

El capítulo 7 hace énfasis en que las diferentes disciplinas, aplicaciones y objetivos requieren de diferentes niveles e intensidades de datos. En nuestro caso de estudio, la agregación de las curvas de relaciones de intercambio, son muy poco afectadas por la resolución de los datos, Sin embargo, los diferentes niveles e intensidades de datos afectan de sobremanera la variabilidad espacial de todas las variables analizadas. El estudio encara el tema de diferentes niveles de agregación de la información por diferentes disciplinas, pero los resultados son muy específicos y no es posible su extrapolación. Es importante desarrollar metodologías con una perspectiva futurista. Descubrimientos al azar pudieron haber dado excelentes resultados en el pasado, pero en una investigación orientada hacia el desarrollo, necesitamos escuchar a nuestros usuarios para saber cuales son sus requerimientos de información.

## Samenvatting

Wetenschappers in het veld van landgebruik en natuurlijke hulpbronnen krijgen in toenemende mate te maken met beperking op het gebied van gegevensbeschikbaarheid. Nieuwe technieken zoals simulatiemodellen vragen om gedetailleerde en kwantitatieve bodem en klimaatgegevens. Grote kaartenheden met representatieve weerstations of representatieve bodemprofielen negeren een belangrijk deel van de ruimtelijke variabiliteit in het landschap. Nieuwe technieken zoals geografische informatiesystemen (GIS), geostatistiek, en remote sensing openen nieuwe mogelijkheden. Een goed voorbeeld op het gebied van bodemkunde zijn de snelle ontwikkeling op het gebied van digitale bodemkartering. De belangrijkste doelstelling van dit onderzoek is een oplossing te vinden voor de databeperkingen van meteorologische gegevens van weerstations door het interpoleren van gegevens van weerstations en om de waarde van nieuwe gegevenssets te onderzoeken voor studies naar natuurlijke hulpbronnen en landgebruik. Het onderzoek heeft plaatsgevonden in twee gebieden in de hooglanden van de Peruaanse en Ecuadoriaanse Andes: (i) de vanggebieden van La Encañada en Tabomayo in Peru (op een hoogte van 2950 tot 4000 meter boven zeeniveau) met landbouw in marginale gebieden en (ii) de vanggebieden van Chitan en San Gabriel in Ecuador (op een hoogte van 2700 tot 3840 meter boven zeeniveau) met commerciële landbouw gericht op de productie van aardappel en melk. Tijdens de eerste stap zijn empirische en mechanistische modellen voor de interpolatie van klimaatsgegevens ontwikkeld, gekalibreerd, geëvalueerd en gevalideerd om toegepast te worden in gebieden met een complexe topografie. Daarnaast is het gebruik van seizoensvoorspelling van klimaat met behulp van mondiale circulatie modellen om landbouwkundige beslissingen te ondersteunen bekeken. De effecten van gedetailleerde ruimtelijke klimaatsgegevens als bodemvormende factor zijn onderzocht als basis voor digitale bodemkartering om de desaggregatie van kaartenheden en

de vraag hoeveel informatie we daadwerkelijk nodig hebben voor studies naar landgebruik en natuurlijke hulpbronnen. De resultaten van deze studie omvatten twee procesmatige modellen om maximum en minimum temperaturen, en regenval te interpoleren. Daarnaast zijn 4 empirische modellen om zonnestraling te schatten geëvalueerd en gekalibreerd. De mogelijkheid om gewasvoorspellingen uit te voeren voor het productie seizoen door middel van het gebruik van mondiale circulatie modellen is geanalyseerd door het koppelen van statistische en gewas modellen geaggregeerd op het niveau van een vanggebied. De theorie van klimaat als bodemvormende factor op het niveau van kleine schalen (de zonale bodems) is aangetoond ook bruikbaar te zijn op grote schalen door het gebruik van gedetailleerde, geïnterpoleerde klimaatsgegevens. Een studie met een systeem voor de analyse van landgebruik heeft aangegeven dat verschillende resoluties van invoergegevens niet eenduidige richtlijnen geven ten aanzien van de kwaliteit van beoogde eindresultaten. Voor iedere casus moet een gevoeligheidsanalyse aantonen welke specifieke resolutie noodzakelijk is in relatie tot bijvoorbeeld de doelstellingen van het project, de gebruikte modellen en de noodzaak van verschillende belanghebbenden.

## References

---

- Aceituno, P. and A. Montecinos. 1993. Circulation anomalies associated with dry and wet periods in the South American Altiplano. Proc. Fourth Int. Conf. On Southern Hemisphere Meteorology. Hobart. Australia. *Bulletin of the American Meteorological Society*, 330-331.
- Ångström, A., 1924. Solar and terrestrial radiation. *Quarterly Journal of the Royal Meteorological Society*, 50: 121-125.
- Aselin, L. and A.D. Griffith, 1988. Do spatial effects really matter in regression analysis? *Papers of Regional Science Association*, 65: 11-34.
- Antle, J., G. Baigorria, V. Barrera, W. Bowen, C. Crissman, C. Romero, J. Stoorvogel and D. Yanggen. 2001. Impacts of terracing, agroforestry, and irrigation on the sustainability of the crop-livestock system of the Peruvian Andes: An application of the Tradeoff Analysis approach. Workshop, Integrated Management for sustainable agriculture, forestry, and fisheries. 28 – 31 August, CIAT.
- Antle, J.M. and S.M. Capalbo, 2001. Econometric-process models for integrated assessment of agricultural production systems. *American Journal of Agricultural Economics*, 83: 389-401.
- Antle, J.M., S.M. Capalbo and C.C. Crissman. 1998. Econometric and simulation modeling of the Carchi potato production system. p. 145-180. In: Crissman, C.C., Antle, J.M., Capalbo, S.M. (eds.), *Economic, Environmental, and Health Tradeoffs in Agriculture: Pesticides and the Sustainability of Andean Potato Production*, Kluwer Academic Publishers, Boston.
- Atwater, M.A. and J.T. Ball. 1978. A numerical solar radiation model based on standard meteorological observations. *Solar Energy*, 21: 163-170.

- Avissar, R. 1993. An Approach to bridge the gap between microscale land-surface processes and synoptic-scale meteorological conditions using atmospheric models and GIS: potential for applications in agriculture. p. 123–134. In: Goodchild, M., B. Parks, and L. Steyaert. (eds.) Environmental Modeling with GIS. Oxford University Press.
- Avissar, R. and Y. Mahrer. 1988. Mapping frost-sensitive areas with a three-dimensional local scale numerical model. Part II: Comparison with observations. *Journal of Applied Meteorology*, 27: 414–426.
- Baigorria, G.A., C.C. Romero and M. Olivares. 2002. La Encañada and Tambomayo Watersheds, Cajamarca, Peru. In [CD-ROM]: Disk 7 of 9. Himalayan Andean Collaborative Watersheds Projects. CIP – IDRC – CRDI. BC, Canada.
- Baigorria, G.A., E.B. Villegas, I. Trebejo, J.F. Carlos and R. Quiroz. 2004. Atmospheric transmissivity: distribution and empirical estimation around Central Andes. *International Journal of Climatology*, 24(9): 1121-1136.
- Baldwin, M., C.E. Kellogg, and J. Thorp. 1938. Soil classification. Yearbook of agriculture, USDA, Printing Office, Washington, DC: 979-1001.
- Bardossy, A. and E. J. Plate. 1992. Space-time model for daily rainfall using atmospheric circulation patterns. *Water Resources Research*, 28(5): 1247–1259.
- Barros, A.P. and D.P. Lettenmaier. 1993. Dynamic modeling of the spatial distribution of precipitation in remote mountainous areas. *Monthly Weather Review*, 121: 1195-1214.
- Barry R.G. and R.J. Chorley. 1980. *Atmósfera, tiempo y clima*. (In Spanish). Editorial Omega S.A. Third edition. Barcelona, Spain. 395 p.
- Bastos, E.J.B., B.M. Funatsu, A. Bonfim, E.C. Moraes and J.C. Ceballos. 1996. Estimativa da radiação solar global para a América do Sul via

- satellite. (In Portuguese, with English abstract.) p. 596-600. In: Proceedings. IX Congresso Brasileiro de Meteorologia, Campos do Jordão, Sao Pablo, Brasil.
- Bell, J.C., D.F. Grigal, and P.C. Bates. 2000. A soil-terrain model for estimating spatial patterns of soil organic carbon. p. 295-310. In J.P. Wilson and J.C. Gallant (eds.) *Terrain analysis principles & applications*. John Willey & Sons Inc.
- Benichou, P. and O. Le Breton. 1987a. Prix Norbert Gerbier 1986: Prise en compte de la topographie pour la cartographie des champs pluviométriques statistiques. (In French) *La Météorologie* 7th series, 19. Direction de la Météorologie Nationale. Boulogne-Billancourt, France.
- Benichou, P. and O. Le Breton. 1987b. Prise en compte de la topographie pour la cartographie de champs pluviométriques: la méthode Aurelhy. (In French) In: *Agrométéorologie des régions de moyenne montagne*. Proc. Toulouse, 16-17 April 1986 (INRA, Ed.). *Les Colloques de l'INRA*, 39: 51-69. Paris, France.
- Berri, G.J. (ed), 1998. *Practical Application of Seasonal to Interannual Climate Prediction and Decision Making in Agriculture and Water Resources Management in Africa*. IRI – ACMAD – WMO. IRIP-CR-N97/1. Palisades, NY.
- Bogaert, P. and D. D'Or. 2002. Estimating soil properties from thematic soil maps: The Bayesian maximum entropy approach. *Soil Science Society of America Journal*, 66: 1492-1500.
- Bonan, G.B., 1989. A computer model of the solar radiation, soil moisture, and soil thermal regimes in boreal forest. *Ecological Modelling*, 45: 275-306.
- Bouma, J., J. Stoorvogel, B.J. van Alphen and H.W.G. Booltink. 1999. *Pedology, precision agriculture, and the changing paradigm of*

- agricultural research. *Soil Science Society of America Journal*, 63: 1763–1768.
- Bowen, W., H. Cabrera, V. Barrera and G. Baigorria. 1999. Simulating the response of potato to applied nitrogen. p. 381-386. In: CIP Program Report 1997-1998. CIP.
- Bristow, K. and G. Campbell, G. 1984. On the relationship between incoming solar radiation and daily maximum and minimum temperature. *Agricultural and Forest Meteorology*, 31: 159-166.
- Carruthers, D.J. and T.W. Choularton. 1982. Airflow over hills of moderate slope. *Quarterly Journal of the Royal Meteorological Society*, 108: 603-624.
- Ceballos, J.C. and G.B.A. Moura. 1997. Solar radiation assessment using Meteosat 4-VIS imagery. *Solar Energy*, 60: 209-219.
- Cengiz, H.S., J.M. Gregory and J.L. Seabaugh. 1981. Solar radiation prediction from other climate variables. *Transactions of the ASAE Journal*, 24: 1269-1272.
- Chow, V.T., D.R. Maidment and L.W. Mays. 1988. *Applied Hydrology*. McGraw-Hill. NY.
- Collins, F.C. and P.V. Bolstad. 1996. A Comparison of Spatial Interpolation Techniques in Temperature Estimation. Third International Conference/Workshop on Integrating GIS and Environmental Modeling. Santa Fe, NM. [Online] Available at: [http://www.ncgia.ucsb.edu/conf/SANTA\\_FE\\_CD-ROM/sf\\_papers/collins\\_fred/collins.html](http://www.ncgia.ucsb.edu/conf/SANTA_FE_CD-ROM/sf_papers/collins_fred/collins.html). Verified: September 5<sup>th</sup> 2003.
- Crissman, C.C., J.M. Antle and S.M. Capalbo (eds.), 1998. *Economic, Environmental and Health Tradeoffs in Agriculture: Pesticides and the Sustainability of Andean Potato Production*. CIP and Kluwer Academic Publishers.



- Daly, C., R.P. Neilson and D.L. Phillips. 1994. A digital topographic model for distributing precipitation over mountainous terrain. *Journal of Applied Meteorology*, 33: 140-158.
- De la Cruz, J., P. Zorogastúa and R.J. Hijmans. 1999. Atlas Digital de los Recursos Naturales de Cajamarca. Departamento de Sistemas de Produccion y Manejo de Recursos Naturales. Documento de Trabajo No. 2. CIP – CONDESAN. Lima, Peru.
- Dissing, D. and G. Wendler. 1998. Solar radiation climatology of Alaska. *Theoretical and Applied Climatology*, 61:161-175.
- Dubayah, R. and P.M. Rich. 1995. Topographic solar radiation models for GIS. *International Journal of Geographical Information Science*, 9(4): 405-419.
- Florinsky, I.V., R.G. Eilers, G.R. Manning, and L.G. Fuller. 2002. Prediction of soil properties by digital terrain modeling. *Environmental Modelling and Software*, 17: 295-311.
- Food and Agriculture Organization (FAO) and United Nations Educational, Scientific and Cultural Organization (UNESCO). 1988. World reference base for soil resources. *World Soil Resources Report 84*. Rome, Italy.
- Frère, M., J. Rijks and J. Rea. 1975. Estudio Agroclimatológico de la Zona Andina (Informe Técnico). (In Spanish) Proyecto Interinstitucional FAO / UNESCO / WMO. Roma, Italia.
- Garatuza-Payan, J., R.T. Pinker, W.J. Shuttleworth and C.J. Watts. 2001. Solar radiation and evapotranspiration in northern Mexico estimated from remotely sensed measurements of cloudiness. *Hydrological Sciences Journal*, 46(3): 465-478.
- Garcia, J.V. 1994. Principios físicos de la climatología. (In Spanish). Ediciones UNALM. Universidad Nacional Agraria La Molina. 244 p.

- Garreaud, R.D., 1999. Multiscale analysis of the summertime precipitation over the Central Andes. *Monthly Weather Review*, 127: 901-921.
- Gilford, M.T., M.J. Vojtesak, G. Myles, R.C. Bonam and D.L. Martens. 1992. South America - South of the Amazon River: A Climatological Study. USAF Environmental Technical Applications Center (USAFETAC/TN — 92/004). Scott Air Force Base, IL.
- Glover, J. and J.S.F. McCulloch. 1958. The empirical relation between solar radiation and hours of sunshine. *Quarterly Journal of the Royal Meteorological Society*, 84: 172-175.
- Göbel, W., A. El Ouali and M. Singh. 1996. Spatial interpolation of precipitation data: an example from Morocco. Presented at the Workshop on Spatialization organized by E.U. Cost and Météo France. 24-25 September. Toulouse, France.
- Goodin, D.G., J.M.S. Hutchinson, R.L. Vanderlip and M.C. Knapp. 1999. Estimating solar irradiance for crop modeling using daily air temperature data. *Agronomy Journal*, 91: 845-851.
- Gultepe, I., G.A. Isaac and K.B. Strawbridge. 2001. Variability of cloud microphysical and optical parameters obtained from aircraft and satellite remote sensing measurements during RACE. *International Journal of Climatology*, 21: 507-525.
- Hansen, J.W., 2002. Realizing the potential benefits of climate prediction to agriculture: issues, approaches, challenges. *Agricultural Systems* 74, 309-330.
- Hargreaves, G. and Z. Samani. 1982. Estimating potential evapotranspiration. *Journal of Irrigation and Drainage Engineering – ASCE*, 108: 225-230.
- Hartkamp, A.D., K. De Beurs, A. Stein and J.W. White. 1999. Interpolation Techniques for Climate Variables. NRG-GIS Series 99-01. Mexico, D.F.: CIMMYT.

- Hay, L.E., G.J. McCabe, D.M. Wolock and M.A. Ayers. 1991. Simulation of precipitation by weather type analysis. *Water Resources Research*, 27: 493-501.
- Hevesi, J.A. 1992. Precipitation estimation in mountainous terrain using multivariate geostatistics. Part I: Structural analysis. *Journal of Applied Meteorology*, 31: 661-676.
- Horel, J., A. Nahmann and J. Geisler. 1989. An investigation of the annual cycle of the convective activity over the tropical Americas. *Journal of Climate*, 2: 1388-1403.
- Hungerford, R.D., R.R. Nemani, S.W. Running and J.C. Coughlan. 1989. MTCLIM: A Mountain microclimate simulation model. Research Paper INT-414. Intermountain Research Station. Forest Service. US Department of Agriculture. 53 p.
- Hunt, L.A., G. Hoogenboom, J.W. Jones and J. White. 2000. ICASA files for experimental and modelling work. International Consortium for Agricultural System Applications. Honolulu, HI.
- International Benchmark Sites Network for Agrotechnology Transfer (IBSNAT). 1988. Experimental design and data collection procedures for IBSNAT: the minimum data set for system analysis and crop simulation. Technical Report 1, third edition. Department of Agronomy and Soil Science, University of Hawaii. Honolulu, HI.
- International Research Institute for climate prediction (IRI), 2003. World precipitation probability forecast for the season of November – January 2004 (made in October 2003). [Online] Available at: <http://iri.columbia.edu/>. Verified: October 30th 2003.
- Isaaks, E.H. and R.M. Srivastava. 1989. *An Introduction to Applied Geostatistics*. Oxford University Press. NY. 561 p.
- Jenny, H., 1941. *Factors of soil formation: a system of quantitative pedology*. McGraw-Hill Book Company, Inc. NY.

- Jenson, S.K. and J.O. Domingue. 1988. Extracting topographic structure from digital elevation data for geographic information system analysis. *Photogrammetric Engineering and Remote Sensing*, 54(11): 1593-1600.
- Jones, J.W., G. Tsuji, G. Hoogenboom, L.A. Hunt, P.K. Thornton P.W. Wilkens, D.T. Imamura, W.T. Bowen and U. Singh. 1998. Decision support system for agrotechnology transfer: DSSAT v3. p. 157-177. In: Tsuji, G.Y., Hoogenboom, G., Thornton, P.K. (eds.), *Understanding Options for Agricultural Production*. Kluwer Academic Publishers, Dordrecht, The Netherlands.
- Jongmans, A.G., T.C. Feijtel, R. Miedema, N. v Breemen, and Veldkamp, A., 1991. Soil formation in a Quaternary terrace sequence of the Allier, Limagne, France. *Geoderma*, 49: 215-239.
- Keith, F. and J.F. Kreider. 1978. *Principles of Solar Engineering*. Hemisphere, Washington, DC.
- Kyriakidis, P.C., J. Kim and N.L. Miller. 2001. Geostatistical mapping of precipitation from rain gauge data using atmospheric and terrain characteristics. *Journal of Applied Meteorology*, 40: 1855-1877.
- Lee, R., 1978. *Forest Microclimatology*. Columbia University Press, NY. 276 p.
- Lenters, J.D. and K.H. Cook. 1997. On the origin of the Bolivian High and related circulation features of the South American climate. *Journal of Atmospheric Science*, 54: 656–677.
- Lookingbill, T.R. and D.L. Urban. 2003. Spatial estimation of air temperature differences for landscape-scale studies in montane environments. *Agricultural and Forest Meteorology*, 114: 141-151.
- Lopez, M.R. 2000. Patrones espaciales en fertilidad del suelo dentro del area de San Gabriel – Carchi – Ecuador. (In Spanish, with English

- abstract). Thesis. Wageningen University & Research Centre, Wageningen, The Netherlands.
- Mahmood, R. and K.G. Hubbard. 2002. Effect of time of temperature observation and estimation of daily solar radiation for the northern Great Plains, USA. *Agronomy Journal*, 94: 723-733.
- Marquinez, J., J. Lastra and P. Garcia. 2003. Estimation models for precipitation in mountainous regions: the use of GIS and multivariate analysis. *Journal of Hydrology*, 270: 1-11.
- Martinez-Lozano, J.A., F. Tena, J.E. Onrubia and J. De la Rubia. 1984. The historical evolution of the Ångström formula and its modification: review and bibliography. *Agricultural Forest Meteorology*, 33: 109-128.
- Materer, S., 2001. The role of potato production in diversified household economic portfolios: Study of San Jose Llanga, Bolivia. Thesis. Agricultural Economics, University of Missouri Columbia, MO.
- McKenzie, N.J. and P.J. Ryan. 1999. Spatial prediction of soil properties using environmental correlation. *Geoderma* 89: 67-94.
- Mellor, D. 1996. The modified turning bands (MTB) model for space-time rainfall. I. Model definition and properties. *Journal of Hydrology*, 175: 113-127.
- Meza, F. and E. Varas. 2000. Estimation of mean monthly solar global radiation as a function of temperature. *Agricultural and Forest Meteorology*, 100: 231-241.
- Ministerio de Agricultura y Ganadería (MAG) and Office de la Recherche Scientifique et Technique Outre Mer (ORSTOM). 1980. Cartas de suelos de la sierra ecuatoriana a 1:50,000. Cartas Tufiño No. 6 y No. 10, 2nd rev. (In Spanish) PRONAREG, Quito, Ecuador.
- Moore, I.D., A.K. Turner, J.P. Wilson, S.K. Jenson, and L.E. Band. 1993. GIS and the land surface – subsurface process modelling. p. 196-230.

- In M.F. Goodchild, B.O. Parks and L.T. Steyaert (eds.) Environmental modelling with GIS. Oxford University Press.
- Mueller, T.G. and F.J. Pierce. 2003. Soil carbon maps: Enhancing spatial estimates with simple terrain attributes at multiple scales. *Soil Society of America Journal*, 67: 258-267.
- Neuwirth, F., 1980. The estimation of global and sky radiation in Austria. *Solar Energy*, 24: 421-426.
- Overmars, K.P., 1999. Developing a Method for Downscaling Soil Information from Regional to Catena Level. Thesis. Wageningen Agricultural University, Wageningen, The Netherlands.
- Overmars, K.P., G.H.J. de Koning, and A. Veldkamp, 2003. Spatial autocorrelation in multi-scale land use models. *Ecological Modelling*, 164:257-270.
- Peixoto, J.P. and A.G. Oort. 1992. *Physics of Climate*. American Institute of Physics. NY. 520 p.
- Pellegrini, G.J. 1995. Terrain shape classification of digital elevation models using Eigenvectors and Fourier transforms. UMI dissertation Services.
- Prescott, J.A., 1940. Evaporation from a water surface in relation to solar radiation. *Transactions of the Royal Society of South Australia*, 64: 114-125.
- Quantin, P. 1997. Caracterización, génesis y geografía de los horizontes endurecidos de suelos volcánicos. p. 11-18. In C. Zebrowski, P. Quantin, and G. Trujillo (ed.) *Suelos volcánicos endurecidos* (In Spanish.) Proc. Int. Symp., 3rd. Quito, Ecuador. Dec. 1996. Impresora Polar, Quito, Ecuador.
- Queney, P. 1948. The problem of airflow over mountains: A summary of theoretical studies. *Bulletin of the American Meteorological Society*, 29: 16-26.

- Rawlings, J.O., 1988. Applied Regression Analysis: a Research Tool. Wadsworth & Brooks/Cole Advanced Books & Software. CA.
- Richardson, C.W. and D.A. Wright. 1984. WGEN: a model for generating daily weather variables. USDA, Agricultural Research Service, ARS-8.
- Ritchie, J.T., T.S. Griffin and B.S. Johnson. 1995. SUBSTOR: functional model of potato growth, development and yield. p. 401-435. In: Kabat, P., Marshall, B., van den Broek, B.J., Vos, A., van Keulen, H. (Eds.), Modelling and Parametrization of the Soil-Plant-Atmosphere System. Wageningen Pers, Wageningen, The Netherlands.
- Romero, C.C. and L. Stroosnijder. 2001. A multi-scale approach for erosion impact assessment in the Andes. In: Proceedings of the Third International Symposium on Systems Approaches for Agricultural Development [CD-ROM computer file]. CIP.
- Romero, C.C., 2005. A multi-scale approach for erosion impact assessment in the Andes. PhD. dissertation. Wageningen University. Wageningen, The Netherlands.
- Rosenberg, N.J. 1974. Microclimate: The biological environment. A Wiley-Interscience publication. 315 p.
- Sagan, C., 1997. The Demon-Haunted World: Science as a candle in the dark. Random House, Inc. US.
- Schoeneberger, P.J., D.A. Wysocki, E.C. Benham, and W.D. Broderson. 1998. Field book for describing and sampling soils. Natural Resources Conservation Service, USDA, National Soil Survey Center, Lincoln, NE.
- Servicio Nacional de Meteorología e Hidrología del Perú (SENAMHI) and Ministerio de Energía y Minas (MEM). 2003. Atlas de Energía Solar del Perú. (In Spanish). Project PER/98/G31: Electrificación rural en base a energía fotovoltaica. Lima, Peru. 115 p.

- Sinclair, M.R. 1994. A diagnostic model for estimating orographic precipitation. *Journal of Applied Meteorology*, 33: 1163-1175.
- Singh, U., J.T. Ritchie and P.K. Thornton. 1991. CERES-CEREAL model for wheat, maize, sorghum, barley, and pearl millet. *Agronomy Abstracts*, 78.
- Smith, R.B. 2003. A linear upslope-time-delay model for orographic precipitation. *Journal of Hydrology*, 282: 2-9.
- Soil Survey Staff, Natural Resource Conservation Service, 1993. *Soil Survey Manual*, United States Department of Agriculture, Handbook No. 18, Washington DC.
- Stoorvogel, J.J., J.M. Antle, C.C. Crissman and W.T. Bowen. 2001. The tradeoff analysis model version 3.1: A policy decision support system for agricultural (User guide), Laboratory of Soil Science and Geology, Wageningen University, Wageningen, The Netherlands.
- Stoorvogel, J.J., J.M. Antle, C.C. Crissman and W.T. Bowen. 2004a. The tradeoff analysis model: integrated bio-physical and economic modeling of agricultural production systems. *Agricultural Systems*, 80: 43-66.
- Stoorvogel, J.J., J.M. Antle and C.C. Crissman. 2004b. Trade-off analysis in the Northern Andes to study the dynamics in agricultural land use. *Journal of Environmental Management*, 72: 23-33.
- Tapia, M., 1995. *La Encañada, Caminos Hacia la Sostenibilidad*. (In Spanish) ASPADERUC, CONDESAN-CIP, Fondo Perú-Canadá. Proyecto PIDAE. Lima, Peru.
- Thornton, P.E., S.W. Running and M.A. White. 1997. Generating surfaces of daily meteorological variables over large regions of complex terrain. *Journal of Hydrology*, 190: 214-251.
- Tiktak, A., F. van den Berg, J.J.T.I. Boesten, D. van Kraalingen, M. Leistra and A.M.A. van der Linden. 2000. *Manual of FOCUS PEARL version*



- 1.1.1. RIVM Report 711401008, Alterra Report 28. National Institute of Public Health and Environment, Bilthoven, The Netherlands.
- Tourre, Y.M. (ed), 2000. CLIMLAB2000 Manual (version 1.1.0). International Research Institute for climate prediction. Palisades, NY.
- Troll, C. 1968. The cordilleras of the tropical Americas: Aspects of climate, phytogeographical, and agrarian ecology. p. 15-56. In C. Troll (ed.) Geo-ecology of the mountainous regions of the tropical Americas. Fred Dummlers Verlag, Bonn, Germany.
- Tsuji, G.Y., G. Hoogenboom and P.K. Thornton. 1998. Understanding Options for Agricultural Production. Kluwer Academic Publishers. UK.
- UNESCO, 2000. Water use in the world: present situation / future needs. [On line] Available at: [http://www.unesco.org/science/waterday2000/water\\_use\\_in\\_the\\_world.html](http://www.unesco.org/science/waterday2000/water_use_in_the_world.html). Verified: 11<sup>th</sup> August. 2003.
- USDA-NRCS, 1998. Keys to Soil Taxonomy. Eighth edition. Soil Survey Staff.
- US Environmental Protection Agency. 1988. Pesticides in groundwater database. 1988 Interim Report. EPA, Washington, DC.
- Valdivia, R.O., 2002. The economics of terraces in the Peruvian Andes: An application of sensitivity analysis in an integrated assessment model. Thesis. Montana State University – Bozeman, MT.
- Van Breemen, N. and P. Buurman. 1998. Soil formation. Kluwer Academic Publishers, Dordrecht, The Netherlands. 377 p.
- Van Soest, F. 1998. A method for downscaling soil information from regional to catena level. Thesis. Wageningen Agricultural University, Wageningen, The Netherlands.
- Wagenet, R.J. and J.L. Hutson. 1989. Leaching estimation and chemistry model: A Process-based model of water and solute movement, transformations, plant uptake, and chemical reactions in the

- unsaturated zone. Continuum, Vol. 2 (version 2). Center for Environmental Research, Cornell University, Ithaca, NY.
- Weymouth, G. and J. Le Marshall. 1994. An operational system to estimate insolation over the Australian region. p. 443-449. In: Proceedings of Pacific Ocean Remote Sensing Conference. Australia.
- Whiteman, C.D. 2000. Mountain Meteorology: Fundamentals and applications. Oxford University Press. 355 p.
- Wörlén, C., K. Schulz, B. Huwe and R. Eiden. 1999. Spatial extrapolation of agrometeorological variables. Agricultural and Forest Meteorology, 94: 233-242.
- Yanggen, D., C.C. Crissman and P. Espinoza. (eds.), 2002. Impactos del uso de plaguicidas en la producción, salud y medioambiente en Carchi: un compendio de investigaciones y respuestas multidisciplinarias. (In Spanish.) Ediciones Abya-Yala, Quito, Ecuador.
- Zebrowski, C. 1997. Los suelos con cangahua en el Ecuador. p. 128-137. In C. Zebrowski, P. Quantin, and G. Trujillo (ed.) Suelos volcánicos endurecidos. (In Spanish.) Proc. Int. Symp., 3rd. Quito, Ecuador. Dec. 1996. Impresora Polar, Quito, Ecuador.
- Zehetner, F., W.P. Miller, and L.T. West. 2003. Pedogenesis of volcanic ash soils in Andean Ecuador. Soil Science Society of America Journal, 67:1797-1809.

## Annex I

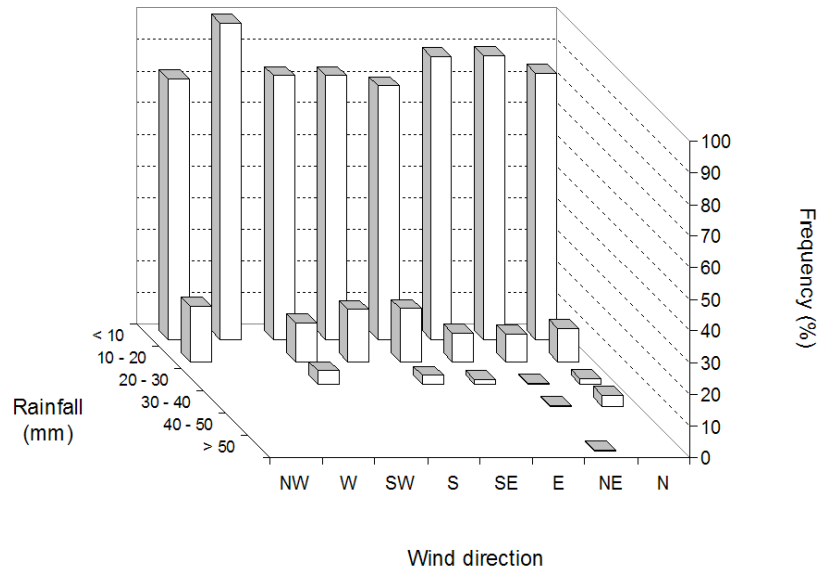


Fig. I.1. Frequency analysis of rainfall according to the wind direction. Watersheds of Chitan and San Gabriel.

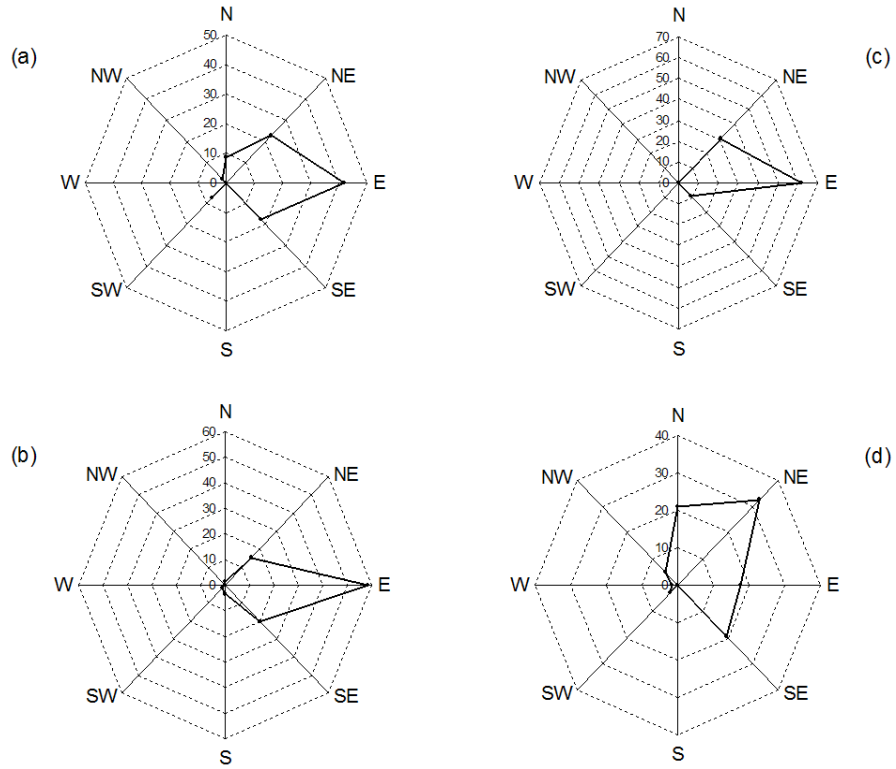


Fig. I.2. Seasonal frequency analysis of wind direction. (a) summer, (b) autumn, (c) winter and (d) spring.



## Curriculum Vitae

Guillermo Antonio Baigorria Paz was born on the 14<sup>th</sup> of March 1969 in Lima, Peru. After attending the private elementary and high school of San Luis Maristas – Barranco he entered the Universidad Nacional Agraria La Molina (UNALM) in 1985, obtaining his Bachelor degree in sciences in 1990 and graduated as Meteorologist in 1994. In 1991 the International Potato Center (CIP) awarded him with a fellowship for a M.Sc. in Agricultural Production in the same university of La Molina obtaining his degree in 1996.

From 1994 to 1998 he performed first as a lecturer and next as an Auxiliary professor in the Physics and Meteorology Department of the UNALM. At the end of 1998 he was awarded with a fellowship for a Ph.D. in the Laboratory of Soil Science and Geology, Department of Environmental Sciences, Wageningen University and Research Centre (WURC). The fellowship was provided by the Soil Management Collaborative Research Program (SM-CRSP) under the project entitled: 'Tradeoffs in Sustainable Agriculture and the Environment in the Andes: A Decision support system for policy makers'. For logistical advantages he moves at CIP as a national recruited staff where he worked until the end of 2004.

During his career, he performed as visitor professor in several universities and postgraduate schools in Peru. From 2001 to 2003, he was the scientific advisor in the Peruvian Atlas of Solar Energy developed by the National Service of Meteorology and Hydrology of Peru using the methodologies developed on his thesis.

Guillermo is married to Consuelo Cecilia Romero León, also defending her Ph.D. thesis on 19<sup>th</sup> April 2005. Since the beginning of 2005 he is a Post-Doctoral Research associated to the Agricultural & Biological Engineering Department at the University of Florida. He can be contacted at [gbaigorr@ifas.ufl.edu](mailto:gbaigorr@ifas.ufl.edu).